Universidade do Minho
Escola de Engenharia

Pedro Miguel Ferreira Mouta

Instrumentation of a cane to detect and prevent falls

Dissertação de Mestrado

Mestrado Integrado em Engenharia Biomédica

Ramo de Eletrónica Médica

Trabalho efetuado sob a orientação de:

Doutora Cristina P. Santos, Universidade do Minho

Janeiro de 2020

ACKNOWLEDGMENTS

I want to thank my mentor, professor Cristina Santos for leading the work in the right direction and proving valuable knowledge and experience each step of the way. Moreover, I would like to mention immense gratitude to the doctoral student Nuno Ferrete Ribeiro, who was outstanding, not only at the level of scientific guidance but also at supporting, advising, and being always present throughout this year.

Thank you to my laboratory colleagues for keeping the excellent energy present and the camaraderie during this year. Besides, I want to thank the suggestions and availability provided.

I also want to thank Inês Carvalho for being present in all the important moments of my life and giving the strength to never give up when the obstacles appear. I am genuinely proud of you.

I want to thank and acknowledge my friends for always giving the motivation to keep going forward and recommendations in the various projects of my life.

Finally, I want to thank my parents and siblings, in particular to my mother and father over the unconditional support over these last few years. Besides to provide me with the best conditions for my education, they were also an emotional pillar, always indicating the best way forward. Thank you for all your strength and encouragement. I have exceptional pride in both of you.

Thank you very much everyone

Pedro Miguel Ferreira Mouta

STATEMENT OF INTEGRITY

I hereby declare having conducted this academic work with integrity. I confirm that I have not used plagiarism or any form of undue use of information or falsification of results along the process leading to its elaboration.

I further declare that I have fully acknowledged the Code of Ethical Conduct of the University of Minho.

RESUMO

O número de quedas tornou-se uma das principais causas de lesões e mortes na comunidade geriátrica. Como resultado, o custo do tratamento das lesões também aumenta. Portanto, é necessário o desenvolvimento de estratégias relacionadas com quedas e que exibam capacidade de monitorização em tempo real sem colocar restrições ao usuário. Devido às suas vantagens, os acessórios do dia-a-dia podem ser uma solução para incorporar sistemas relacionados com quedas, sendo que as bengalas não são exceção. Além disso, a avaliação da marcha pode ser capaz de aprimorar a capacidade de uso de uma bengala para usuários mais idosos. Desta forma, é crucial o desenvolvimento de estratégias que reconheçam estados de queda, do passo anterior a uma queda e dos diferentes eventos da marcha de uma bengala. Esta dissertação tem como objetivo desenvolver estratégias capazes de identificar as situações anteriormente descritas com base num sistema incorporado numa bengala que coleta informações inerciais e de força, a *Assistive Smart Cane (ASCane).*

A estratégia referente à deteção de quedas consistiu em testar os dados adquiridos através da *ASCane* com três algoritmos de deteção de quedas (baseados em *thresholds* fixos), com um algoritmo de *thresholds* dinâmicos e diferentes classificadores de *machine learning* encontrados na literatura. Estes métodos foram testados e modificados para dar conta do uso de informação adquirida através de uma bengala. O melhor desempenho alcançado em termos de sensibilidade e especificidade foi de 96,90% e 98,98%, respetivamente.

Relativamente à deteção dos diferentes eventos da *ASCane* em situações controladas e da vida real, um detetor de eventos da marcha foi e comparado com um sistema de *ground truth*. Além disso, foi também realizado um estudo de *machine learning* envolvendo oito métodos de seleção de *features* e nove classificadores diferentes de *machine learning*. Os resultados mostraram que a precisão dos classificadores foi bastante aceitável e apresentou, como melhores resultados, 98,32% de precisão para situações controladas e 94.82% para situações do dia-a-dia.

No que concerne à deteção de passos pré-queda, a mesma abordagem de *machine learning* foi realizada. Os modelos foram precisos (precisão = 98,15%) e com a implementação de um filtro de pós-processamento, todas as deteções de falsos positivos foram eliminadas e uma queda foi passível de ser detetada 1,019s antes do final do respetivo passo de pré-queda e 2.009s antes do impacto.

PALAVRAS-CHAVE: QUEDAS, PASSOS PRÉ-QUEDA, EVENTOS DE UMA BENGALA, ASSISTIVE SMART CANE

ABSTRACT

The number of falls is growing as the main cause of injuries and deaths in the geriatric community. As a result, the cost of treating the injuries associated with falls is also increasing. Thus, the development of fall-related strategies with the capability of real-time monitoring without user restriction is imperative. Due to their advantages, daily life accessories can be a solution to embed fall-related systems, and canes are no exception. Moreover, gait assessment might be capable of enhancing the capability of cane usage for older cane users. Therefore, reducing, even more, the possibility of possible falls amongst them. Summing up, it is crucial the development of strategies that recognize states of fall, the step before a fall (pre-fall step) and the different cane events continuously throughout a stride. This thesis aims to develop strategies capable of identifying these situations based on a cane system that collects both inertial and force information, the Assistive Smart Cane (ASCane).

The strategy regarding the detection of falls consisted of testing the data acquired with the ASCane with three different fixed multi-threshold fall detection algorithms, one dynamic multi-threshold and machine learning methods from the literature. They were tested and modified to account the use of a cane. The best performance resulted in a sensitivity and specificity of 96.90% and 98.98%, respectively.

For the detection of the different cane events in controlled and real-life situations, a state-of-the-art finite-state-machine gait event detector was modified to account the use of a cane and benchmarked against a ground truth system. Moreover, a machine learning study was completed involving eight feature selection methods and nine different machine learning classifiers. Results have shown that the accuracy of the classifiers was quite acceptable and presented the best results with 98.32% of overall accuracy for controlled situations and 94.82% in daily-life situations.

Regarding pre-fall step detection, the same machine learning approach was accomplished. The models were very accurate (Accuracy = 98.15%) and with the implementation of an online post-processing filter, all the false positive detections were eliminated, and a fall was able to be detected 1.019s before the end of the corresponding pre-fall step and 2.009s before impact.

KEYWORDS: FALLS, PRE-FALL STEPS, CANE EVENTS, ASSISTIVE SMART CANE

CONTENTS

LIST OF FIGURES

List of Tables

List of Acronyms and Abbreviations

ACC	Accuracy
ADL	Activities of Daily Living
BOS	Base of Support
CFS	Correlation Based Feature Selection
CMSW	Cane Mid-Swing
COG	Center of Gravity
COM	Center of Mass
CV	Cross-Validation
DA	Discriminant Analysis Classification
DT	Dynamic Threshold
F1S	F1 Score
FBC	Full Base Contact
FD	Fall Detection
FCO	Full Cane Off
FF	Foot Flat
FGC	First Ground Contact
FN	False Negative
FOG	Freeze of Gait
FP	Fall Prediction
FS	Sampling Frequency
FSM	Finite State Machine
FT	Fixed Threshold
GPS	Global Positioning System
Gyr	Gyroscope
HO	Heel Off
HS	Heel-Strike
KNN	K-nearest neighbour
LASSO	Least Absolute Shrinkage and Selection Operator
LDR	Light Dependent Resistor

LFT	Lower Fall Threshold
LLCFS	Local learning-based clustering feature selection
LRF	Laser Range Finder
Mag	Magnetometer
maxLE	Maximum finite-time Lyapunov exponent
MCC	Matthews correlation coefficient
MMST	Middle Mid-Stance
MMSW	Middle Mid-Swing
MSM	Maximum Support Moment
NA	Not Applicable
PCA	Principal Component Analysis
PCO	Partial Cane Off
PD	Parkinson's Disease
PF	False Positive
PFS	Pre-Fall Step
PREC	Precision
RQ	Research Questions
SENS	Sensitivity
SPEC	Specificity
SVM	Sum Vector Magnitude
SVmaxmin	Differences between the maximum and minimum acceleration
TN	True Negative
TO	Toe Off
TP	True Positive
UDFS	Unsupervised Discriminative Feature Selection
UFSOL	Unsupervised Feature Selection with Ordinal Locality
UFT	Upper Fall Threshold
USA	United States of America
Z2	Vertical Acceleration
ZMP	Zero Moment Point

1. INTRODUCTION

This dissertation presents the work developed in the scope of the fifth year of the Integrated Master's in Biomedical Engineering during the academic year of 2018/19.

This dissertation was developed at BiRD LAB (Biomedical Robotic Devices Laboratory) of the Center of MicroElectroMechanical Systems (CMEMs), at University of Minho, Braga, Portugal. This dissertation addresses the development of offline strategies to distinguish not only normal gait from a fall and Pre-Fall Step (PFS) situations, but also to detect cane events (both in controlled and real-life situations) with information acquired in a system embedded into a regular cane, which was named Assistive Smart Cane (ASCane).

1.1 Motivation

Human walking is a complex and fundamental human physical activity that can be done in an assortment of ways and directions. It requires joint mobility, muscular strength, and coordination of the central nervous system [1]. However, human gait can be modified by several muscular deformities and neurological injuries, whose predominance tends to increase with ageing. In the United States of America (USA) alone, there is a considerable number of people who have been affected by walking disorders, for example, 4.7 million with stroke, 400 thousand with multiple sclerosis and 100 thousand with cerebral palsy [2]. Thereby, walking diseases lead to disorders and abnormalities of the gait, which are the main symptoms utilised to diagnose and evaluate the advancement of a person's gait impairments [1].

Falls are the **second main reason of death by accident worldwide**, which represents not only one of the significant undesired accidents but also a challenge to patient safety, and therefore, their care quality [3]. In 2000, in the USA alone, **$19 billion** were spent on **medical costs of fall-related injuries** [4]. Since the population is ageing, their bodies go through numerous physical changes making them more fragile and more predisposed to falls [5]. So, it is expected that both the number of falls and the costs to treat them increase substantially. The estimated **medical costs concerning falls in 2015** were approximately **$32 billion**, where $31.3 billion were from nonfatal falls alone [4]. By 2020, expenses linked to injuries from falls to senior citizens are expected to cost roughly $43.8 billion [6].

Nowadays, falls in the elderly population is a subject of interest amongst the scientific community. Systems that can detect, but, more importantly, to predict a fall, are crucial to reducing the costs, physical and psychological consequences of a fall. Fall-related systems mainly focus on the development of

wearable methods in which a fall is automatically detected. Nonetheless, the system will weight on the individual and hinder its flexibility [7]. Amongst the elderly that fall at home, a large amount does not have their assistive device with them at the moment of the fall. Consequently, sustain severer injuries when they fall without their assistive device.

The **study of human locomotion** has the potential of assessing gait pathologies and locomotion performance as well as **predicting, preventing and detecting falls**. Regularly, gait analysis is carried out in a motion analysis laboratory with expensive, yet, very accurate systems (e.g. optical systems, force plates). However, these systems are limited to laboratory standards. The challenge is to provide comparable results with low-cost, unobtrusive solutions for constant all-day and any-place monitoring [8]. The detection of human gait events can possibly be used in the rehabilitation field, specifically, in the design of tuned therapy strategies per the patient requirements and venture to promote a more effective functional motor recovery [1].

1.2 Problem statement and scope

In order to detect not only falls but also PFS situations, it is required continuous gait monitoring. Recently, numerous fall-related studies have been carried out. Nevertheless, most of them require a substantial number of sensors placed in the living environment to work successfully.

Consequently, the use of accessories where elderly may take with or wear on, e.g. necklaces, watches or canes, can be a serious alternative. However, using these accessories to monitor the subject continuously involves a considerably sized battery. Therefore, the use of smaller devices will result in a low power supply for a short amount of time, which is not optimal. The constant hand movement is also a factor to discard its use which is too high to monitor for long periods.

Therefore, embedding sensors into a cane can be the best choice since these assistive devices are widely used amongst the geriatric community, and the number of prescriptions is increasing due to gait/balance disorders and lower limbs weakness. Furthermore, an evaluation of the canes gait can be capable of enhancing the ability of cane usage, also reducing the possibility of possible falls amongst them. Consequently, it was possible to produce a system capable of providing information regarding the gait of a cane. Firstly, a **Fall Detection (FD)** system was implemented comparing the different FD methodologies existent in the literature. Secondly, two methods were accomplished to segment a cane stride into **six cane events**. More specifically, an adapted state-of-the-art algorithm for human gait event detection and a combination of machine learning classifiers and feature selection methods. Moreover, to

identify **PFS** situations, the same machine learning study accomplished for cane event segmentation was performed.

These requirements are the core to the development of a gait monitoring wearable system embedded into a cane, presenting an innovative character and allowing to improve some problems of the actual fall and gait analysis related systems.

1.3 Goals and research questions

The main goals of this thesis are the development of offline strategies to distinguish not only normal gait from a fall and pre-fall situations but also to detect cane events with information acquired in a system embedded into a regular cane. To accomplish these goals, it is necessary the understanding of several aspects of human walking, along with the knowledge of sensors' characteristics, attachment location and the most characteristic gait parameters to this situation.

Thereby, with this thesis, it is necessary to achieve the following goals:

- **Goal 1:** The first goal consists of a survey and interpretive study of pertinent information concerning **falls** and **technological approaches** to detect and avoid them. It is intended to understand the different stages of a fall, how falls are classified in the literature, their risk factors and consequences, as well as the existent systems, methods and algorithms. In this goal, it is also essential to know which are the typical gait parameters studied, used sensors and their corresponding attachment location.
- **Goal 2:** This goal aims to make an extensive analysis about several studies, techniques and **devices already developed** that are already **embedded into canes**. Namely, what type of sensors are used and their corresponding placement, what experimental protocol was carried out, what features were computed, and what type of algorithm was employed into the system. Also, it is expected to recognise the limitations in the existing devices aiming at proposing new solutions.
- **Goal 3:** The third goal is the **development of the monitoring system**, namely, the investigation and identification of the materials to ensure a sturdy, universal and adaptable system. Moreover, it will be identified the electronic components required for the data acquisition system, processing unit, and additional components which can be included.
- **Goal 4:** This goal consists of a survey for **FD strategies already implemented** and its **implementation in the ASCane**. An experimental protocol needs to be established, and several tests should be performed on the acquired data, as well as a comparative analysis

considering the recent works in the literature and the eventual improvements completed to account the use of a cane.

- **Goal 5:** The fifth goal is to identify the different event phases of a cane during human locomotion that can be distinguished. Following, the acquired inertial data will be used as an input to a modified Finite-State-Machine (FSM) for gait event detection for gyroscopic foot data and understand how a cane event detection can be accomplished. Moreover, a machine learning study will be achieved to uncover an adequate approach to distinguish proper **segment a stride into six different phases** from a single vector of features representative of a single time frame. Several feature selection methods, as well as various machine learning classifiers, should be tested and compared to reach the best possible results.
- **Goal 6:** The last goal aims at **distinguishing normal from PFS** with the same machine learning approach as the previous goal. Therefore, it will be possible to merge in one system a fall, a PFS and cane event detection. The overall work has been described throughout this master's thesis.

The following Research Questions (RQ) are expected to be answered in the present work:

- **RQ1:** Which is the best FD strategy to be implemented in a cane? This RQ is addressed in Chapter 5.
- **RQ2:** Which are the features and machine learning classifier with greater potential to distinguish the different cane events during the users' walking? This RQ is addressed in Chapter 6.
- **RQ3:** Which are the features and machine learning classifier with greater potential to distinguish between normal and pre-fall situations in data acquired from a cane? This RQ is addressed in Chapter 7.

1.4 Contribution to knowledge

The main contributions of this work are:

- The initial development of an instrumented cane system for human gait analysis, fall and PFS detection, from a technology readiness level of 0 up to a level 3.

- A FD technique applied to data acquired from a cane. Numerous experiments were conducted to discover which FD method achieved the best results considering the processing power required and detection time.
- A tool that can differentiate between the various cane events during human locomotion. It was tested offline, and an online test was mimicked. An analysis and comparison of the different implemented approaches were fulfilled to reach the best possible results.
- A tool that accurately distinguishes between normal and PFS. This tool and its main concepts were tested offline and online simulated. Detailed comparisons between all methods tested were accomplished.

1.5 Publications

From work produced throughout this academic year, it was possible to publish two conference papers.

Conference Papers

- P. Mouta, N. F. Ribeiro, L. Gonçalves and C. P. Santos, "An Overview of Fall-Related Systems Developed in Canes", 2019 IEEE 6th Portuguese Meeting on Bioengineering (ENBENG), Lisbon, Portugal, 22-23 February 2019.
- P. Mouta, N. F. Ribeiro, L. Moreira and C. P. Santos, "Assistive Smart Cane (ASCane) for Fall Detection: First Advances", 2019 15th Mediterranean Conference on Medical and Biological Engineering and Computing (MEDICON), Coimbra, Portugal, 26-28 September 2019

1.6 Thesis outline

This dissertation is organised as follows. An introduction concerning falls, their different stages, the problems they constitute to the elderly, and how to classify them is available in Chapter 2. It is also presented a state-of-the-art regarding the technological approaches to falls, how they can be classified, which features systems use to discern between normal gait, falls and PFS, and the most used sensors and respective attachment location in the scientific literature.

In Chapter 3 it is presented a general overview of fall-related strategies implemented into canes, which sensors they embed and their corresponding location, the gait parameters used, which algorithms were employed, and, finally, the results attained. It was also accomplished an extensive research for commercial canes and patents with fall-related embedded systems.

Chapter 4 presents the developed solution, discussing the importance of its components, specifying their functions, and a general overview of the software implemented to explain all the systems that make up the global system developed.

An offline fall detection system is described in Chapter 5. In this chapter, a comprehensive overview of different FD algorithms in literature is performed and tested with data acquired from the AScane. Afterwards, analysis and discussion of the results were accomplished to understand how the algorithms can be modified to achieve a more accurate FD.

In chapter 6, the AScane is used to collect gait's data from several subjects in four different walking conditions. Then, a modified state-of-the-art FSM algorithm for human gait event segmentation was benchmarked against a ground truth of the acquired data, which was developed with the information acquired from the MTw Awinda (Xsens Netherlands) and Force Sensitive Resistors (FSR) systems. Furthermore, the best machine learning model was chosen based on different feature selection methods, in which the trade-off between the number of computed features and model performance was acknowledged. Finally, with the best set of parameters, the classifier was mimicked online, and a post-processing technique was developed to further increase the segmentation performance. Respective results and discussion are also presented.

An offline PFS detection system is described in Chapter 7. In this chapter, the AScane is used to collect gait's data from several subjects regarding walking and pre-fall situations. This information was, initially, filtered, separated by normal and pre-fall situations and used to estimate the features previously found in the literature. Then, through different feature selection methods, the most significant combination of features were used to train different machine learning models. The best combination of parameters was determined using various performance metrics. The results are also discussed.

The conclusions of this work are available in Chapter 8. The proposals to continue this work in the future are also written in this chapter.

2. FALLS AND RELATED TECHNOLOGICAL APPROACHES: STATE-OF-THE-ART

2.1 Introduction

The definition of a fall has been varying over the years. In 1897, the Kellogg International Working Group on the Prevention of Falls in the elderly defined a fall as “unintentionally coming to the ground, or some lower level not as a consequence of sustaining a violent blow, loss of consciousness, sudden onset of paralysis as in stroke or an epileptic seizure”. Later, this definition was updated to include several other

health issues such as dizziness or even cardiac collapse, all of which might result in a fall and its possible consequences [9]. The World Health Organization stated that falls are the second main reason of death by accident worldwide, representing not only one of the main unwanted accidents but also a challenge to patient safety, and Therefore, their care quality [3].

Falls in older adults represent a common and increasing health problem. One-third of the elderly suffer at least one fall each year, frequently resulting in serious health complications. According to the International Database of the U.S. Census Bureau, the typical proportion of individuals older than 65 years in developed countries in 2015 was roughly 17%. This proportion is expected to reach 30% in 2050 [4], [10]. Regarding statements from the same federal agency, there will be a **210% growth of the population aged 65 and over** within the next 50 years, in part due to ageing from the baby boomers generation [11]. Projections for 2150 have shown that one-third of the population will be represented by the elderly, which makes the goal of sustaining a healthy ageing a priority at the European level [12].

The **probability of a fall increases with age** since **32% to 42%** of people over 75 years suffer a fall in the same period. Previous fallers have a $\frac{2}{3}$ chance of suffering from a fall in the following year, and over 50% of residents in institutional care have had at least one fall over one year. About 65% of women and 44% of men fall inside their usual residence. Most falls occur in the most frequently used rooms such as bedrooms, kitchen and dining room [13].

2.2 Different Stages of a Fall

Some studies have proposed a multiphase fall model towards providing a more in-depth observation of the fall event for improving automatic FD systems where the fall manages to be divided into different phases, including a pre-fall, critical, post-fall, and recovery phases [9]. Other authors divide the critical phase into the falling and impact stages [10], [14].

The first stage of a fall is the moment in which the person performs Activities of Daily Living (ADL) which can include actions that sometimes can be classified as a fall due to sudden and rapid movements performed such as jumping and sitting down [9], [10], [14].

The critical phase can be defined by a lowering of the Center of Mass (COM) that can no longer be recovered by protective strategies. It is associated with the sudden movement of the body towards the ground, ending with a vertical shock [10]. While falling, there is a short moment where the person is in free-fall, which is characterised by an approximation of the three acceleration axis to zero [15]. Regarding its duration is expected to last from 0.3 up to 0.8 seconds [9], [10]. Then, the body typically hits the

ground or an obstacle. Regarding its acceleration, an abrupt polarity inversion of its vector in the direction of the trajectory is verified, which can be easily detected by an accelerometer or a shock detector.

The post-fall phase is of varying duration, considering the different type of injuries that can be sustained in a fall. Normally, the faller remains immovable in a posture and a place. The end of this phase can be detected with the start of the next one, the recovery phase, usually including COM movement or the surpass of a predefined time interval [9], [10], [14].

Finally, the recovery phase can be either intentional and independent, where the faller stands up in his own or is assisted by someone. Its duration fluctuates since it can be anything from a full recovery to its absence [14]. In case there is no rescue in this event, a fall can be followed by a "long lie," which is defined as the involuntarily remaining on the floor for at least an hour after a fall [16]. All the acceleration changes abovementioned of a person during a fall are represented in Figure 2.1.

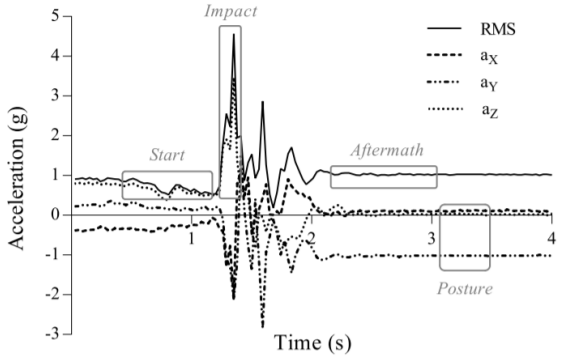

Figure 2.1: Acceleration changes during an accidental fall.

2.3 Classification and type of falls

The identification of different types of falls is essential to fall-related strategies to provide appropriate measures to assure the safety of the patient. Concerning the literature, there are not standardised fall type criteria. Thus, in each work, the researchers propose their division and classification of falls and ADL trials as can be seen from Table 2.1.

Table 2.1: Types of falls and ADLs discriminated in different studies

Study	Falls and ADL description
[17]	Fall: (i) forward, (ii) backward, (iii) lateral left, (iv) lateral right and, (v) falling on the stairs. ADL: (i) standing, (ii) sitting in a chair, (iii) sitting on the floor, (iv) lying, (v) walking, (vi) running, (vii) going upstairs, (viii) going downstairs, (ix) bending.

Study	Falls and ADL description
[18]	Fall: (i) forward due to a trip, (ii) backwards due to a slip, (iii) left lateral and (iv) right lateral. ADL: 9 participants kept the smartphone for a week to record everyday behaviour.
[19]	Fall: (i) forward, (ii) lateral left and (iii) lateral right. ADL: (i) standing up, (ii) sitting down in a chair, (iii) walking average pace.
[20]	Fall: (i) forward, (ii) backward, (iii) lateral left and (iv) lateral right. ADL: (i) sit-to-stand, (ii) stand-to-sit, (iii) level walking, (iv) walking up and (v) downstairs, (vi) answering the phone, (vii) picking up an object, (viii) getting up from supine.

Falls can be discriminated by its direction and the incident that cause it, such as trips and slips. Bai et al. [15], studied the acceleration signal for different ADL and fall directions. The researchers concluded that the **acceleration when falling is entirely different from that of ADL** (jumping, standing up, walking and standing down) and fall direction was able to be determined by comparing the accelerations on all three axes before and after the fall. Nevertheless, some ADL can be misinterpreted as a fall since some of its characteristics exists in typical actions such as crouching, which also demonstrates a fast downward motion [21].

Smeesters et al. [22], examined the effect of disturbances (faint, slip, step down, trip) and gait speed (fast, normal, slow) in fall direction and impact location. They concluded that disturbance type and gait speed knowingly affected the fall direction impact location. Regardless of gait speed, trips and steps down frequently result in forward falls, leading to abdominal pelvis impact. With faster gait speeds, slips and faints result in the same outcome. Decreasing gait speed, slips result more often in sideways or backwards falls, leading to hip or buttocks impact. Regarding impact velocities, they were constant, 1.51 ± 0.50 m/s, excluding step down that result in lower impact velocity. The age, gender, height, mass and physical activity did not suggestively affect fall direction, impact location or impact velocity.

2.4 Risk factors

Before any fall-related strategies can be implemented or analysed, it is essential to identify those individuals who have a higher fall risk. **Falls** occur as a result of **dynamic interactions between numerous risk factors** categorised into two types: intrinsic and extrinsic factors. Therefore, analysing fall risks is a challenging problem due to the multifactorial mechanisms behind a fall [23]. Falls among

older people are often allied with intrinsic factors, these are mainly age-related since older people suffer from a more severe weakening within its balance system, but more significantly, linked with pathophysiological aspects affecting any of the systems involved in balance. Extrinsic factors are connected to environmental hazards such as poor lighting, slippery floors and uneven surfaces, footwear/clothing and unsuitable walking aids/assistive devices [24]. Roughly one-third of fallers using a walking aid were prescribed with a device insufficient for their needs, not improving their gait the desired amount [25]. As a result, it is vital to identify the people who are more prone to falls to take full advantage of the intervention planned. Although several studies identify risk factors related to falls, a direct comparison is hindered due to different methodologies applied. This section presents risk factors associated with falls and including them into the two categories mentioned above. It is essential to understand that multiple factors are always involved in a fall since they do not have a single cause because most of the risk factors are linked [26].

2.4.1 Gender, Ethnicity and Age

There is proof of racial differences regarding fall rates in the USA. The fall rate from the highest to lowest is white men, white woman, black man and black woman, although **fall risk increases with age** among different races. The risk and frequency of falls increase with age with its greatest **intensification at the age of 80** [23], [24], [26]–[28].

Considering geographical and socioeconomic variations, caucasian women are more likely to suffer from a fall outdoors than African American women up to 1.6 times and twice as likely to land on surfaces suchlike ice, dirt and snow. They are not only 3.8 times more probable to fall straight down (along with the vertical direction), but also twice as plausible to fall laterally or posteriorly compared to falling forward [24], [27]. Although women are more likely to suffer from nonfatal falls, men are more prone to experience fatal falls, possibly due to the practice of more risky behaviours [27].

2.4.2 Psychological Status

Although the relationship between falls and psychological factors still are unclear, the **fear/anxiety of falling and depression are related to an increased risk of fall**. Depression can be bound to the decrease in physical activity, gait speed and muscle strength, which are linked to lethargic behaviour typical in people with this disorder [29]. Fear of falling is due to several different aspects, such as reduced physical activity and a history of falls. Since up to 70% of people who suffered a fall recently and 40% of people who not account for falls lately recognises the existence of this fear which can lead to

the decrease of physical and social activities [24], [29]. Fear of falling makes people lose self-confidence in their safety, restricting their ADLs [10].

2.4.3 Medication intake

The most common medications are the ones that interact with the central nervous systems, for instance, benzodiazepines, sedatives and tranquillisers, which cause cognitive impairment, dizziness, sedation and a decrease in neuromuscular function [27]. Studies show that with the **intake** of four **medications, the fall risk increases significantly**, the consumption of five or more is associated with a nine-fold increase of the cognitive weakening and fear of falling [24]. The intake of different drugs has consequences that include drug reactions, drug interactions and cognitive impairments and urinary incontinence. Which is why the patient clinical history is critical while prescribing such medications [28].

2.4.4 Physical conditions

Physical disabilities can increase the risk of falls. This type of risk factor is directly linked to ageing. Table 2.2 presents several physical risk factors associated with falls, the ones mentioned were examined and compared between individuals who experienced a fall and with those who did not.

As a person ages, muscle weakness, particularly in the lower limbs, debilitated neurologic feedback and chronic illnesses may be experienced. These changes, in combination with other risk factors, increase the likelihood of a fall. One study showed that a patient with a combination of four risk factors has about 78% chance of falling [30]. Starting with the medical conditions associated with the intensification of the fall risk, they can be subclassified dependent on the functional system associated.

Table 2.2: Reported physical fall risk factors in older people [31], [32]

Risk Factor	Mean RR[a]	Range
Muscle Weakness	4.4	1.5 – 10.3
Gait deficit	2.9	1.3 – 5.6
Balance deficit	2.9	1.6 – 5.4
Mobility limitation	2.5	1.0 – 5.3
Visual deficit	2.5	1.1 – 3.5
Impaired ADL	2.3	1.5 – 3.1
Postural hypotension	1.9	1.0 – 3.4
Cognitive impairment	1.8	1.0 – 2.3

[a] RR: Relative risk (Prospective studies)

The occurrence of falls among neurological patients is very high, carrying high costs for health institutions, and the prevalence of neurological disorders is increasing as a result of changes in population demographics. A study regarding falls in recurrent neurological diseases ranked the most frequent neurological disorders with the highest fall rate, which led to the results shown in Figure 2.2 [33].

From Figure 2.2, patients with Parkinson's disease (71%) and stroke (89%) are more likely to fall than patients with every other type of neurologic disease. They were followed by a collection of diseases with an average of four times the likelihood of falling consisting of dementia, epilepsy, movement disorders and peripheral neuropathy.

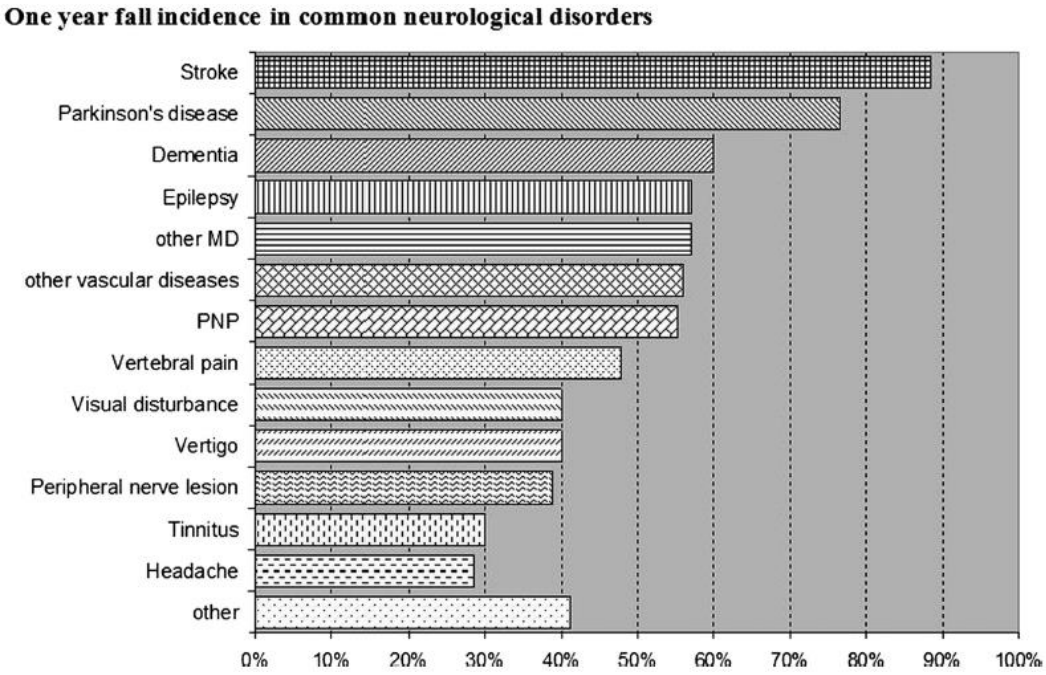

Figure 2.2: Difference in frequency of having at least one fall within the 12-month period for patients suffering from the 13 most commonly encountered neurological disorders, taken from [33].

Stroke-related neurological conditions contribute to a large number of falls in the community since individuals with stroke do not only present a high fall risk during the acute phase but also during the poststroke phase considering that are various conditions that may develop after [34].

From studies performed in people who suffered from strokes, it is suggested that the individuals are more prone to fall when walking involves considerable cognitive control. Consequently, patients are usually incapable of walking and talking simultaneously or slow down when performing a current mental task. Stroke-related balance and gait deficits, which were acknowledged by clinical assessments, contribute to a large number of falls in these patients [34].

To maintain balance, the vertical projection of the body needs to be upheld inside the limits of the Base of Support (BOS). In tasks where the BOS changes size or position, such as ADL, the Center Of

Mass (COM) has to be relocated with the new BOS in order not to fall. When an environmental perturbation changes the COM near the limits of the BOS or even out of them, the person needs to be able to counterforce the external forces applied to the one's body in order to maintain balance. Regarding one's gait, it must be able to produce adequate mechanical energy in order to walk and cause progression of gait. It must be able to attain sufficient clearance of the foot to avoid stumbling, the necessary stance stability of the weight-bearing lower limb and the correct positioning of the swinging leg. However, some deficits caused by stroke prevent the requirements mentioned above such as such decreased postural stability during quiet standing, tardy and fewer coordinated responses, reduced propulsion at push-off, lessened leg flexion through the swing phase, reduced stability throughout the stance phase and reduced automaticity of walking [34].

Parkinson's Disease (PD) is a neurodegenerative disease that presents motor and non-motor signs and symptoms [28]. Studies indicate that people affected by this neurological illness experience falls and around 70% of them are affected by recurrent falls even in the early stages of the disease. It has been assessed that 76% of falls in PD patients require health care services and 33% result in fractures [35][36]. Patients with PD often walk with diminished gait speed, shorter stride length, stooped posture, and reduced arm swing [37].

Furthermore, amongst PD patients whose fall resulted in fractures, the mortality rate is approximately 10.6%. PD patients fall in various directions, and different body parts are wounded during such falls. Most of the population tend to fall forward. Some researches stated multiple fall directions and the association between the falling course and fractures obtained [35]. The two main mechanisms underlying recurrent falls in PD patients were identified as being the Freeze of Gait (FOG) and balance impairment.

Freezing is defined as "an episodic inability to generate effective stepping" even though there is a desire to walk [38]. Thus, FOG is a predictor for falling forward, when it happens their Center of Gravity (COG) keeps moving forward when their feet stop moving, which leads to falling forward while balance impairment, akinetic-rigid subtype, and neuropsychiatric symptoms were linked with falling backwards or sideways [35]. This feature is most prevalent not only while initiating gait, turning, or approaching a destination but also is commonly triggered by environmental features such as narrow hallways, doorways and large crowds. There are three types of FOG described in individuals with PD. The most common type observed is represented with trembling of legs, which is frequently linked with an effort to overcome the block that is associated with FOG. Akinesia is a condition where individuals suffer from loss of ability to move their muscles. Festination is a gait disturbance described as small and quick steps executes to

retain the COG between the feet while the trunk leans forward involuntarily, shifting the COG forward [38] Gait Disorders [39]. Therefore, a prevention strategy for falls in PD patients, could be established grounded in their main falling direction [35].

Female individuals have a higher incidence of both falls and fractures among PD patients, which is the same regarding the general population [40]. Although hip fractures have been described as the most common location of fractures and have revealed the strongest association with PD, in [40], upper limb fractures were the most common type sustained. However, the location of the fractures is determined by several factors. For case, osteoporosis and body mass index have been proven to be associated with increased risk of hip fractures, and low bone mineral density predominantly affects the risk of fracture for the hip, wrist, and spine [40]. The related factors and characteristics regarding the different falling directions in an individual with Parkinson's disease and their gait are illustrated in Figure 2.3. a) and b), respectively.

Although dementia was not one of the neurological disorders with the highest fall rate, its predominance in the population is still significative. Dementia is a category of neurological syndromes which restrict the social and occupational functioning of predominantly elderly and are characterised by the progressive deterioration in cognition. The primary subtypes of dementia include vascular dementia and Alzheimer's disease. Although in people younger than 65, the predominance of dementia is rare, its incidence increases exponentially in individuals older than that [42].

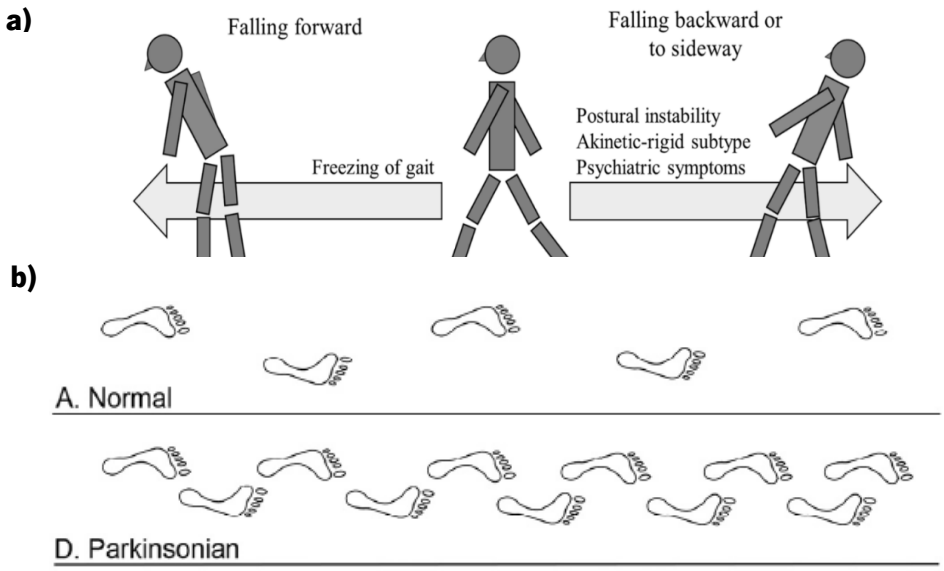

Figure 2.3: a) Scheme of the mechanism and characteristics of PD forward fallers and non-forward fallers; b) Graphic representation of Parkinson's gait versus normal gait.

Even though there are no studies about the type of falls in individuals diagnosed with dementia, falls are often a part of the disease, hence the reason to implement preventive strategies to prevent them.

Dementia is classified as an independent risk factor in falls due to its symptoms such as disorientation, dromomania, postural and neurovascular instability [41],[42].

Regarding the incidence of falls in patients with dementia, it varies according to the type of study conducted, with studies that recorded data retrospectively obtaining considerably lower estimations of fall rates than those using prospective methods. Considering studies with prospective methods, people with dementia are two times more prone to fall than cognitive healthy older people. Regarding actual fractures sustained due to falls is estimated to be roughly 7% and 50% of the fractures are to the femoral neck [41].

2.4.5 Non-use or non-access to assistive devices

Amongst the elderly that sustains a fall at home, a large amount does **not possess an assistive device with them at the moment of the fall.** People sustain **more severe injuries** when they fall without their assistive device. Data implies that a large percentage of people end up quitting their prescribed assistive device. Moreover, they underestimate the significance of the cane to their safety. Believing that the prescribed device decreases falls, doesn't necessarily ensure device use. The known risk of falling is not significant enough to justify engaging in the self-protective behaviour of using the device [43]. Older adults do no use their canes or walkers, particularly in their homes where the most considerable number of falls occur, even though knowing that it can help avert a fall. Instead, they steady themselves by holding themselves against walls and furniture. Two factors that influence device use that has not been adequately discussed are the disregard of older adults concerning fall prevention strategies (e.g. proper use of canes and walkers), and their rejection about fall prevention actions [44].

A research accomplished by Luz et al. [45] suggests that people will not practice the required precautions to avoid an adverse event (such as a fall) till people accept that the risk presents a notable threat to them personally. Precautionary behaviour needs to be significant enough to their security that overcomes every potential reason for not engaging in this behaviour. Patient education regarding the connection within device use and fall-related injuries could improve the discernment of their own risk and the importance of device use that could surpass the negative psychosocial context and stigma which discourages use. Furthermore, the development and investigation of approaches to maximise device use are demanded such as environmental reminders and employing new technologies to develop new types of canes and walkers which could overcome the social stigma associated with device use.

2.5 Consequences of a fall

As stated before, **falls are a public health issue** that predominantly affects older people and can result in injury, hospitalisation, injuries, mobility impairment and even death. Fabricio et al. [46] conducted a study not only to investigate the history of falls reported by the geriatric community, but also to name likely associated factors, the place of occurrence, causes, and consequences. The most frequently observed consequence were fractures (64%), occurred in 53% of men and 70% of women. The most common fractures were of the femur (62%), followed by radius (12.5%), clavicle (6.25%), and others such as spinal column, ulna, scapula, patella, and nose. Fear of additional falls (44%) and the remaining consequences reported are presented in Figure 2.4. The population of the study was comprised of 251 older adults older than 60 years [46]. Furthermore, Figure 2.5 resumes the causes and effects of the mentioned problem by using a Tree Problem Diagram.

2.6 Fall-Related Tools And Existing Strategies

As stated, fall-related medical care is linked to high financial expenditure, and it is expected to grow significantly. Falls amongst the elderly community does not only concern the health practitioners but also the scientific community. **Fall Prediction (FP) and FD systems are vital** to answer this problem and can assist in **reducing the financial, physical, and emotional consequences of a fall.** Consequently, numerous research papers have tackled falls and in methods of detecting and preventing them, exploiting a wide range of sensing methods. At the moment, it is essential to differentiate between the different fall-related systems. To this day, literature reviews lack a standard ground classification since each analysed study presented a different classification based on the understanding of the problem of falling and the expected contribution. Thus, a comprehensive review was accomplished.

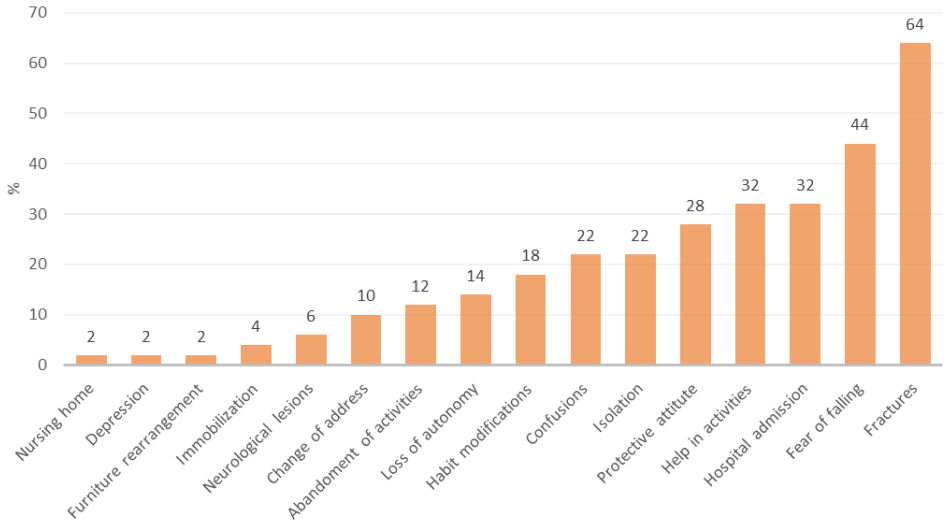

Figure 2.4: Consequences presented by older adults after falls (Adapted from [46]).

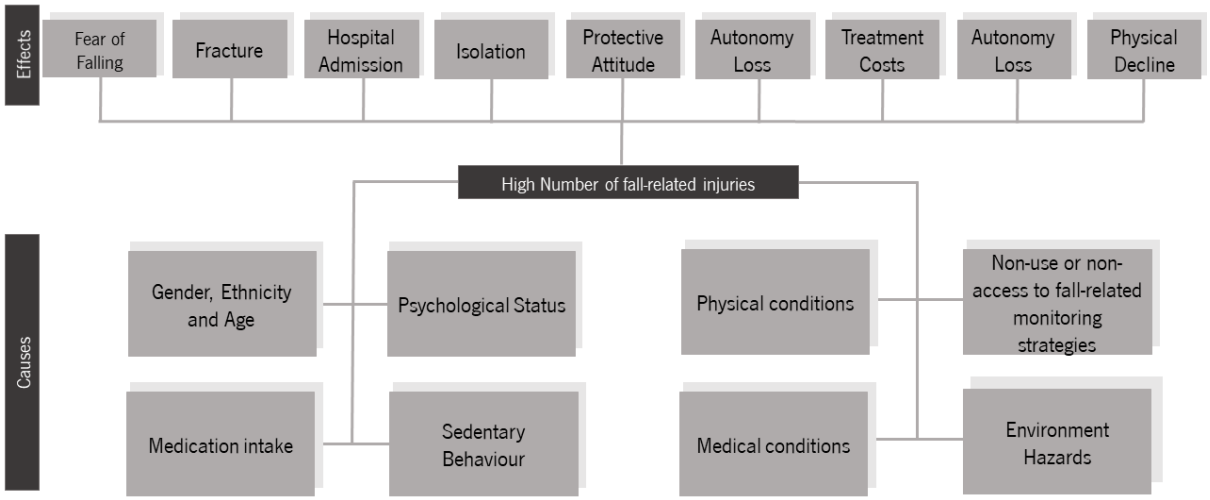

Figure 2.5: Tree Problem Diagram.

2.6.1 Fall Detection Systems

Usually, FD systems rely on impact detection [5], [10], [14]. According to the literature, these systems can be differently classified, and there are many efforts to structure them. Hsieh et al. [10], categorise FD systems according to its type of detection, which includes user-manual and automatic systems. User-manual systems are intended to send emergency messages through user manipulation. Nevertheless, in case of loss of consciousness, they are useless, not providing the medical care necessary. Contrarily, automatic FD systems are planned to detect falls without any user manipulation. These devices alert the user and healthcare provider after a fall to accelerate and improve the medical care provided to the user [10], [47].

FD systems can also be divided depending on what type of sensor the system employs. A survey achieved by Delahoz et al. [5] presented the primary three-class division of current FD systems: camera-based sensing, ambient sensors and wearable sensors.

Systems can make use of cameras to detect falls due to their typically short time of occurrence. Consequently, the patients' posture and shape vary significantly, which is the key factor in this type of system. For example, Stone et al. [48] presented a two-stages FD algorithm and validated the system with an available dataset comprising 454 falls. The first stage of the detection system characterises a person's vertical state in-depth image frames and then segments on-ground events from the vertical state time series. The second stage employs an ensemble of decision trees to compute a percentage of confidence that a fall preceded an on-ground event. It is required a high computational power to detect a fall in real-time since on average, a picture is composed of at least 345,600 individual pixels that need to be analysed. One of the significant concerns with camera-based systems is user privacy. As a result,

instead of recording the patients' movements, the systems record their surrounding with body-mounted cameras.

Ambient device-based FD systems normally surveil the subject of interest surroundings to track his movements and behaviour. This type of systems is normally installed when the subject refuses to wear any device on his body. Typically, pressure, infrared, vibration, acoustic and motion PIR sensors are mounted in the SOI vicinity [49].

As previously stated, abrupt fluctuations in body motion parameters such as orientation or acceleration may be due to a fall. To measure such parameters, sensors must be placed onto the body of the subject. Wearable systems generally employ inertial sensors such as accelerometers, inclinometers, gyroscopes, barometers, goniometers and magnetometers to identify not only sudden changes in human gait but also to assess the subjects balance and monitor displacement [50]. They are typically low-cost and small, which makes them an attractive solution. They also can be easily placed in the human body or can be attached to daily life accessories. Numerous studies on sensor placement have been done. Kangas et al. [51] studied low-complexity FD algorithms for wearable accelerometers with different body placement. It was concluded that while the waist and head were valid positions, the wrist was not. Bourke et al. [52] positioned sensors on the trunk and thighs and described the trunk as a better position. Fang et al. [53] stated that more reliable performance is achieved when the sensor is installed near the center of mass. The results revealed that the chest was the optimal location. The subject's waist was recommended rather than the chest since it was a more comfortable position. Figure 2.6 summarises the sensor positions used in existing FD systems.

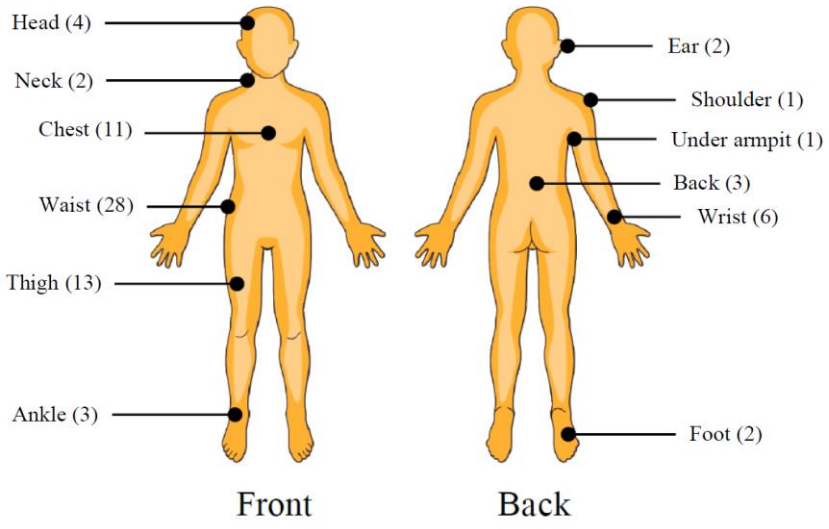

Figure 2.6: Different positions and number of studies for sensor placement in wearable FD systems (adapted from [54]).

Pierry et al. in [55] contemplated a survey and evaluation of real-time accelerometry based FD systems. Their classification was established on methods that evaluate acceleration, that merge acceleration with additional sensor data and methods that do not assess acceleration at all. Most systems use accelerometers along threshold-based algorithms to detect fall-related events due to an abrupt polarity inversion of the acceleration of the subject when hitting the ground.

Ambient and Vision-based systems being limited to only some aspects of ADL or certain locations, while wearable-based FD systems allow the monitorization of individuals under real-life conditions in their natural environment, including both indoor and outdoor ADL. Even though wearable sensors are more attractive, they can be uncomfortable for the person depending on their size and location on the [10], [14]. Table 2.3 contains the results of the conducted search regarding FD systems, which includes the type of sensors employed, their corresponding specifications and location, the computed features, and if it is wearable or not.

Table 2.3: Features used in FD systems, as well as the sensors, their corresponding location, specification, and wearability of the developed system.

Type of sensor	**Sensor Specification**	**Features used**	**Wearable**	**Placement of sensor**	**Work**
Doppler range control radar	-	Melfrequency Cepstral Coefficient;	-	Floor	[56]
Magnetometer	Android Smartphone	Sum Vector Magnitude (SVM); Magnitude of angular displacement;	+	Hip	[57]
Accelerometer	Triaxial Fs: 400Hz	SVM; Dynamic Sum Vector; Differences between the maximum and minimum acceleration (SVmaxmin); Vertical Acceleration (Z2);	+	Wrist, Waist and Forehead	[58]
	Triaxial Fs: 50Hz		+	Waist level	[16]
	Triaxial Fs: 100Hz	Rotation angle of accelerometer coordinate in 3D space;	+	Waist	[59]
	Triaxial	Activity Signal Magnitude Area; SVM;	+	Neck, waist, foot and hand	[60]

Type of sensor	Sensor Specification	Features used	Wearable	Placement of sensor	Work
	Triaxial Fs: 40Hz	SVM; Signal Magnitude Area; Postural Orientation; Tilt Angle;	+	Waist	[61]
	Triaxial Fs: 100Hz Range: ±11g	SVM;	+	Thoracic vertebrae	[19]
	Triaxial	SVM; Delta Changes; Average Resultant Acceleration; Resultant of Standard Deviation; Z-Score;	+	Trouser pocket	[62]
	Smartphone Fs: 33Hz	Transversal acceleration	+	Trouser pocket	[63]
	Smartphone	SVM; Absolute Vertical acceleration;	+	Chest, thigh and waist.	[11]
	-	SVM; Rotation angle; Slope; The SVM of acceleration in the horizontal plane;	+	Waist	[64]
	Smartphone	SVM; Magnitude of angular displacement; Roll, Pitch and Yaw; Quaternion	+	Hip	[57]
		SVM; Maximum SVM; Minimum SVM; Average SVM;	+	Chest and waist	[65]

Type of sensor	Sensor Specification	Features used	Wearable	Placement of sensor	Work
		Root mean square SVM Acceleration exponential moving average; Signal magnitude area;			
	Triaxial Range: ±2 g), Fs = 200	SVM; Fast changed vector; Vertical acceleration; Posture angle;	+	Waist	[66]
		Skewness; Skewness (X, Y and Z Smooth Median Filter axis); Skewness of SVM; Skewness of SVM (Smooth Median Filter axis); Kurtosis; Kurtosis (X, Y and Z Smooth Median Filter axis); Kurtosis of SVM; Kurtosis of SVM (Smooth Median Filter axis); Mean; Mean of SVM; Variance; Variance of SVM;	+	Waist	[67]
Atmospheric air pressure sensor	Fs: 1.8Hz	Differential pressure	+	Waist	[67]
FSR	-	8 orthogonal principal components;	+	Under booth feet	[68]

Type of sensor	Sensor Specification	Features used	Wearable	Placement of sensor	Work
Microsoft Kinect	-	Vertical state of a segmented 3-D object; Minimum Vertical Velocity; Maximum Vertical Acceleration; Vertical Velocity;	-	Placed Around the room	[48]
	-	Velocity; Acceleration; Width/Height ratio;	-	Placed Around the room	[69]
Gyroscope	Triaxial Fs: 1000hz	SVM; Total Angular Change; Resultant Angular Acceleration;	+	Thoracic vertebrae	[19]
	Triaxial Fs: 50Hz	Resultant angle change; Maximum resultant angular acceleration; Fluctuation frequency;	+	Waist	[70]

Existing systems primarily focus on detecting a fall rather than predicting it. Therefore, FP and prevention systems are of the **highest importance to achieve** since there is an imperative need for the development of strategies that can minimise not only the cost associated with the consequences of the fall but also improve the quality of life for persons who suffer from them [28], [47].

2.6.2 Fall Prediction Systems

Although FD and FP systems share some common ground such as commissioning sensors to complete their task and the use of collected data through computer algorithms including artificial intelligence, there are critical differences between these two systems [5].

FP systems aim at notifying the subjects before the occurrence of a fall, thus avoiding the consequences of it. These systems ought to identify most of the scenarios and events leading to a fall and deliver a framework based on data acquired from different scenarios, sensors and subjects from the target population for increased reliability and safety [47].

It is essential to distinguish two different systems linked to FP. **Fall Risk Assessment Tools** (FRAT) **identifies persons of high fall risk** upon specific and protocoled interventions. Three types of assessment are relevant regarding falls and the decrease of mobility in the geriatric population [71], [72]:

i) Comprehensive medical assessments - accomplished by geriatricians or nurse practitioners in order to evaluate and rehabilitate patients with fall risk involving evaluation of the patients fall history, strength, cognition, balance, gait, chronic diseases, mobility, nutrition, and prescriptions;

ii) Nursing fall risk assessments - which has been performed mainly in health institutions commissioning popular measures, tools or scales used to assess the risk of fall. Some examples are the Morse Fall Scale, St Thomas Risk Assessment Tool in Falling Elderly Inpatients (STRATIFY), Resident Assessment Instrument (RAI), Fall Risk Assessment Tool, Hendrich Fall Risk Model, High Risk for Falls Assessment Form, or Royal Melbourne Hospital Risk Assessment Tool. Patients are classified into risk categories, which enables clinicians to associate risk assessment with specific interventions. Therefore, the need for health facilities to develop their scales is null, which could affect the type of treatment and care of fall patients since scores and scales would not be comparable across similar types of facilities;

iii) Functional mobility assessments - accomplished by physical therapists or physicians, such as Timed-Up and Go test (TUG), Berg Balance scale (BBS), Physiological Profile Assessment (PPA) and Tinetti Performance Oriented Mobility Assessment (POMA).

Differently, **pre-impact FD systems** also aim at detecting a fall before it happens in real-time, although with a **shorter lead time**. For example, Tamura et al. [73], developed a wearable airbag which incorporates a pre-impact FD system based on accelerometer and gyroscope's signals to trigger their inflation. In this study, it is assumed that the subject is in free fall, and before the impact, the airbag is triggered, and the patient's head, neck, hip, and thigh are protected.

According to [74], alterations in ADL are early signs of cognitive and physical decay, which is related to gait deficiencies and an imminent fall. Therefore, these systems can identify irregularities, trace all variations in gait parameters and, finally, identify dangerous and emergencies. The development of these type of systems nowadays faces numerous challenges such as their performance in real-like conditions since high outcomes are achieved in experimental/controlled environments and hardly any studies collect data of elderly generations. User engagement is also a subject that requires attention as recent surveys have shown that wearable systems have less appeal due to the lack of interaction and familiarity with the recent technological advances since habitually, these types of systems combine data

from multiple sensors and transmit them wirelessly to a central computational device. Integrity and privacy concerns are raising in FP systems due to the large vision-based systems transmitting real-time images that share user sensitive information to networks who can suffer from hacking [47]. Table 2.4 contains the results of the conducted search regarding FP systems. It includes the type of sensors employed, heir corresponding specifications and location, the computed features, and if it is wearable or not.

Table 2.4: Features used in FP systems, as well as the sensors, their corresponding location, specification, and wearability of the developed system.

Type of sensor	**Sensor Specification**	**Features**	**Wearable**	**Placement of sensor**	**Work**
Force Plate	Fs: 100Hz	Velocity of centre-of-pressure	-	Subject stand on it	[75]
	Fs:20Hz	Ground reaction forces; Center of Pressure	-	Subject stand on it	[76]
IMU	Fs: 50Hz Res: 0.05° Range: ±5g ±1,200°/s	Maximum finite-time Lyapunov exponent (maxLE)	+	Lower back	[75]
Accelerometer	Biaxial; Range: ±1.7 g, Res: 1mV/mg Fs: 125Hz	maxLE; Step length; Step duration; Heel contact velocity,	+	Hip	[77]
	Tri-axial Fs: 200Hz	Acceleration Fast Fourier Transform	+	Waist	[78]
	Tri-axial Fs: 40Hz	TUG Time Duration; RMS of HP Filtered SVM; Signal Magnitude Area;	+	Waist	[79]
	Tri-axial	Cadence	+	Lower back	[23]

Type of sensor	Sensor Specification	Features	Wearable	Placement of sensor	Work
Camera	Kinect Fs: 30Hz	Position; Speed; Acceleration; CoM;	-	SOI Vicinity	[80]
	Fs: 120Hz	maxLE	-	Booth Heels	[77]

A broader search about which features are analysed in studies regarding gait was accomplished, and the results containing which features were computed, what sensor was used to acquire the data and the type of study conducted are described in Table 2.5.

Table 2.5: Potentially relevant metrics for FP, and the sensors used to obtain them.

Feature	Study Type	Sensor	Reference
Cumulative Horizontal Acceleration; Velocity (X, Y and Z axis); Displacement (X, Y and Z axis); Cumulative horizontal displacement; Cumulative horizontal sway length (X, Y and Z axis); Mean sway velocity (X, Y and Z axis); Displacement range (X, Y and Z axis);	Displacement of centre of mass during quiet standing	Accelerometer	[81]
Acceleration (X, Y and Z axis);	Movement Classification	Accelerometer	[82]
Energy (X, Y and Z axis); Energy of SVM;	Detection of Everyday Activities	Accelerometer	[83]
Mean (X, Y and Z axis); Mean of SVM; Correlation (XY, YZ and XZ);	Optimal Features to Classify Falls	Accelerometer and Gyroscope	[84]

Feature	Study Type	Sensor	Reference
Maximum and minimum of SVM (raw signal and LP filtered); % window where LP SVM is less than 0.9;			
Approximate entropy; Frequency Analysis; Wavelet Decomposition	Quantifying movement patterns	Accelerometer and Gyroscope	[85]
	Classification of Walking Patterns	Accelerometer	[86]
Root Mean Square (X, Y and Z axis); Root Mean Square of SVM; Peak-to-peak values (X, Y and Z axis); Peak-to-peak values of SVM; Minimum values (X, Y and Z axis); Harmonic Ratio Ratio Index (X, Y and Z axis); Ratio Index of SVM; Ratio Index of Peak-to-peak values	Stability and harmony of gait	Accelerometer and Gyroscope	[87]

Chaccour et al. [49], proposed a **global standard reference scheme for all FD and FP systems**. The proposed method is a **three-category based classification**. Firstly, fall-related systems are separated into two groups: FD and FP systems. FD systems use the fall impact to trigger an alarm, whereas the FP Systems compute features of gait and balance. Due to a large number of studies and to the shortage of a global classification, fall-related systems can be arranged concerning their technology. The three main categories are Wearable based Systems, Non-wearable based Systems (NWS) and Fusion or hybrid-based Systems (FS). The proposed classification criterion is depicted in Figure 2.7.

2.6.3 Fall Prevention Strategies

Recognising active interventions to prevent falls and fall-related injuries amongst older adults is a field of research in geriatrics. Numerous published clinical guidelines evaluate the evidence for fall prevention strategies and present directions for evaluation and intervention [88]. Fundamental to the success of the before-mentioned interventions is not only to shape the minds, stands and roles of older

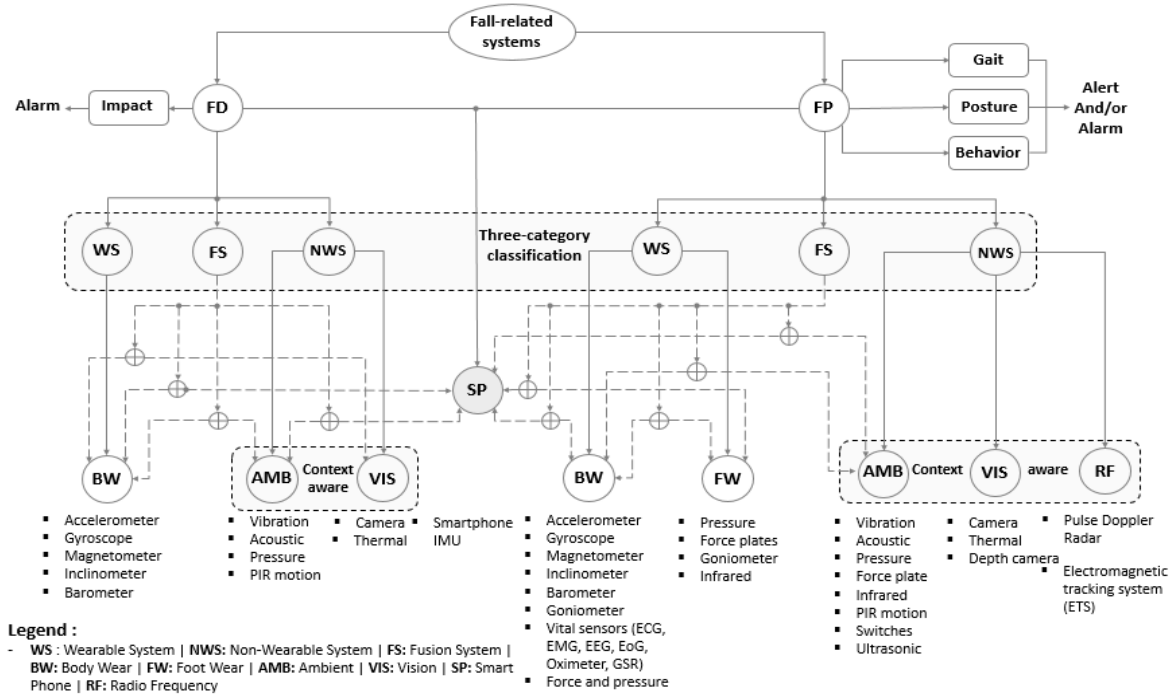

Figure 2.7: A three-category based global classification scheme of fall-related systems according to [52].

people themselves, but also the health and social care specialists who assist, and the broader communities in which the senior live. Someone will change his lifestyle if it is within their capacity to achieve so, if he possesses the means to execute change, if the changes are recognised as being of good to him and if the resultant advantages exceed the value in overcoming the hurdles [89].

Commonly, fall prevention interventions can be classified within particular general categories [28], [88], [89]. **Exercise** has become a commonly considered **intervention in fall prevention**. It is proved that exercises can **decrease fall risk** factors such as poor balance, muscle weakness, gait impairment [88], and reaction time [89]. Endorsing fitting physical activities or exercises to enhance strength, balance, and flexibility is one of the most suitable and cost-effective approaches to prevent falls amongst the geriatric community [89]

Diet and lifestyle influence morbidity and mortality, therefore, aged people must adopt a diet and a lifestyle that can minimise the risk of morbidity. A healthy well-balanced diet is fundamental to healthy ageing. A proper intake of protein, calcium, essential vitamins and water are necessary for a healthy life. If deficiencies do exist, it is prudent to expect that weakness, weak fall recovery and increase risk of injuries will ensure. A diet composed with a proper intake of calcium and vitamin D is found to improve bone mass amongst the elderly with low bone density and their musculoskeletal function. It also reduces the risk of osteoporosis and falling [89][88].

Environmental evaluation and adjustment are another promising fall prevention strategy. Usually is practised as a method of recognising and excluding possible risks, such as clutter, poor lighting and throw rugs. The environment is then revised to increase mobility and security, for example, with the installation of grab bars, raising toilet seats and even lowering bed height. Nowadays, many self-administered home safety checklists are created to evaluate older people homes, and to support in identifying hazards and propose recommendations for promoting a safer environment. For patients with a higher fall risk, usually, this assessment is accomplished by trained professionals, such as nurses or occupational therapists. This in-home evaluation allows the health professionals to access how the patient functions within the home, which help to name security problems that may not be identified with a self-administered checklist [90]. Any risk-taking behaviours also improve the risk of falling in older age, such as climbing ladders, standing on unsteady chairs, hurrying with limited attention to the conditions or not using mobility devices prescribed such as a cane or a walker [88].

2.7 Machine Learning Algorithms in Fall Detection

Machine learning is a field of computer science regarding programs and algorithms that learn from experience. Just as the type of sensors used in fall-related system change aside from the technological progress, FD algorithms also change. Xu et al. [7], reviewed the FD algorithms on the most cited works **before** and after **2014** until the end of 2017 and found that since formerly the **most used sensors were accelerometers** which detect accelerations in specific parts of the body, threshold-based algorithms were the most used. With the technological progress and the increasing usage of vision-based sensing with FD algorithms, **the application of machine learning techniques has been significantly increasing**, as seen in Figure 2.8, since the sensors nowadays can perceive more details in human activities [7]. For example, Aguiar et al. [91], using information from a built-in smartphone accelerometer, retrieved features and threshold information to detect a fall through DT. Moreover, Pierleoni et al. [92], with data acquired from an accelerometer, gyroscope, and magnetometer, used Support Vector Machines to choose acceleration thresholds to develop a FD algorithm.

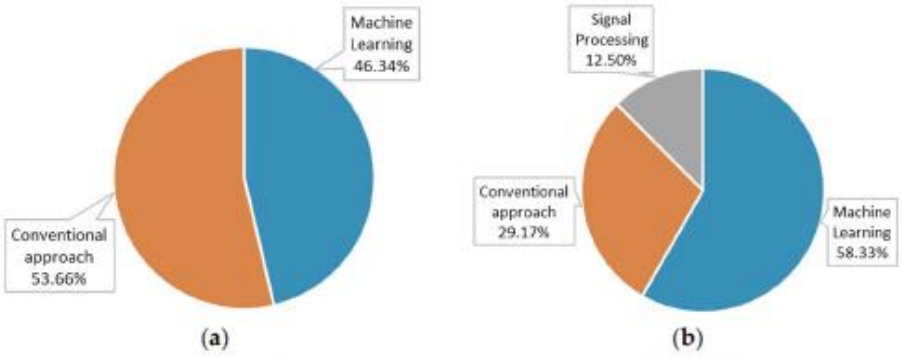

Figure 2.8: Tendency of algorithms used in FD system: (a) main categories of algorithm used before 2014; (b) main categories of the algorithm used before. Taken from [7].

2.7.1 Model Evaluation

In the evaluation of classification models, if their application leads to a misclassification, the performance of the chosen classifier decreases, increasing the error rate. Hence, classifier evaluation is essential in the learning progress allowing to access the performance of different algorithms which cannot be compared any other way. Alternatively, to access the classifier performance, Cross-Validation (CV) can also be accomplished.

CV assesses how the results of a statistical analysis will generalise to an independent data set. It is mostly used in machine learning, and one wants to estimate how accurately a predictive model will perform in practice. Normally it is given a dataset of known data to the classifier on which training is run and a dataset of unknown data on which the model is tested. Thus, the model will be tested only with unseen data to signal problems such as overfitting, selection bias and to understand how the model generalises to a different dataset which indicates who the system will perform when applied to real-world problems. CV involves partitioning a sample of data into complementary subsets, training the model with one subset and testing it with another. To reduce variability, multiple rounds of CV are performed using different partitions, and the validation results are averaged over the rounds to give an estimate of the model's predictive performance. This technique is the method of choice in fall-related systems [5]. Usually, the results are stored in a confusion matrix, as seen in Figure 2.9, which allows visualising the performance of the classifier.

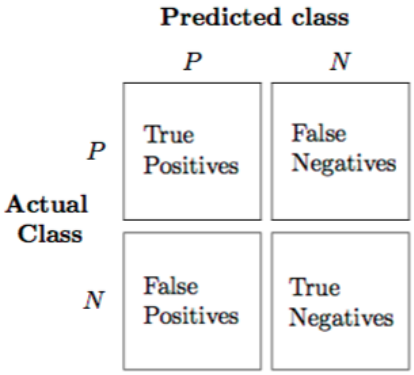

Figure 2.9: Confusion Matrix Example

Numerous designations are frequently used along with the description of sensitivity, specificity and accuracy. They are True Positive (TP), True Negative (TN), False Negative (FN), and False Positive (PF). Sensitivity (SENS), Specificity (SPEC) and Accuracy (ACC) are defined in terms of TP, TN, FN and PF. ACC is an evaluation measure that indicates the percentage of correct results that the classifier obtained, equation 2.1. The major disadvantages of ACC are the neglect of the differences between the types of errors and their dependence on the class distribution of the data, since it is usually important, in practical examples, the differentiation between the different types of errors.[3].

$$\text{Accuracy} = \frac{\text{TP}+\text{TN}}{\text{TP}+\text{TN}+\text{PF}+\text{FN}} \tag{2.1}$$

Although this metric is one of the first to analyses when evaluating the classifier, when the number of tests is not balanced, that is, the number of tests of each class is different this metric cannot clearly describe the effectiveness of the classifier. For this reason, it is necessary to calculate other metrics that capture the more specific aspects of the evaluation. PREC, is the metric that indicates the percentage of correct positive results of all positive results obtained by the classifier, given by equation 2.2.

$$\text{Precision} = \frac{\text{TP}}{\text{TP} + \text{PF}} \tag{2.2}$$

SENS, presented in equation 2.3, measures the proportion of current positives that are correctly identified.

$$\text{Sensitivity} = \frac{\text{TP}}{\text{TP} + \text{FN}} \tag{2.3}$$

SPEC displays the proportion of negatives that are correctly identified, and this metric is presented in equation 2.4.

$$\text{Specificity} = \frac{\text{TN}}{\text{N} + \text{PF}} \tag{2.4}$$

The Matthews Correlation Coefficient (MCC), is a metric used in Machine Learning for the evaluation of the quality of binary classifications, i.e., there are only two classes, consequently if there is a higher number of classes, the classification is done by joining several classes with respect to another, this process being iterative until there are no other possible combinations, this metric is presented in equation 2.5.

$$\mathrm{MCC} = \frac{\mathrm{TP} * \mathrm{TN} - \mathrm{PF} * \mathrm{FN}}{\sqrt{(\mathrm{TP} + \mathrm{PF})(\mathrm{TP} + \mathrm{FN})(\mathrm{TN} + \mathrm{PF})(\mathrm{TN} + \mathrm{FN})}} \tag{2.5}$$

The F1 Score (F1S) combines PREC and SENS. By equation 2.6, we can observe that the TN number is not considered in the calculation formula, so we can have the same value of this metric if we have a high or low TN value in the classification results.

$$\mathrm{f1\_score} = \frac{2 * (\mathrm{SENS} + \mathrm{PREC})}{\mathrm{SENS} + \mathrm{PREC}} \tag{2.6}$$

Cohen's Kappa (KAPPA) is a very valuable performance metric when faced with a multi-class classification problem. In those cases, measures such as ACC, or PREC may not provide the full understanding regarding the performance of the classifiers. For the computation of KAPPA is necessary the relative observed agreement among raters (Po) and the hypothetical probability of chance agreement (Pe), as seen in equation 2.7.

$$\mathrm{Kappa} = 1 - \frac{\mathrm{Po} - \mathrm{Pe}}{1 - \mathrm{Pe}} \tag{2.7}$$

2.8 Discussion

A contextualization about falls, including its different stages, costs, classification criteria, risk factors and consequences, was presented. Then, all fall-related strategies common in literature were discriminated, including the recent trends, associated limitations, difficulties, and future research areas for designing fall-related system with prediction capabilities.

FP is a complex multifactorial problem which includes the interaction between several risk factors already disclosed. Current **FD and FP systems are primarily tested in controlled conditions** and do not take into account the interactions within the various fall risk factors. Furthermore, these systems need to be capable to contextualise the problem of falling in real-life scenarios where the accuracy of the systems is assessed. Also, **future systems will require the merge for indoor and outdoor fall assessment** with the smallest obtrusiveness to the subjects. The principal difficulties in producing

adequate FP systems involve assessing its reliability amongst frequent fallers and the geriatric community, safety and privacy in data transmission and power optimisation.

Since the time interval between the detection of an imminent fall and its impact is relatively small, the **devices being developed must increase this lead time**. Consequently, the establishment of a framework that considers the perceptual information in order to monitor movement execution in real-time and use it to prevent unwanted situations such as falls is imperative**. The system must distinguish normal gait from fall and PFS situations, using proper gait's parameters using a sensorial system during ADLs.**

3. CANES AS A FALL-RELATED SYSTEM

3.1 Introduction

The scientific community has been proposing several different solutions concerning fall-related technology, the most common one **attaching a sensor to the subject's body**. Even though the system can detect the fall, **the system will weight on the individual** [51], [52]. In contrast, **image-based methods** employ specific algorithms to liberate the subject of any wearable system. The entire system is **constrained due to environmental reasons** and must be installed in a suitable place [48]. Most of the developed projects focus on FD and employ methods supported by vision, wearable and environmental approaches discussed in Chapter 2, subsection 2.6, "Fall-Related Tools And Existing Strategies".

Initially, all developed systems trusted on the individual to trigger an alarm by pressing a button when a fall happened. In the case of inaccessibility of the alarm system, loss of consciousness or even if the subject is in a coma or disabled, all system is insignificant. Nowadays, most research focuses on developing methods in which a fall is automatically detected, and an alarm is triggered. The majority uses acceleration sensors, or image processing algorithms along with vision-based sensors. Regardless, many sensors need to be installed so the system can work effectively, nonetheless, installing sensors on the body of the elderly can reduce the flexibility of their movement, and the indoor sensors cannot detect the accidents that happen outside the surveyed areas [49][10].

Thus, the **use of accessories** where elderly may take with or wear on, e.g. necklaces, bracelets, watches or canes, **can be a serious alternative**. Since a real-time monitoring system needs a considerably sized battery to operate for a reasonable period, the use of smaller devices will result in a low power supply for a short amount of time. Consequently, the systems need to be charged several

times a day, which is not optimal. The constant hand movement is also a factor to discard its use, which is too high to monitor for long periods. So, if we would like to insert sensors on these objects for FD and FP, then **canes can be a great choice** due to its size, but also since they are commonly used by the geriatric community [93].

3.2 Canes

Assistive devices such as canes are defined as mechanical implements specifically intended to assist individuals with disabilities to accomplish their needs, providing biomechanical support for their mobility [94]. Canes are often prescribed to patients with indications of gait/balance disorders and weakness in inferior members, which are one of the leading indicators of falls [95]. Typically, canes are prescribed to people with a reasonable level of impairment and when minimal stability is needed [96], [97]. They are operated by the individual dominant hand or the hand opposite of its weakness or injury since it can **shift up to 25% of the individual's weight** [97], [98]. By reducing weight supported on the individual legs, these devices can aid **ease pain related from injuries or clinical pathology's** such as hip fracture, or compensate for weakness or impaired motor control of the leg [96]. Canes **increase the person stability** by widening the base of support, reducing the weight load on the inferior extremities, and giving the user a sense of safety, which results in a lower fall risk [45]. The **use of mobility aid devices is expected to increase** since the elderly community is growing, and device ownership increased with age [45]. More than 4 million people in the USA alone use a cane.

Hui-Ching [99] conducted a research in order to study the use and the attitude of the geriatric community towards the use of assistive devices. The attained results revealed that most older people had **a neutral to a positive outlook towards the adoption of assistive devices** in their lives. Moreover, the will to preserve their independence and rely less on personal assistance was crucial to the use of assistive devices. Furthermore, there was no notable relationship linking the use of assistive devices and living situations. Even though social influences were noticeable in the use of assistive devices, they were insignificant. The existing negative attitude towards these devices pointed out to be through their first use, and after a period**, older people accepted and began to enjoy their assistive devices**. It was also concluded that the reasons for the abandonment of assistive devices were mainly design related, and due to the device bulkiness, reliability, performance and difficulty of use.

The association between the use of mobility aid devices and the increased risk of sustaining a fall are to this day not clear. The fall risk and limitation upon the use of canes develop from several factors

including the inappropriate use and abandon of canes, usage of the device in hazardous environment and disruption of balance as a result of attention between cane mobility and manipulation [94].

3.3 Canes in literature

3.3.1 Search strategy & Eligibility Criteria

A comprehensive search was accomplished in order to understand the following topics: i) what fall-related strategies are implemented with canes; ii) how canes are instrumentalized; iii) how and what algorithms are implemented; and iv) what researchers did to validate their system to be able to construct an innovative cane capable of detecting and avoiding falls.

On October 9th, 2018, the search was completed in the IEEE Xplore Digital Library, Scopus and Web of Science with the keywords (“Cane” OR "Walking Stick") AND ("Near Fall" OR "Fall Detection" OR "Fall Prediction" OR "Fall Prevention" OR "Falling") and in total 325 articles were found. To decide which ones were most relevant, articles were selected based on whether the system has implemented fall detection/prediction mechanisms with built-in technology into the cane, in total 9 articles were selected.

3.3.2 Search Results

All the found studies implemented FD systems and only some FP strategies. Di et al. [100]–[103] and Yan et al. [104] tried to avoid falls by using a cane robot with an omni-wheel base different from the other instrumented canes. Di et al. developed several systems with embedded fall-related methodologies. In 2011, designed an omni-wheeled cane robot with an FD and FP system. With a combination of two LRF and six force sensors, a fall was detected through the computation of the COG of the subject which was estimated due to the force applied in the cane and from the subject’s legs and body position. In order to prevent a fall, an impedance control system was implemented in which the robotic cane moved in order to equal the fall direction to the direction from the robot and the user. However, the experimental protocol did not include falls, and its results were not disclosed [103]. Later, in 2013, another prototype of an intelligent cane robot also comprising FD and FP was developed based on the Zero Moment Point (ZMP) Stability Theory. Associating the collection of different data from an accelerometer, gyroscope, magnetometer, LRF and pressure sensors, the ZMP is estimated. Since this feature equals the ground point where the total moment produced due to inertia and gravity is null, when the ZMP surpasses the support polygon, a fall is imminent. Moving the robotic cane in the direction of the eminent fall, ensuring the ZMP remains inside the boundaries. Thus, a fall is prevented. In this work, the experimental protocol and results are not revealed [101], [102]. For last, in 2016, the same research team realised a

comparison between the employment of two different algorithms for FD based on a real-time calculation of the individual's COP and its leg motion which obtained an accuracy of 75% and 91,2% respectively. Regarding the FP mechanism, a similar impedance control system to the one previously described was implemented. With the fall prevention results, it was concluded that the algorithm based on the relative acceleration of each leg is faster by 30%, detecting a fall in less than 210 mms [100].

Yan et al. [104] developed a cane-type walking-aid robot in which his system was based on the Human-Robot Coordination Stability which can describe the stability of the integrated human-robot system during the user operating the cane robot. Although the results from their experiments were not uncovered, they concluded that the system reached the expected effect for stability measure and provided a new way for FD and fall prevention. The previous articles described a cane robot with an omni-wheel base, and for the computation of the individuals, COP included wearable foot pressure sensors, which is not the intended.

Excluding robotic systems with a wheeled base, generally, contact and triaxial inertial sensors are the most common sensors embedded into canes. More specifically, accelerometers, gyroscopes, magnetometers and FSR with a Sampling Frequency (FS) between 15 and 100 Hz. Its location can be in one of three places, near the canes handle [95], [105], into the handle [95], [104], or in its base near the tip [12], [98].

Concerning the implemented algorithms, it is possible to say that the strategies can be considered as complete in terms of low-power consumption, considering that almost all developed system implemented threshold-based algorithms of the acceleration data for classification [12], [98], [105]. After the collection of enough acceleration data from different fall directions, thresholds are computed, and when its values exceed a single value or several thresholds in a specific sequence over a time period, a fall is detected. This method is prone to give PF outcomes to many exceptional scenarios. As a result, algorithms used in fall-related systems tend to increase the number of devices with embedded machine learning algorithms; nevertheless, its implementation in canes is yet to be completed. Therefore, Lan, M. et al. [95], employed an algorithm based on subsequent matching which instead of focusing on instantaneous values from suchlike acceleration threshold-based strategies, it emphasises the general signal shape.

From the acceleration data acquired, features can be extracted from the signal in the time domain. The Sum Vector magnitude is the most commonly computed feature [95], [98], [105] because the fall direction and the posture of the subject are almost impossible to predict considering there is not

a pattern observed in a single acceleration axis. When the acceleration data from all the different axis are summed, a pattern describing the different stages of a fall is observed [105].

Regarding the experimental protocol and age/health status of the subjects, only half of the systems disclosed it. All the systems were tested with healthy subjects [95], [100], [105] excluding Lachtar, A. et al. [12], which is not ideal whereas the target population for fall-related systems is the elderly community. The fall direction can be divided into forward, backward and sideward [12], [95], yet, [105] only consider forward and backwards falls and [100], [104] only account for falls in the forward direction. The number of trials for each case is divided between 10 [105] and 30 [12], [95]. According to the experimental protocols, the success detection rate of the systems can achieve between 84% (forward and backwards falls) [105] and 100% (forward falls) [12], [95].

As a result, information about sensors used on canes and their location were combined. In Figure 3.1, four cane's locations, as well as three body locations (to assist the cane device) are pointed, and associated numbers correspond to sensors used by found studies. The matching between numbers, sensors and studies is found in Table 3.1.

All information regarding the systems mentioned above including their features, sensors, algorithms and/or strategies, sensors' attachment location, type of falls and ADL considered, subjects' information, experimental protocols, performance/results and other important information are disclosed in Table 3.2.

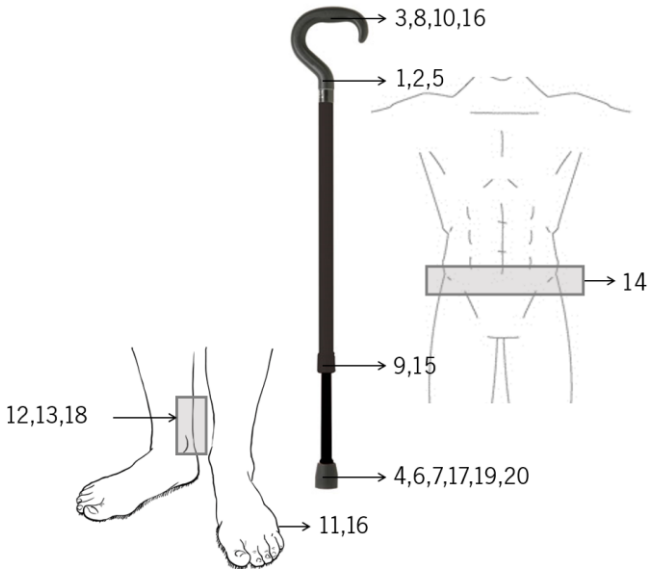

Figure 3.1: Four cane's locations, as well as three body locations where sensors are attached (numbers correspond to sensors – description available in Table 3.1).

Table 3.1: Matching between numbers from Figure 3.1, sensors and found studies

Study	Accelerometer	Gyroscope	Pressure Sensor	LFR	Force/Torque Sensor	Magnetometer
[95]	1	2	3,4			
[105]	5					
[98]		6				
[104]				7	8	
[100]				9	10,11	
[101][102]	12	13,14		15	16,17	18
[12]	19					20

Table 3.2: Features, sensors, algorithms and/or strategies, sensors' attachment location, type of falls and ADL's considered, subjects' information, experimental protocols, performance/results used in different fall-related strategies related to canes.

Study, Type of work	Sensor type and specification	Sensor placement	Falls and ADL	Sample size (n), Age, health status	Experimental protocol	Features	Algorithm development	Accuracy
[95], FD	1 Acc (Triaxial, Fs: 26 Hz) 3 Gyr (Uniaxial, Fs: 26 Hz) 2 Pressure Sensors (Fs: 26 Hz)	Near the handle Perpendicular to each other near the handle Cane tip and handle	Fall: Forward, backward, side and free-fall ADL: Slow walk, Fast walk, sit & stand, stand still, swing, lay on the lap	n = 3 (healthy, 2 men, 1 woman, dissimilar body builds)	Each type of fall performed 30 times ADL's performed 30 times excepting standstill (30 second period)	SVM (x and y-axis)	Subsequence matching	100% forward; 97,8 % Backward; 98,9% Side; 100% Free-fall
[98], FD	1 Gyr (Biaxial, Fs:15Hz)	The base of the stick	NA	NA	NA	SVM (axis parallel to the ground)	Threshold	NA
[105], FD	1 Acc (Triaxial, Fs: 42 Hz, sens: ±8g, res:0.1g)	Top of the cane before the handle	Fall: forward, backward ADL: Walking normal, trot, stroll Cane: freely falling, thrown out	n = 3 (young)	Each mode (fall + cane) was performed 10 times. Walking: walk-in hard ground for 1 minute	SVM (x, y and z-axis)	FSM with several thresholds	84%
[12], FD	1 Acc (Triaxial, Fs: 100Hz) 1 Mag (Triaxial, Fs:100Hz)	Base of cane	Fall: forward, backward, sideways ADL: Slow walk, fast walk, swing, sit and stand, lay on the lap, free fall	n = 1 (elderly)	30 trials for each type of fall and ADL	Linear and gravitational acceleration	Multi-Threshold	100% forward; 96,7% backwards; 100% sideways

Study, Type of work	Sensor type and specification	Sensor placement	Falls and ADL	Sample size (n), Age, health status	Experimental protocol	Features	Algorithm development	Accuracy
[100]FD/FP	1 force/torque sensor	handle	Fall: forward Walk: normal/abnormal	n = 3 (male)	Each subject walked for 12 min forward, turn right/left, stumbled 12x	COP	Threshold	75%
	4 Flexiforce Load sensors	Insole of feet						
	1 laser rangefinder	Robot base				Relative acceleration of each leg	Fuzzy Control System	91,2 %
[101][102] FD/FP	1 force/torque sensor	Handle	NA	NA	NA	ZMP	Threshold	NA
	4 Flexiforce Load sensors	Insole of feet						
	1 laser rangefinder	Robot base						
	9 axis sensor (Accelerometer, Gyroscope, Magnetometer)	Back of heel						
[104], FD/FP	4 Force/Torque sensor	Under the handle	Fall: forward	NA	NA	Robot Stability Users Stability	Threshold	NA
	2 LRFs	Robots Body towards/ backwards the user						
[103], FD/FP	2 LRFs	Robots Base / Robots body at hip height	Walking: Stop, straight forward, straight in other directions, turn right, turn left	NA	Subjects lean to the right	COG; Distance between user and robot;	Multi-threshold	NA
	6 Force/torque sensor	Handle						

3.4 Commercial Canes

Even though FP systems are relatively new regarding canes, FD systems have been employed for a considerable amount of time as we can see from the bibliographical search above. After an extensive search for commercial canes with fall-related embedded systems, it was possible to find two products in which one is available for sale.

3.4.1 iStand SmartCane™

The iStand Smart Cane, Figure 3.2, is a device manufactured by WhatBox, Inc., that offers families a trackable cane with Global Positioning System (GPS) and a FD system. The device has Bluetooth capabilities which allow it to pair with the iStand cane mobile application, ending the communication gap and allowing real-time visibility for family, friends and caregivers. All notifications are sent through Facebook or text messages in the event of a lost Cane, low battery, or FD. Every cane has a flexible shaft for joint comfort and a no-trip base that stands alone [106].

Optional features, which are only available for a monthly fee, include a 911 panic button, daily activity collection such as the number of falls sustained and fingernail sticker with a QR Code that can be scanned by any smartphone to help a person with Alzheimer's to find the way home or call its caregiver if he/she gets lost. The device is currently available only in the US for $99 [106].

Figure 3.2: iStand Smart Cane. Taken from [106]

3.4.2 Dring Smartcane

The Dring Smartcane from French start-up Nov'in, Figure 3.3, appear for the first time in the Consumer Electronics Show in 2017 towards people with decreased mobility. The cane has a built-in GPS, Acc and Gyr to track the individual's movements, is also equipped with an alert system that connects directly with the GSM network suppressing the need of a smartphone to be paired with. In case of a fall, the cane can send back an alert to a selected caregiver which can respond with a confirmation that is sent to the device, letting its user know that someone has been warned. With the purpose of every device being able to adapt to a specific user, artificially intelligent algorithms were implemented to process the data which helps understand a user's habits and movements to infer low activity, tiredness and other changes in walking patterns that can be related to a deteriorating condition. The device also has long battery life. The company estimates several weeks between two consecutive charges. The release date of the device is yet to be disclosed [107].

Figure 3.3: Dring Smartcane. Taken from [107].

3.5 Patent Review

3.5.1 Search Strategy

On October 10th, 2018, an advanced patent search on international patents was performed on Espacenet /http://spacenet.com), which allows free access to over 100 million international inventions and technical developments. The search parameters for the smart search based on title and abstract were (“Cane” OR "Walking Stick") AND ("Fall" OR "Near Fall" OR "Fall Detection" OR "Fall Prediction"

OR "Fall Prevention" OR "Falling"). The selection of patents was based on available schemes, and appropriate titles and abstracts.

On October 11th, the previous procedure was also performed this time on the United States Patent and Trademark Office (http://patft.uspto.gov). The selected keywords the same as also the selection process.

3.5.2 Search Results

Regarding the search process accomplished, a total of 17 patents were selected in the end. On Espacenet, 404 patents were found, and only 50 were selected based on its title. In turn, 6756 patents were found on the United States Patent and trademark office, where 25 patents were selected similarly as Espacenet. Ultimately, from the 75 patents selected, 17 were included based on abstract, description and drawings.

Figure 3.4 illustrates a flow diagram of the entire study selection process. All articles were excluded because they focused in several different areas, such as sugarcane cleaning, separator, harvester, purifier and planter, bamboo canes, walking aids which do not fall, fall-related systems not related to canes, improvements in canes, walking aid holders, skin treatments and methods related to the biomass industry.

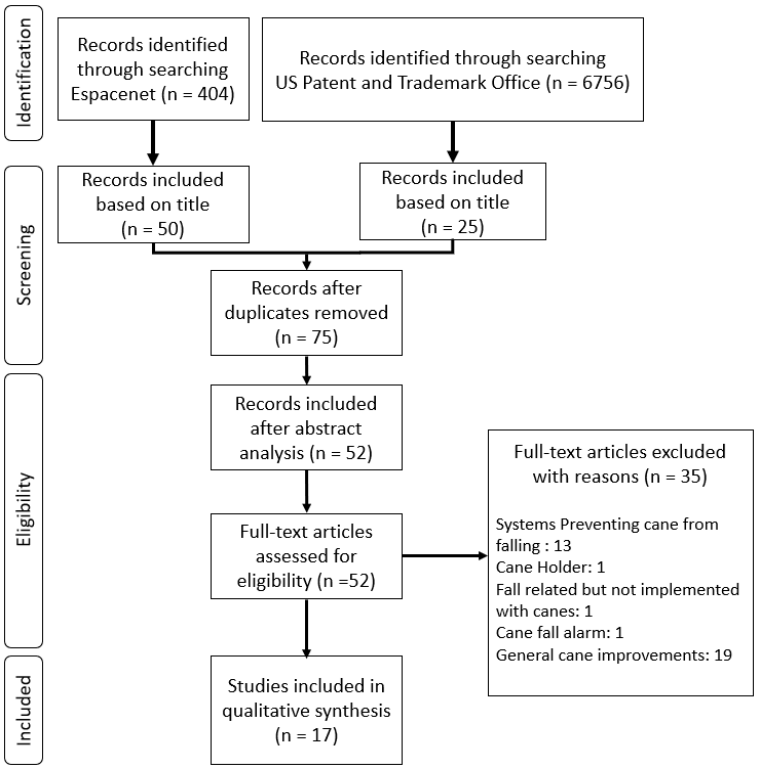

Figure 3.4: Flow Diagram PRISMA.

From the 17 chosen patents, it was selected the three that most closely relate to the concepts developed, Table 3.4. This can be related to concepts developed on two strands: whether it has fall detection/prediction mechanisms and whether or not it has only built-in technology into the cane.

Table 3.3: The three most similar patents with name, number and scheme to the FD and FP system developed

Name and Reference	Anti-falling walking stick for an old person [108]	Robotic cane devices [109]	Walking Support Device and Fall Prevention Method [110]
Patent Number	CN20141567378 20141023	US 20130041507 A1	JP20140103331 20140519
Scheme	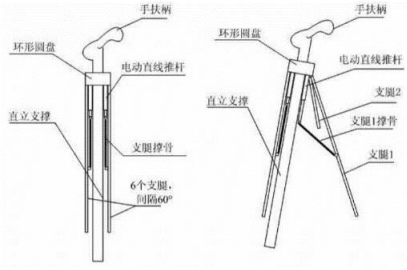	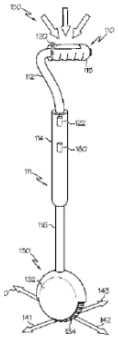	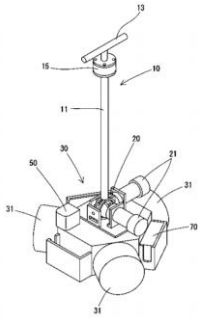

All the three chosen patents present FP mechanisms. The patent regarding the anti-falling walking stick comprises a walking stick shell, a supporting unit, a three-dimensional axial accelerated speed monitor and a central analysing unit in which the accelerated speed of the stick is supervised by a balance sensor, and the system can be unfolded automatically to keep it stable. When the subject walks unstably, is about to fall or even its already falling, a supportive leg can pop up automatically. Therefore, the user, can be successfully supported, and he/she is prevented from being wounded, or the injury degree is decreased by the new triangular support of the walking stick. Since a person can sustain falls in different directions, the central analysis unit analyses the received data, computes the characteristics of the changes and determines the direction of the fall. Thus, whether the leg needs to be ejected, and if necessary, selects the two branches closest to the fall direction to pop up [108].

The robotic cane device includes a grip handle equipped with force sensors, a cane body extending from the grip handle, a motorised omnidirectional wheel, a balance control sensor and a controller module. With the data acquired and computed, the omnidirectional wheel will attempt to retain the robotic cane in a substantially upright position. As regards to the FP mechanism, if the grip force value surpasses the grip force threshold such that the motorised omnidirectional wheel quickly provides a counterforce

that is contrary from a user weight projection, a fall can be avoided [109]. Finally, the walking support device and fall prevention also comprises an omni wheeled base with a fall prevention mechanism linked to the computation of the subjects ZMP much like Di, P. et al., 2013, [101], [102]. An LRF attached to the upper surface of the base of the system can detect the positions of both legs below the knees, measuring its distance to each leg. If case the ZMP of the pedestrian surpasses the plane connecting both its legs and the robotic system, it is determined that the user is in a pre-fall state. As a result, the system moves to the direction opposite to the fall direction, returning the individuals ZMP to inside the plane [110].

3.6 Discussion

After a thorough, careful and comprehensive search, it can be concluded that till this day, **it has not been developed a cane system that focuses on the temporal window that precedes a fall and prevents/minimises it by predicting a fall.**

Regarding commercial canes only one was available for sale concluding that the only systems comparable to the envisioned only embed FD mechanisms. As far as patents go, from the three selected, none can also be directly compared to the projected system. Only the robotic cane system with an omni-wheeled base comprises fall prevention algorithms.

Several steps have already been taken in this direction, and one of the conclusions reached is that **wearable systems**, despite their advantages, are still seen with some **rejection by patients regarding** their use. Furthermore, these devices are reliant on the subject, not only remembering to wear the device but also choosing to wear the device. Also, the installation of many sensors in the elderly can affect the flexibility of their movement.

The main challenge in this area is to develop highly accurate devices that are as unobtrusive as possible. As stated, the number of prescribed walking aids is increasing due to gait/balance disorders and lower limbs weakness. Since they are relatively low cost, the **cane is an ideal candidate for universal healthcare and implementation of fall-related mechanisms incorporating FD and FP methods**.

4. System Overview

Up to the moment, it has been concluded that it has not been developed a cane system that focuses on the temporal window that precedes a fall and prevents/minimises it by predicting a fall. Further, limitations of the currently developed systems were raised, so it is mandatory to accomplish the critical literature research and carry out all the essential requirements to be met. In this chapter is presented the proposed solution. Thus, it is presented the importance of each used components and their functions to explain all the systems that make up the global system developed: The Assistive Smart Cane (ASCane).

4.1 Basic Architecture of Fall-related Systems

Fall-related systems follow three main phases of operation: **sense, analysis and communication/operation**. The first phase is where suitable physical quantities are measured using appropriate sensors including, for instance, accelerometers, gyroscopes, temperature sensors and magnetic field sensors. According to Chapter 2, the **tri-axial accelerometer is the most employed sensor** in fall-related projects [111].

Subsequently, the data and signals acquired need to be analysed. To accomplish it, relevant features are computed, and decisions are made by classifying those extracted features. Most of the fall-related systems use threshold-based algorithms due to its low computational cost and reduced battery consumption. The application **of machine learning algorithms has increased dramatically** over the few past years due to the increased computational power of the latest microcontrollers [7]. Aziz et al. [111] compared the accuracy of FD algorithms, more specifically, threshold-based versus machine learning. The fall and non-fall trials data were acquired from controlled laboratory conditions and after evaluating five different machine learning techniques (Logistic Regression, Naïve Bayes, Nearest Neighbor, Decision Tree, Support Vector Machine) and five different threshold-based algorithms (Kangas2Phase, Kangas3Phase, BourkeUFT, BourkeLFT, Bourke4Phase). It was concluded that **machine learning algorithms provided higher overall SPEC and SENS.**

Whenever a fall-related system detects or predicts a fall, it communicates with the user, pre-selected caregivers and another system to prevent the imminent fall. In many systems, the device expects feedback from the user by verifying the preliminary decision and, consequently, improve the overall sensitivity of the system. Furthermore, rather than alerting the user for the pending fall, other systems can be activated (e.g. cane robot [100], [104]) to protect the user from harmful consequences of a fall,

as disclosed in section 2.7. The underlying architecture of the proposed strategy for the current device is depicted in Figure 4.1.

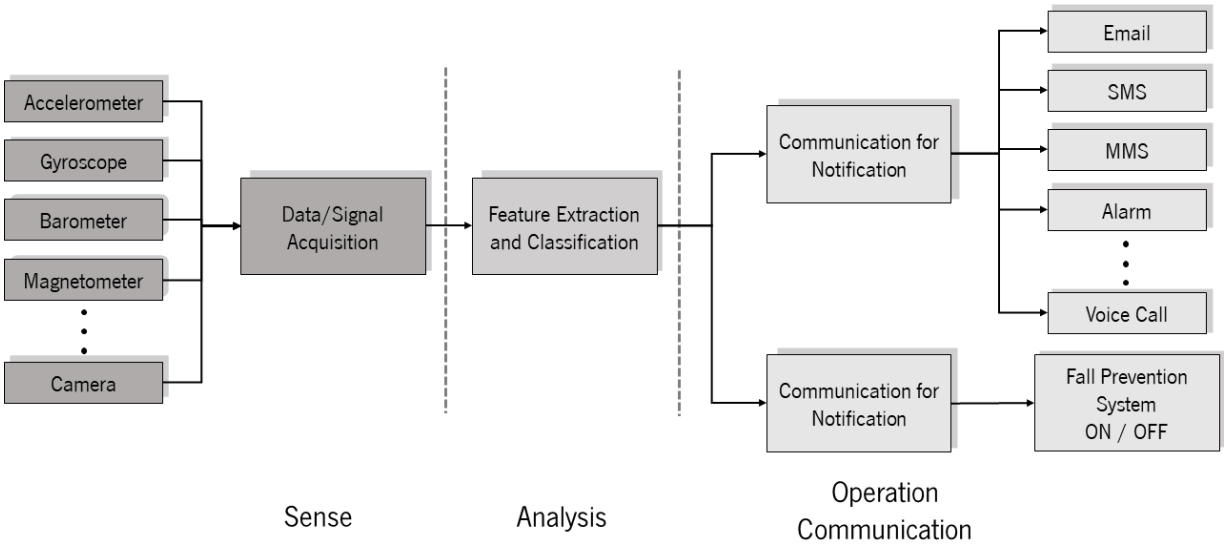

Figure 4.1: Common basic architecture of fall-related systems, adapted from [111].

4.2 Global Architecture

The strategy imposed in this chapter follows the standard architecture of fall-related systems unveiled in subsection 4.1. The implemented system is composed of six central systems: the Processing Unit, the Inertial Acquisition System, the Data Storage System, the Haptic Feedback System, the cane tip Force Acquisition System and the Lighting Acquisition System.

These primary systems and the respective components are displayed in Figure 4.2. The system was power supplied by a portable computer through the micro USB connector with +5V. The inertial measurements are collected through the IMU (MPU 9250), and the processing unit (STM32f303k8) receives this information to process the acquired data and save it to the micro SD card. Also, the force applied on the canes' tip is saved onto the SD card through the FSR. Depending on the readings from the ultrasonic sensor (MB 1010), the processing unit delivers signals to the haptic drivers (DRV 2605) to control the vibrotactile units and provide the vibrotactile feedback. The respective breadboard implementation with the different subsystems delimited is depicted in Figure 4.3.

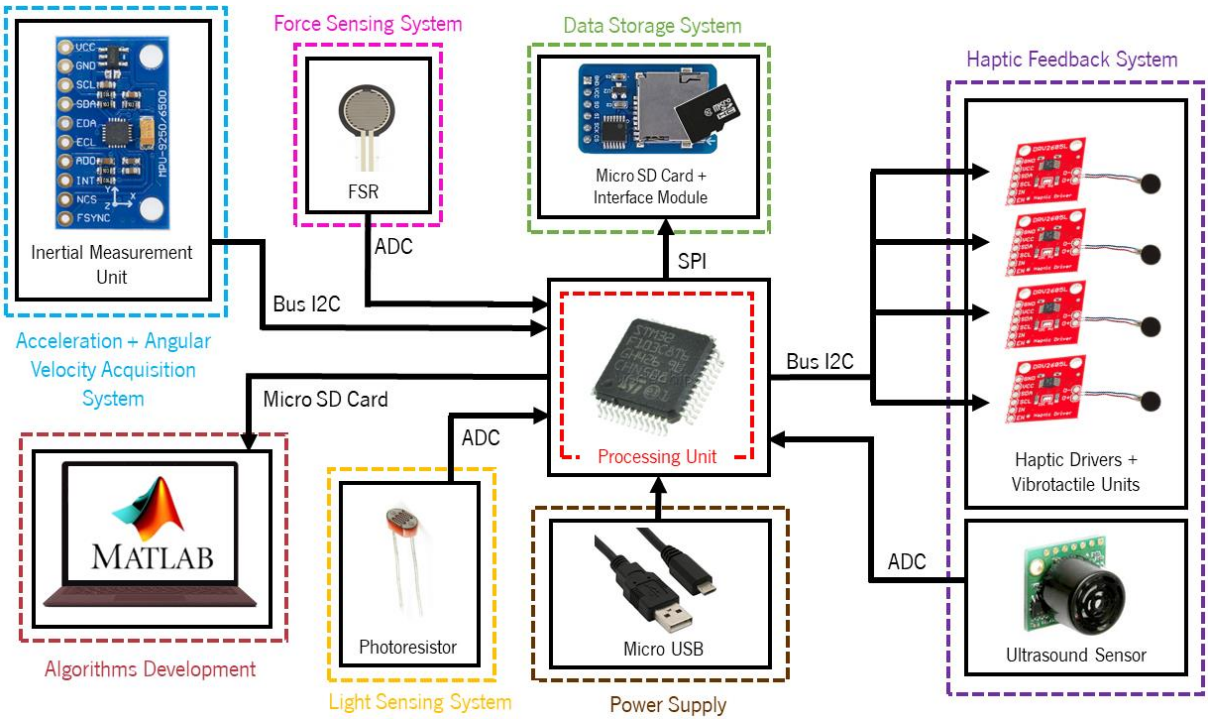

Figure 4.2: The systems architecture overview, illustrating the central systems with the respective components and interfaces between them: the processing unit (delimited at red); the Inertial Acquisition System (delimited at blue) constituted by an MPU 9250; the data storage system (delimited at green) composed by a micro SD card and the respective interface module; the Haptic feedback System (delimited at purple) with the haptic drivers, the vibrotactile units (ERM motors) and the ultrasonic sensor; the power supply (delimited at brown), the Light and Force Sensing System (delimited at yellow and pink, respectively), and the algorithms development tool (delimited at marron).

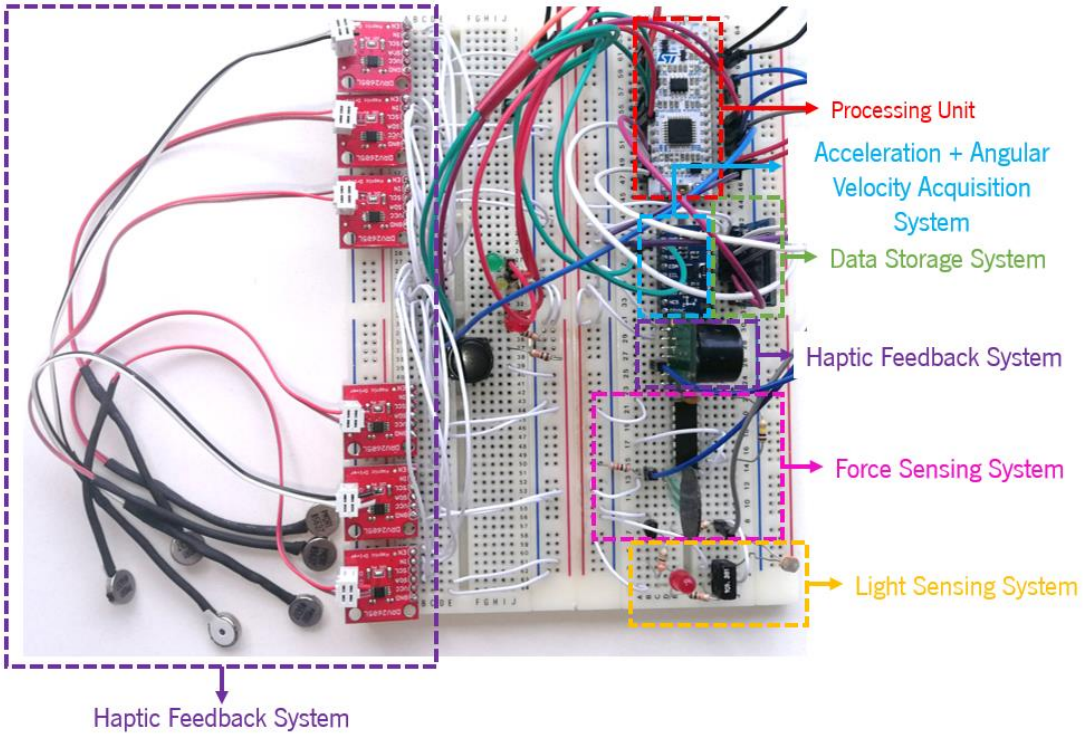

Figure 4.3: The ASCane System breadboard implementation.

4.3 Hardware Overview

4.3.1 Processing Unit

The processing unit is an STM32 Nucleo-32 Development board, with an STM32F303K8 MCU. This development board gives an affordable and flexible way for users to tackle new ideas and develop prototypes with the STM32 microcontroller, picking from numerous combinations of performance, power consumption and features. The microcontroller presents a maximum clock speed of 72 MHz, a wide range of PWM outputs and analogue inputs, supports I2C and SPI communication and up to two ADC 0.20 (up to 21 channels) with a selectable resolution of 12/10/8/6 bits. The STM32 Nucleo-32 board integrates the ST-LINK/V2 debugger, and it comes with the STM32 comprehensive software HAL library. The board can operate on an external supply of 3.3V, 5V or from 7 up to 12V [112]. The mainboard features are listed in Table 4.1.

Table 4.1: STM32f303k8 Characteristics [112]

Parameter	Value
Microcontroller	STM32F303K8
Architecture	ARM
Voltage Supply (USB)	5V
Voltage Supply (External)	3.3V; 5V; 7 – 12V
Memory flash	64 KB
Pins	32
Analog Pins	9
Clock Speed	48 MHz
SRAM	16 KB
ADC	2x12-bit with 9 channels
DAC	2x12-bit with 9 channels
Timers	11

The I2C pins provide communication with the IMU to process the acquired acceleration and angular velocity. It also provides an interface with the Haptic drivers to control the vibrotactile motors, in a PWM mode through the use of the PWM output pins. Also, the SPI pins enable the communication between the SD Card Module Interface and the Arduino board. The board pinout, including the pins legend, is depicted in Figure 4.4.

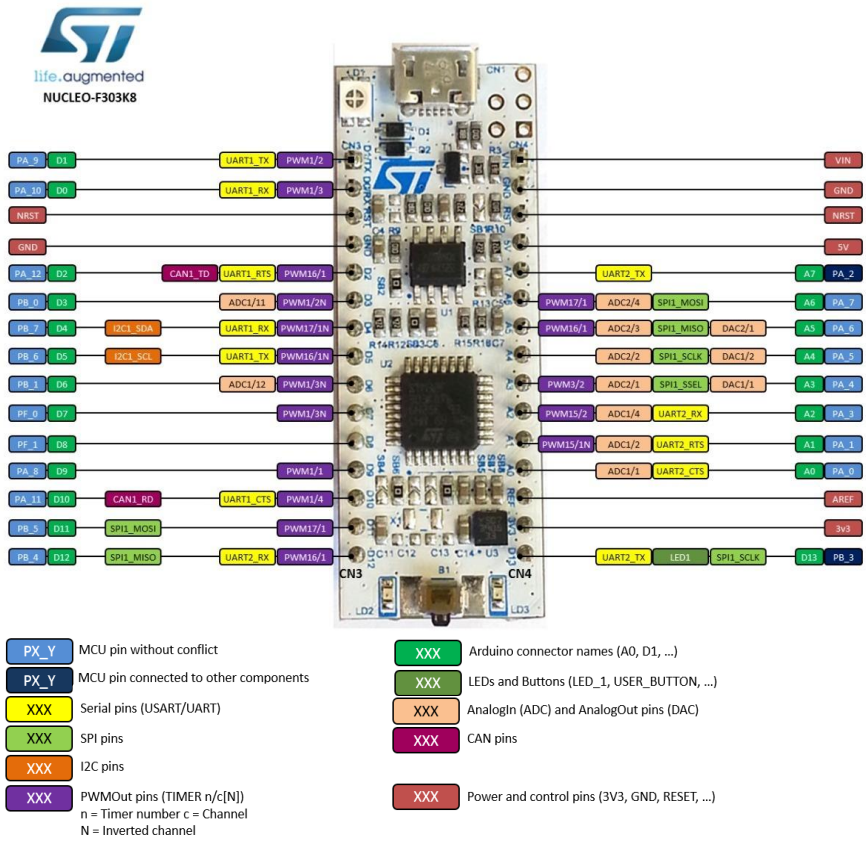

Figure 4.4: Stm32f303k8 board pinout and pins legend [113].

The MCU was programmed in the Keil uVision5 Integrated Development Environment (IDE), with the aid of the STM32CubeMX firmware. This firmware is part of STMicroelectronics STMCube original initiative to make developers' lives easier by reducing development effort, time and cost. By selecting and configuring the MCU peripherals, it generates the code in C, using the HAL library, and create a Keil project with the code generated [114]. The STM32CubeMX Pins used in this project and their corresponding STM32f303k8 Pins, their function and to where they are connected is summarised in Table 4.2 [113].

Table 4.2: STM32CubeMX Pins used and corresponding STM32f303k8 board Pins, their function and connection.

STM32CubeMX Pins	**STM32f303k8 Pins**	**Pin Function**	**Pin connection**
PA0	A0	ADC1 entry 1	Button
PA1	A1	ADC1 entry 2	Ultrasound
PA2	A7	ADC1 entry 3	FSR
PA3	A2	ADC1 entry 4	LDR
PA4	A3	GPIO Output	Yellow LED
PA7	A6	PWM Timer 17 Channel 1	IN (DRV2605)

STM32CubeMX Pins	STM32f303k8 Pins	Pin Function	Pin connection
PA9	D1	GPIO Output	Red LED
PA10	D0	GPIO Output	EN (DRV2605)
PA11	D10	GPIO Output	D3 (SD Card Shield)
PB1	D6	GPIO Output	Green LED
PB3	D13	SPI1 SCLK	CLK (SD Card Shield)
PB4	D12	SPI1 MISO	D0 (SD Card Shield)
PB5	D11	SPI1 MOSI	CMD (SD Card Shield)
PB6	D5	I2C1 SCL	SCL (DRV2605)
			SCL (MPU 9250)
PB7	D4	I2C1 SDA	SDA (DRV2605)
			SDA (MPU 9250)

4.3.2 Data Storage System

To store the acquired gait data during the experimental tests, an SD card with enough memory was used to store the data over a substantial period. Even though the microcontroller processing unit includes 64kB in flash memory, this is an insufficient quantity of built-in storage for the current proposal. Therefore, it was used an SD card, as an alternative.

For an Fs of 200Hz, considering a test duration of 60segunds, and at least 10 trials per subject, it is needed an SD card with at least 10.2 Mb. There are two ways to interface with SD cards: Serial Peripheral Interface (SPI) mode and Secure Digital Input Output (SDIO) mode. The SDIO mode is faster but is more complex, and module used only supports SPI. Also, the SPI protocol can be interrupted while the software code is running, and the SDIO cannot. Figure 4.5 depicts the used connections between the processing unit and the micro SD card Module. Also, Table 4.3 sums the module main features [115].

Table 4.3: Micro SD Card Shield main characteristics [115]

Parameter	Value
Voltage Supply	3.3 V
Dimensions	3.5 cm x 2.2 cm
Interface	SPI and SDIO

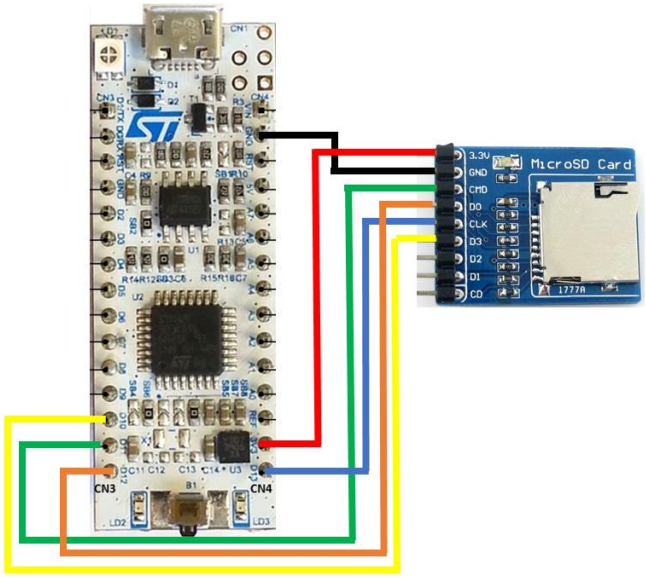

Figure 4.5: Implemented connections between the processing unit and the micro SD card Shield.

4.3.3 Haptic Feedback System

The ability to conduct activities like walking, sit-to-stand and stair negotiation determine the independence of elderly patients. Incapacity in ADL became a frequent obstacle for elderly adults. Accompanying the deterioration of functional capacity and skills, older people are limited in their ADL. Their lives become more and more semi-dependent until they are entirely dependent. Typically, they require to get someone's help to bathe, going down and climbing up the stairs and even walking. Climbing up and downstairs remains one of the five activities that older adults have difficulty at most [116][117].

Typically, assistive devices that incorporate haptic feedback in the form of mechanical vibrations are designed to assist blind users so that they can be guided into some specific direction. Nevertheless, a study accomplished by Boonsinsukh, R. et al. [118], documented that a light touch cue can be given while walking by the use of a cane. This augmented sensory information contributes to increased lateral stability while walking for subjects with stroke. By promoting the activations of weight-bearing muscles towards the paretic leg throughout the stance phase, greater balance is achieved when the paretic leg supports the body weight, which also increases the muscle activation.

Afzal et al. [119], developed a cane concept in which haptic feedback on the canes handle was used for stability in walking. The research team concluded that the system provided rehabilitation during walking, and posture stability with a haptic handle.

Miiõ Studio developed a cane which improves mobility for people who have Parkinson's disease. Amongst the main manifestations of Parkinson's disease is FOG. During FOG episodes, the patient's brain senses an incapacity to move, even though their bodies might still be able to respond to commands. FOG episodes can boost the risk of falls and generally occur in narrow spaces and stressful situations.

The Albert cane, Figure 4.6, employs **haptic feedback through built-in vibrational motors**, **stabilising the rhythm of the user's walk** [120]. Recent studies discovered that not only rhythmic stimulation, whether vibratory, visual, or auditory but also vibratory and auditory alerts can assist patients in avoiding so episodes [121].

Figure 4.6: Albert Cane, designed by Miiõ Studio, taken from [120].

The human tactile sensory system is mediated via the cutaneous mechanoreceptors. They relate to our touch sensitivity, vibration, sense of position and pressure. The mechanoreceptors usually are susceptible to the deformation or stretching and are in numerous parts of the body, such as the skin, muscles and tendons. When stimulated, the sensory system transmits encoded information (e.g. location, intensity and duration) in subgroups of receptors, axons and neurons which stimulate the primary and secondary somatosensory cerebral cortex. Consequently, the receptors and their connection to the central pathways and target areas within the cerebral cortex establish the human vibratory sensory system [122]–[124]. Usually, the receptors react to a form of energy, whether it is mechanical, chemical, thermal or even electromagnetic. Hence, each receptor, according to its distinct modality, serves as a transducer which converts the sensed data into action potentials. In this, skin receptors intervene in tactile sensitivity [122]–[124].

Generally, the skin vibration detection ranges between 80 and 300Hz. Additionally, It is essential to remark that the amplitude of the vibratory mechanical wave does not relate to its frequency, and the perceived magnitude ranges between 17 and 30 dB [122]. Since a continuous decrease of the "firing" frequency of the nerve impulse occurs until it reaches the cerebral cortex, the frequency discrimination of the human body ranges from 80 to 250 Hz [122]–[124]. Therefore, it is crucial to understand that

the capacity of the mechanical receptors and the capacity of the sensorial information of the cerebral cortex, relative to the somatosensory system, are different.

In conclusion, even though the skin can achieve a vibration detection between 80-300 Hz, the cerebral cortex only distinguishes frequencies between 80 and 250 Hz, as is described in Figure 4.7 [122].

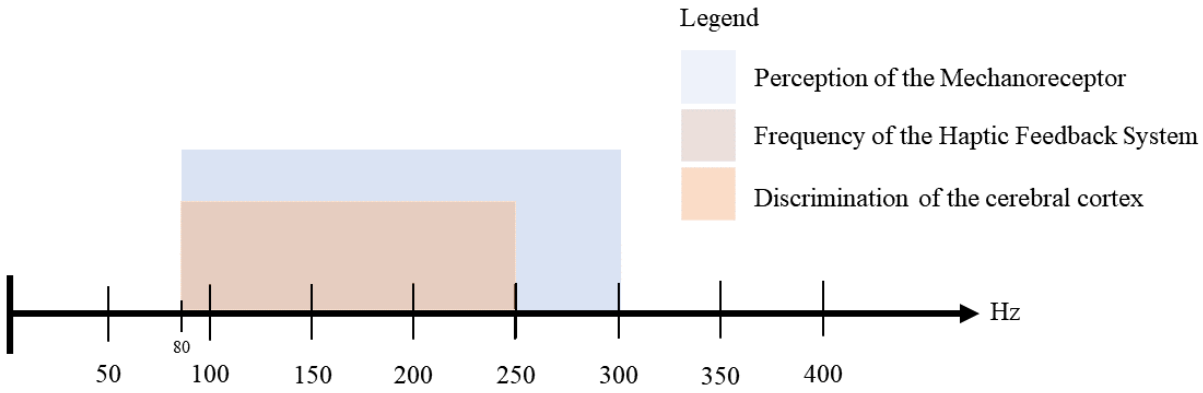

Figure 4.7: Representation of the frequency discrimination in the human body.

The human glabrous skin (skin with no hair) and the skin with hairs present notable differences regarding their vibratory detection. In hairy skin, the vibratory threshold is higher when compared with glabrous skin, which is attributable to the fact that each skin type presents different receptors and afferent fibres [122]–[124]. In Table 4.4, it is presented the body sites with the highest sensitivity, respecting the sensitivity regarding the spatial location, the vibration and the pressure and the discrimination between two points, in descending order [123].

Table 4.4: Body sites listed in order of most sensitive to least sensitive for tactile sensitivity measures [123]

Tactile Sensitivity Measures	**Body Site (listed in order of most sensitive to least sensitive)**
Pressure Sensitivity	Forehead (face), trunk, fingers, lower extremities
Two-Point Discrimination	Fingers, forehead/face region, feet, arms, lower trunk
Point Localization	Face region, fingers, hallux, palms, abdomen, arms, lower legs, upper chest, thigh
Vibration Sensitivity	Hands, soles of feet, larynx region, abdomen, head region, gluteus region

The lower frequencies depend on the sensory fibres associated with the hair follicles in the hairy skin (5-80 Hz). Contrarily, the higher frequencies (60-400 Hz) rely strongly on mechanoreceptors which are present in the glabrous skin. These specific mechanoreceptors, the Pacinian corpuscles, are the most

abundant mechanoreceptors that exist. They are presented in 20 to 70 layers. Therefore, human vibratory perception depends principally on Pacini corpuscles [122].

As reported, the hairless areas of the skin are more sensitive to vibrations, which can be verified by Table 4.4. **The hands and the soles of the feet are the areas with higher vibration sensitivity** [123]. Another critical factor is the patient's adaptation to the feedback. Adaptation happens if a stimulus is given for an extended amount of time. It is described by a decrease in the perception of the intensity of the signal and can occur for any stimulus. It can be avoided if stimuli are manifested for smaller periods. The adaptation stimulus can increase the threshold for the following stimulus [122].

Ultrasonic sensors are fit for close-range obstacle detection up to ten meters and provide multiple range measurements per second. The benefit of these sensors is its inexpensiveness, low power consumption and can continue operating in environmental situations whereas other sensors would fail, such as a smoked filled environment.

To detect obstacles, the LV-MaxSonar®-EZ3™ (MaxBotix® Inc.) ultrasonic sensor was preferred due to its small dimensions, low power requirements (2.5 - 5.5 V), and detection angle, Figure 4.8. The detection capability of this ultrasonic sensor ranges from 0.15 to 6.45 meters, and the sensor operates at 42 kHz [125]. The sensor has two modes of operation. It can output an analogue voltage with a scaling factor of (Vcc/512) per inch. Also, the output is buffered, which corresponds to the most recent range of data. The sensor can also output a pulse-width representation of the detected range. The distance can be calculated using the scale factor of 147uS per inch. The mode of operation chosen was the one which utilises the output analogue voltage [125].

Figure 4.8: LV-MaxSonar®-EZ™ Series High-Performance Sonar Range Finder MB1010, taken from [125].

The Haptic Feedback system is constituted by the Haptic Drivers and the corresponding vibrotactile motors. The vibrotactile units used are the Precision Microdrivers 10 mm Vibration Motor Model Number310-103.005, a type of Eccentric Rotating Mass ERM motors, Figure 4.9 a). Due to their small size and enclosed vibration mechanism, vibrating coin motors are a popular choice for many different applications. The whole constitution of an ERM motor is portrayed in Figure 4.9 b) [126].

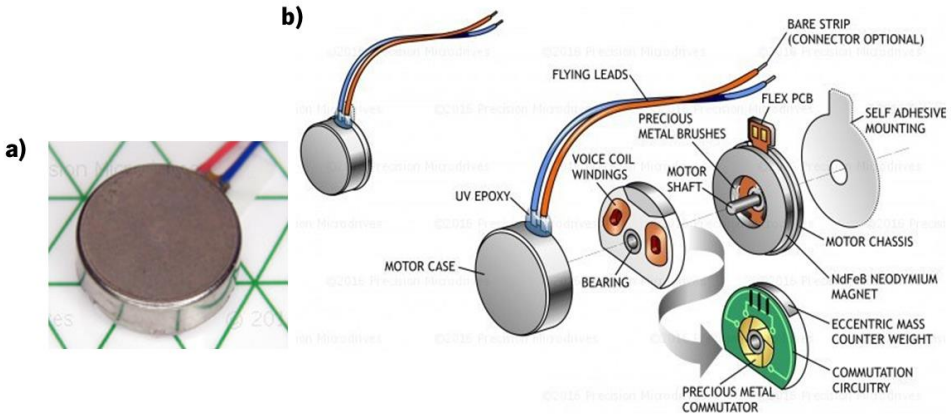

Figure 4.9: a) Precision Microdrivers 10mm Vibration Motor Model Number 310-103 b) the constitution of the ERM motor. Taken from [126].

Concerning the haptic drivers, it was used the Texas Instruments DRV2605L Haptic Motor Driver, which is able of handling two distinct kinds of motors, ERM and Linear Resonance Actuator (LRA). The Haptic Motor Driver breakout board features six pins, as depicted in Figure 4.10. The supply pin (VDD), being recommend a voltage range between 2 and 5.2 V; the two I2C-compatible bus pins (SCL and SDA), the ground pin (GND); the multi-mode input I2C selectable pin (IN/TRIG); and the device enable pin (EN). The haptic drivers were used in PWM interface mode and operated with EN control. They accept a PWM signal at the IN/TRIG pin. The DRV2605 drives the actuator in this mode until the user sets the device to standby mode or to enter another interface mode. In this mode, a constant voltage from the PWM will induce the motor at a steady vibration speed, and, therefore, at a regular frequency and vibration amplitude until the supply is turned off. The EN pin of the DRV2605 device gates the active operation. When the EN pin is logic high, the driver is active. When the EN pin is logic low, the drivers enter the shutdown state, which is the lowest power state of the device [127].

Figure 4.10: DRV2605 Haptic Driver for ERM and LRA from Texas Instruments, taken from [127].

A considerable range of DC voltages can drive these motors. Nevertheless, it exists a "start voltage" which matches the lowest voltage that needs to be applied to ensure the rotation of the motor. As the applied voltage is increased, also the vibration frequency increases in an almost-proportionally way, as depicted in Figure 4.10 [127]. Figure 4.11 also shows the relation between the voltage applied

vs amplitude, current and efficiency of the ERM motor. The used connections between the processing unit and the Haptic feedback system are presented in Figure 4.12.

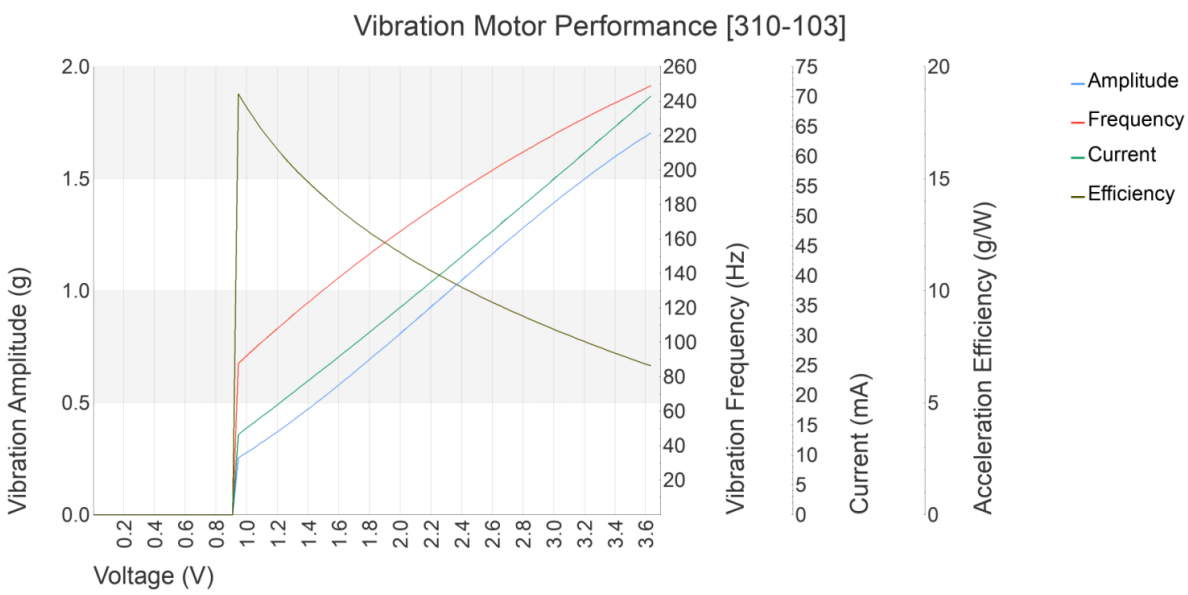

Figure 4.11: Relation between the voltage applied vs frequency, amplitude, current and efficiency of vibration for the Model No. 310-103.005 10mm Vibration Motor - 3mm Type from Precision Microdrivers, taken from [127].

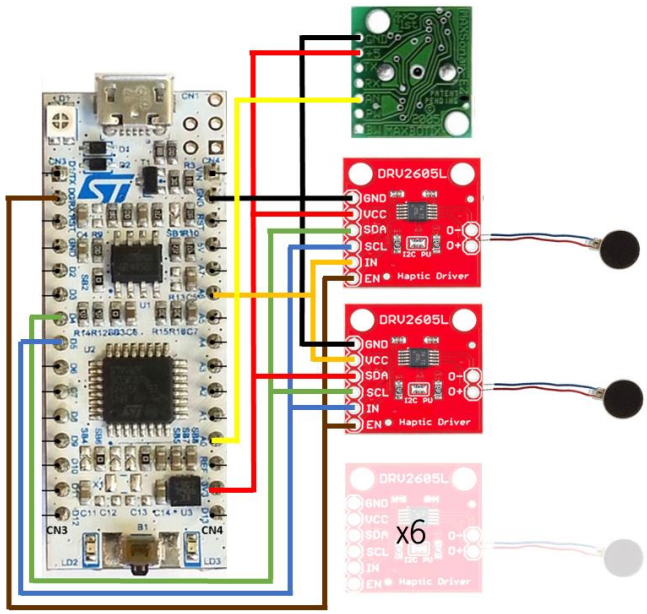

Figure 4.12: Implemented connections between the processing unit and the haptic drives with the respective vibrotactile motors and ultrasonic sensor.

4.3.4 Inertial measurement unit System

The MPU-9250, although only a single chip, internally consists of: an accelerometer and a 3-axis gyroscope - InvenSense MPU-6500, a 3 - axis magnetometer AK8963 from Asahi Kasei Microdevices Corporation and a processing unit called the Digital Motion Processor (DMP). Figure 4.13 displays the

diagram of the MPU-9250 with the main components and mode of communication with the microcontrollers. A communication interface can be established between the main microcontroller and the sensors via 400KHz Fast I2C or 1MHz SPI. The communication protocol chosen was I2C [128].

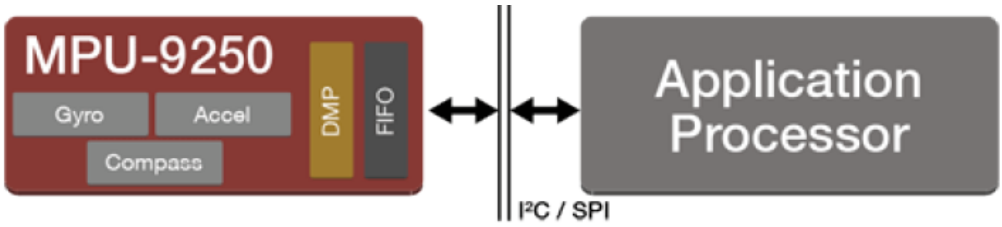

Figure 4.13: Diagram of the MPU-9250 with the main components and its modes of communication

Regarding the sensors reviewed in chapter 2 regarding fall-related systems, accelerometers, and gyroscopes are widely embedded into these systems. So, it is proposed to use those sensors in order to collect the data, which will serve as the primary source of signals used in the ASCane. The IMU will be mounted on the top of the cane since Chen et al. [105] studied acceleration readings in different places of a cane and concluded that the **amplitudes of the acquired data in the "upper" location of the device were higher than the other locations**. Since the higher the amplitude of the variation, discriminative characteristics of the signal are more easily observed, **placing the sensing units in the upper part of the cane is more desirable**. The embedded system also must be able to collect continuous readings from the sensors at a rate which meets the minimum requirements for FD systems.

Bouten et al. [129], conducted a study in which a tri-axial accelerometer was described to conduct daily physical activity. It was concluded that a range of ±6g would suffice. For this reason, the closest possible sensitivity was chosen, ±8g. Regarding the gyroscope, studies regarding its range for human motion purposes were not found for canes. As a result, their operation range will be set according to studies conducted on FD [130]. Consequently, a sensitivity of ±2000°/s was chosen. Figure 4.14 depicts the used connections between the processing unit and the MPU 9250.

Inertial sensors present measurements influenced by drifts and offsets. The characteristics of these changes are described in the datasheets given by the manufacturers. To correct the measurements, a calibration process is required.

The IMU is placed on a surface as horizontal as possible on its different faces as described in Figure 4.15 a). These positions correspond to the alignment of the three accelerometer axis with the gravity. At every position, the gravity value is stored for 6 seconds, considering only the sensitive axis parallel to the gravitational force [131]. This calibration was accomplished every two weeks for 6 weeks, and the calibration values did not change significantly.

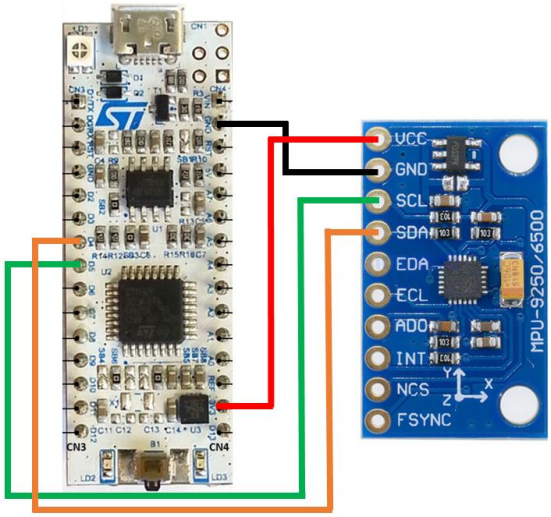

Figure 4.14: Implemented connections between the processing unit and the IMU.

Regarding the gyroscope calibration, its offsets were measured every time the cane starts. A total of 500 samples are saved, and the mean values of each axis are subtracted to values of the readings during the experimental trials. The position of the gyroscope calibration depicted in Figure 4.15 b), which is the IMU orientation inside the ASCane.

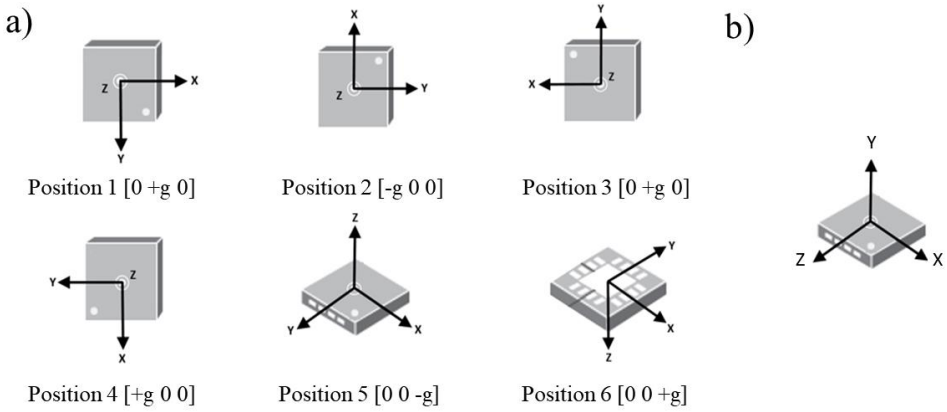

Figure 4.15: a) The six different positions for the extraction of Maximum and Minimum values of the accelerometer b) IMU orientation inside the ASCane.

4.3.5 Force Sensitive Resistor Interface

To obtain a voltage drop from the FSR sensor, a hardware interface is required to connect it with the MCU. For a force-to-voltage conversion, the FSR is connected to a measuring resistor in a voltage divider configuration, Figure 4.16, and the following equation (Equation 4.1) describes the output:

$$V_{OUT} = \frac{R_M \times VCC}{R_M + R_{FSR}} \tag{4.1}$$

The output voltage increases with increasing force. If the resistors are swapped, the output voltage will decrease with increasing force. The measuring resistor, RM (Figure 4.16) , is chosen to maximise the desired force sensitivity range.

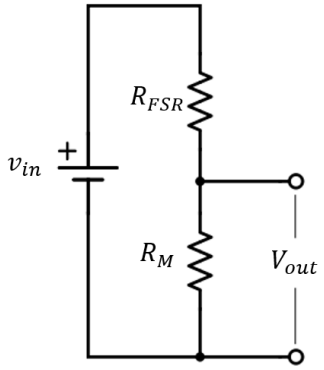

Figure 4.16: Voltage Divide Eletronic circuit

The FSR chosen for the project was the FSR-402 from Interlink Electronics which have a circular sensing area with a diameter 12.7 mm, Figure 4.17. The FSR chosen for the project was the FSR-402 from Interlink Electronics which have a circular sensing area with a diameter 12.7mm and thickness around 0.46mm. In this design, one FSR-402 will be used beneath the canes' tip. The readings from the FSR can identify when the cane is in contact with the ground [132].

Figure 4.17: Interlink Electronics FSRTM 402 Force Sensing Resistor, taken from [132].

4.3.6 Light Sensing Mechanism

The designed circuit is based on an Light Dependent Resistor (LDR), that is, a resistance that varies its resistance by the amount of light that reaches it. An LDR has a semiconductor material inside it, which allows electrons to pass through when struck by light photons. Thereby, when the light strikes bend the LDR, it will enable the passage of electric current. The circuit shown in the following figure allows the construction of a simple adjustable dimmer detector. This circuit has a straightforward operation. The potentiometer together with the resistor R1 and the LDR form a voltage divider which, by the brightness

reaching the LDR, puts a variable voltage on resistor R2, which has the function of limiting the base current of transistor NPN BC547. The potentiometer allows to adjust and set the output voltage of the voltage divider that will be applied to the transistor base through R2.

When the voltage reaching the base of the transistor reaches the value necessary for it to conduct conduction, current begins to flow from the collector to the emitter, as well as from the LED and resistor R3, and it begins to emit light. The described and implemented circuit is depicted in Figure 4.18.

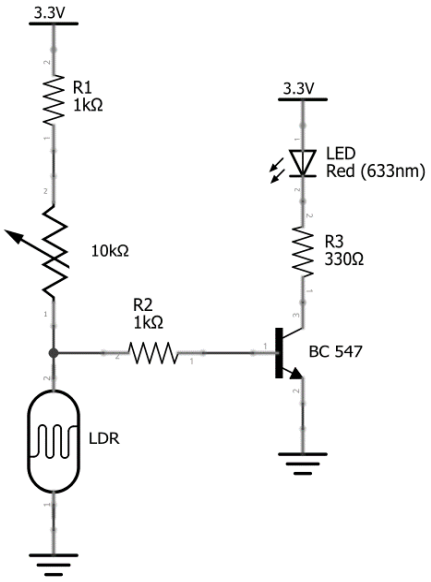

Figure 4.18: Light Sensing Circuit implemented and designed for the ASCane.

4.4 Software Methodology Overview

The main goals of this thesis are the development of strategies to distinguish not only normal gait from a fall and pre-fall situations but also to detect cane events with information acquired in a system embedded into a regular cane. Described in Figure 4.19, the sensor's raw data were collected from trials, and these data were normalized through a calibration process. Subsequently, for each trial acquired, all the features found in the literature were computed, as listed in Table XXIV, Appendix 3. Finally, depending on the what type of detection is desired, different methodologies were accomplished. All the process, starting from the experimental protocol to the results attained, are described in Chapters 5, 6 and 7 for FD, cane event detection, and PFS detection, respectively.

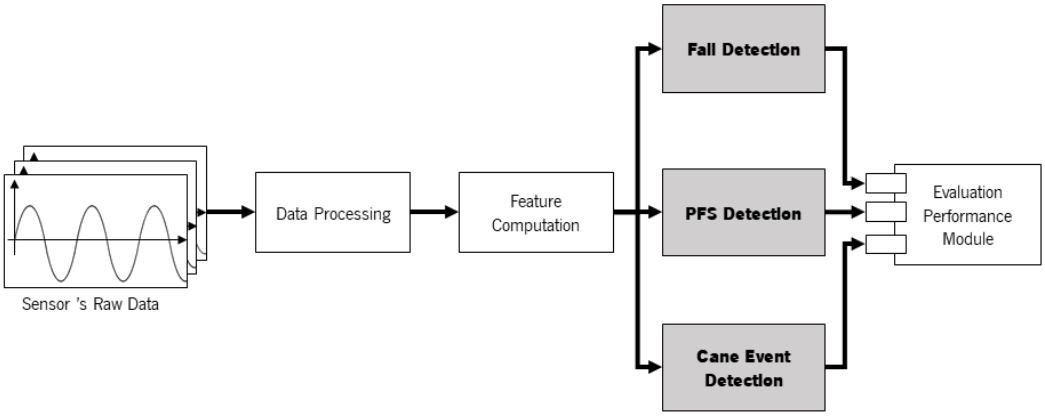

Figure 4.19: Main General block diagram for the methodology implemented.

5. ASCane Fall Detection System

The main goal of this chapter is to achieve a system capable of detecting a fall using inertial sensors embedded into the ASCane. It is hypothesised that the system will only detect falls from an ordinary cane, which corresponds to a fall from its user. A FD system will be implemented and tested by using data from an IMU attached to a cane. This chapter will be divided into four major parts: i) Detailed research of the existing FD methods in the literature; ii) Data collection through trials with healthy young subjects; iii) Implementation of several offline FD methods and some improvements to these methods; iv) Selection of the best FD method based on the collected data.

Wearable FD systems regularly employ accelerometers. However, other sensors are used such as gyroscopes, magnetometers and barometers, have also been explored in the literature. **In FD systems, sensor measurements are fed to an algorithm that identifies fall events**. FD algorithms aim to detect accurately falls and not to generate false alarms during ADL. The algorithms suggested in the literature can principally be classified into two categories: **threshold-based and machine learning algorithms**. Nevertheless, the threshold-based algorithms can implement **fixed or dynamic thresholds** [133].

5.1 Threshold-based Algorithms

In threshold-based algorithms, features are computed from sensorial data and are constantly compared with pre-defined thresholds [51], [52], [134], [135]. A multi-stage threshold system employs at least two different thresholds, and all need to be surpassed in an appropriate order over a specific period.

Bourke et al. [134], studied signals from accelerometers placed at the trunk and thigh, to discover if their peak values could be utilised to distinguish between ADL and falls. The team developed a threshold-based algorithm through the computation of the acceleration SVM. The algorithm is based upon two different thresholds. If the Upper Fall Threshold (UFT) or the Lower Fall Threshold (LFT) is surpassed, a fall is detected. The complete algorithm developed is depicted in Figure 5.1.

Regarding the UFT, for all the trunk and thigh signals, it was established at the smallest magnitude upper fall peak value registered for both locations separately. The UFT is connected to the impact force endured by the body when it impacts with the ground. Concerning LFT, they were set at the level of the smallest magnitude lower fall peak recorded. The LFT is linked to the approximation of acceleration with zero before the contact of the body with the ground.

Thus, four thresholds were determined, as presented in Table 5.1, and transcending any individual limit would register that a fall had happened. Since these thresholds would also be applied to ADL, they were tested against recorded ADL to conclude regarding the extent of misdetection of ADL as falls.

The UFT for each location provided greater SPEC than the LFT value. The UFT from the thighs provided a SPEC of 83.3%, as the LFT presented a SPEC of only 67.08%. For the trunk, the LFT achieved a SPEC of 91.25%, concerning the UFT, all ADL tasks were correctly detected as non-falls, obtaining a SPEC of 100%.

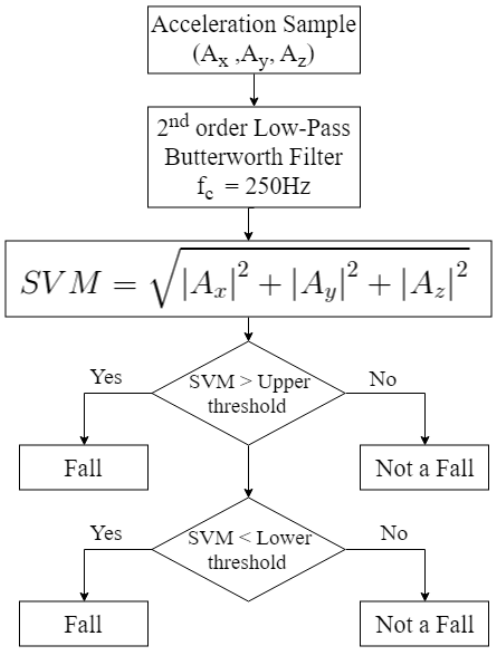

Figure 5.1: Flowchart of the threshold-based FD algorithm using accelerometric data by Bourke et al. [134].

FD upon impact is proven to be possible utilising data solely from a triaxial accelerometer located on the trunk. Nevertheless, if the 3-D accelerometer sensor fails for any reason, the fall cannot be

detected. Consequently, Bourke et al. [52], also developed a threshold-based algorithm which can automatically discriminate between falls and ADL, utilising a bi-axial gyroscope. After acquiring gyroscopic data from the sagittal and coronal planes (ωr, ωp) from both simulated falls (on healthy subjects) and ADLs (from elderly in their own home), it was concluded that the resultant angular velocity peak values for the recorded falls and ADL overlapped. Consequently, by setting a single-threshold, ADL can be misclassified as falls.

In the end, three different thresholds were set. The first threshold (ωres) was established at the lowest recorded resultant angular velocity fall peak value, wich will guarantee that 100% of falls are accurately identified. To differentiate some ADLs that could be detected as fall, the resultant angular acceleration (αres) and the resultant change in trunk angle (θres) were also computed. The resultant angular acceleration indicated the unforeseen change in the trunks rotation and was set at the lowest recorded αres in falls. The final threshold, the θres shows what angle the trunk had swept through in the time just before impact and was also set the lowest recorded θres in falls. The complete algorithm developed is depicted in Figure 5.2, and the corresponding thresholds are shown in Table 5.1.

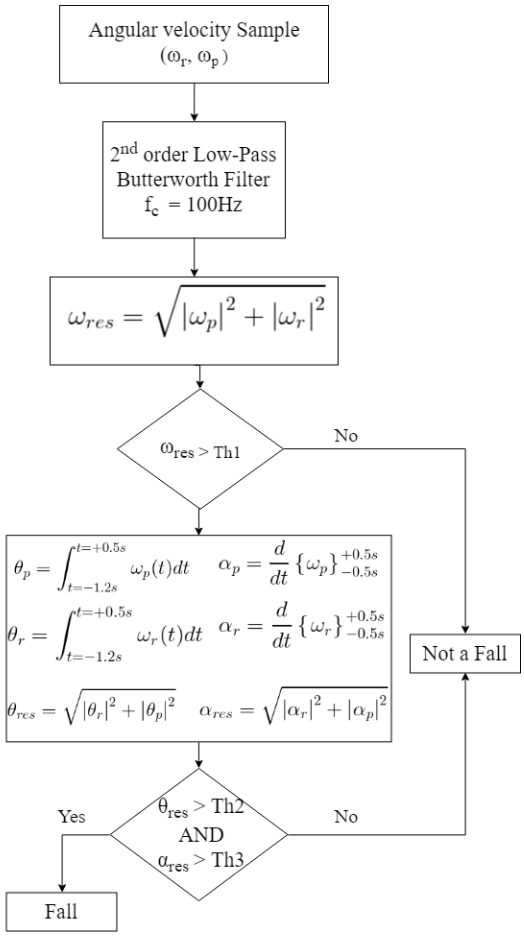

Figure 5.2: Flowchart of the threshold based FD algorithm using gyroscopic data developed by Bourke et al. [52].

A single threshold for ωres rightly classified 97.5% of ADL as non-falls, which corresponds to a SPEC of 97.5%. By combining the threshold for ωres and αres, a SPEC of 99.2% was achieved. Finally, by merging all three thresholds, 100% SPEC was obtained.

The algorithm introduced by Kangas et al.[51], is a multi-threshold algorithm based on the analysis of 4 acceleration parameters from the wrist, head or waist, Figure 5.3. The parameters used were the SVTOT (which contains both the dynamic and static acceleration), SVD (which includes only the dynamic acceleration), Vertical Acceleration (Z2), the differences between the maximum and minimum acceleration (SVmaxmin) and the final posture, which is detected 2 seconds after the impact. The authors attained a FD SENS of 97% and SPEC of 100% from the waist. All the thresholds were adjusted until a maximum a maximum SPEC was reached. All the thresholds set for the different parameters and locations are summarized in Table 5.1.

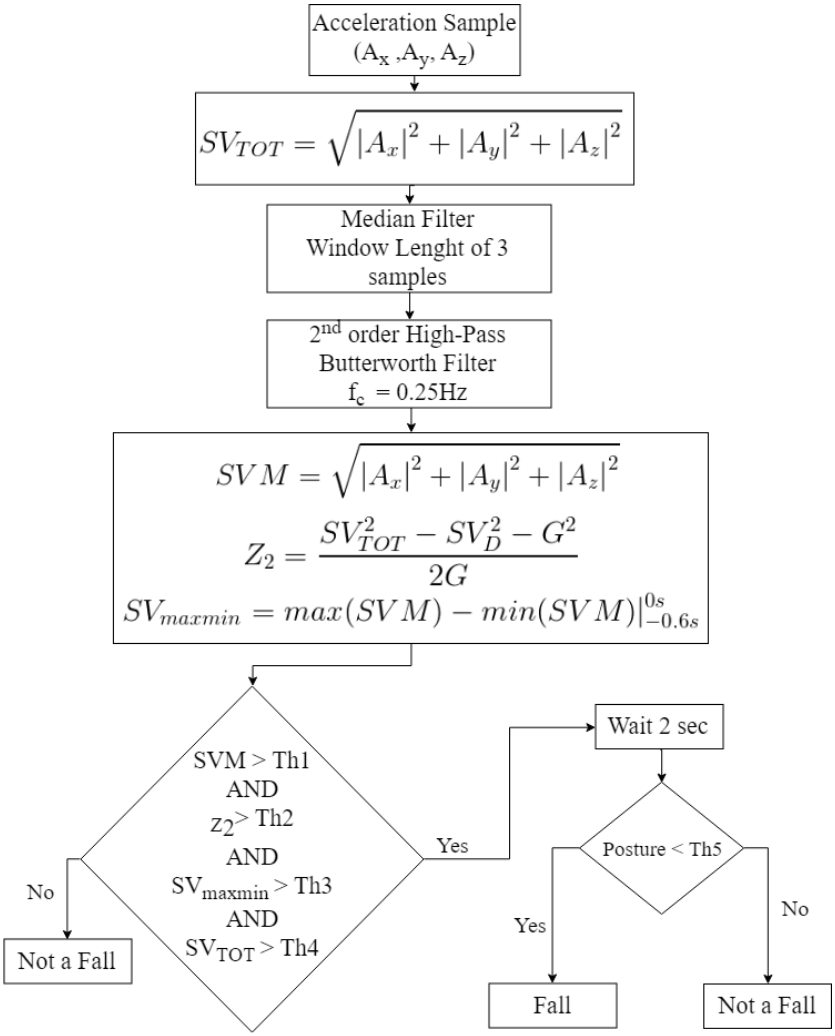

Figure 5.3: Flowchart of the threshold-based FD algorithm with in accelerometric data by Kangas et al. [51].

Table 5.1: Threshold values for the different fixed threshold FD algorithms

Study	Parameter	Location	Value	Type of Threshold
Bourke et al. [134]	SVM (g)	Trunk	3.52	UFT
			0.41	LFT
		Thigh	2.74	UFT
			0.60	LFT
Bourke et al. [52]	ωres (rads/s)	Trunk	3.1	
	αres (rads/s2)		0.05	
	θres (rad)		0.59	
Kangas et al. [51]	SVMTOT (g)	Waist	2.0	UFT
		Head	2.0	
		Wrist	5.2	
	SVD (g)	Waist	1.7	
		Head	1.2	
		Wrist	5.1	
	Z2 (g)	Waist	1.5	
		Head	1.8	
		Wrist	3.9	
	SVMaxMin (g)	Waist	2.0	
		Head	1.7	
		Wrist	6.5	

5.2 Dynamic Threshold Algorithm

Nyan et al. [136], revealed that falls could be identified with an average most extended lead-time of 700 msec under pre-impact FD, with 100 % SPEC (no false alarms) and 95.2% SENS (falls do occur but fails to detect them in 4.8% of trials).

Furthermore, the researcher observed that the application of a dynamic threshold might decrease the false alarm rate. If the fixed threshold is estimated too low, the likelihood of the number of falls happening that are correctly detected will increase. Meanwhile, the PF rate, ADL which are classified as falls, will be increased simultaneously. Contrarily, if a fixed threshold-based method is established too

high, not only the false-positive but also the true-positive rate will decrease. Thus, fixed threshold-based algorithms can be insufficient to achieve the primary goal of fall-related systems due to inter and intra-variability of subjects, and limited sample [51], [52], [134]. These methods should be adaptive and account for variability.

Otanasap et al. [135], developed a dynamic threshold algorithm through accelerometry data, Figure 5.4. A Fixed Threshold (FT) is computed based on the data acquired from the subject while performing ADL, ADLacc. Secondly, the Dynamic Threshold (DT) is formulated by the FT added by a standard deviation calculated with the data gathered in the last second. The algorithm outputs a percentage which discriminates the possibility of a fall, reaching results of 97.4%, 99.5% and 95.3% for ACC, SENS and SPEC, respectively.

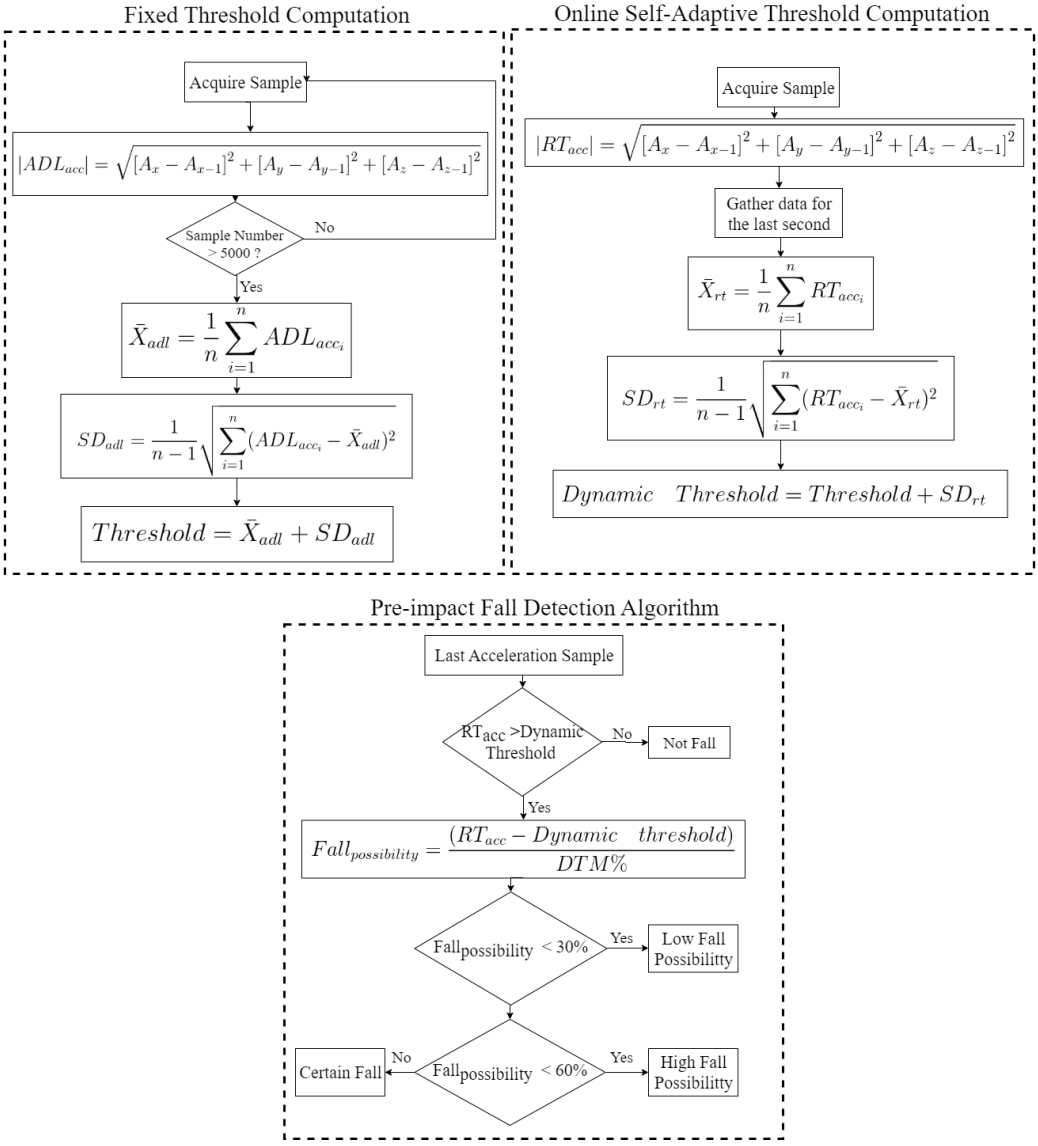

Figure 5.4: Flowchart of the dynamic threshold model for FD using accelerometric data by Otanasap et al. [135].

5.3 Machine Learning Algorithms

In supervised learning, the classifier can learn on a labelled dataset. Therefore, it can construct a model that can predict the correct output about data it has never seen. Each input has the outcome that the algorithm should be able to predict which is used to evaluate its accuracy on training data [137]. There are two main fields where this kind of learning is helpful, which is in classification and regression problems. The first one concerns the type of problem where the output is discrete values which represents a specified category, in the simplest case conceivable, selecting between positive and negative. Regression problems intend to model the underlying behaviour of the data given to the classifier expecting it to provide an output based on past training stages, such as the price of a stock in 6 months [138]. In this type of learning, the output will always be the same for specific input.

The field of unsupervised training is more complex, contrarily to supervised learning, the classifier has to learn to perform specified tasks without telling it how to execute them, that is to say, that only the predictor variables are given, therefore the training time is much longer [137], [138]. The output produced by the system may vary each run for the same input variable.

Regarding reinforcement learning, the classifier outputs are actions, and the only guiding signals are scalar rewards, these ways, the systems learn based on interactions with the surrounding environment. Occasionally restrictions as a set of rules are imposed on the systems that influence its behaviour directly [138]. Since the output depends on the interactions made, it can change if the environment changes even if the input remains the same.

To detect falls, systems normally respect a defined general model composed by different modules. The data collection module is responsible for collect all the information concerning the SOI's gait. Since a dataset can have thousands of features, feature extraction is essential to minimise problems that could originate in future steps. Before the classifiers learn the features and can establish relationships between the dataset introduced, it must be divided into training and test dataset.

5.3.1 Data collection

The first step when collecting data is identifying the variables needed to accomplish the final result. In this case, considering fall-related systems, the collected data is the acceleration, angular velocity, speed and force measurement from different body parts. The data must be collected following a formal procedure to guarantee it is accuracy and validity [5].

5.3.2 Dimensionality reduction & Feature selection

The size of the data currently available is massive and constantly increasing due to technological advances and cheap sensor manufacturing. Hence, researchers can calculate as many features possible from the data collected. Yet, this poses a challenge to the majority of machine learning algorithms due to a large amount of storage and computational power required [139]. Considering that raw data obtained from the sensor have insignificant information, feature reduction aims to diminish the problems aforementioned with choosing a small subset of relevant features removing irrelevant, redundant and noisy features, even though their existence does not affect the learning performance [5][139]. Irrelevant features are the ones that cannot support the classifier to differentiate between different classes, not make it able to predict an outcome [139].

Selecting the most relevant and not redundant information helps to generalise the model, being able to adapt appropriately to new, previously unseen data, obtained from the same distribution as the one used to create the model. Faster and cost-friendly are more advantages of feature selection [140]. Through feature selection, the meaningless information is removed, which translate in the advantages above described [5].

5.3.3 Feature Computation

Feature computation is essential in the way that is a substantial influence in the following stages in which mathematical procedures and algorithms are applied to the information to recognise linear and non-linear combinations among the remaining features. Some of the procedures usually used are standardisation, Principal Component Analysis (PCA), signal enhancement and normalisation. Choosing the features that effectively will be used to construct the model is extremely important, which is why a meticulous study of the problem should be executed [5].

5.3.4 Learning Classifiers

Regarding FD and prevention systems, supervised learning is widely employed, about the remaining subfields, hardly any information can be found about their use in this type of applications [5]. Some of the most used supervised algorithms are: support vector machines, Decision Trees and K-Nearest Neighbours (KNN). Support vector machines are a class of supervised classifiers that attempts to find the hyperplane/line in n-dimensional space that's able to separate different classes. In Support vector machines, the input data is transformed into a higher-dimensional space through non-linear mapping in which they are linearly separable wherein the initial space they are not. The training points

closest to the maximum decision margin are called support vectors, the higher the number of support vectors used, the change of overfitting is more significant since the classifiers are more tailored to the training data. When new data is presented to the algorithm, the data will be classified reliably on the section that it falls [5], [139], [140].

In DT, the goal is to generate a model that predicts the value of a target variable based on numerous input variables. A decision tree is constituted by a condition/internal node, based on which the tree splits into branches. The end of the branch that doesn't split any longer is the decision/leaf.
For its construction, an attribute/node must be selected to place at the root and make one branch for its every possible value, which separates the example into subsets. This process continues iteratively in every branch until every instance of it have the same classification which should happen as fastest as possible since we seek small tree sizes. The decision of which attribute to split is made based on its measure of purity, measured in bits. The level of purity is the number of instances in the node that has the same class. To classify an unknown instance, its directed through the tree accordingly to the values of its attributes in the nodes, when a leaf is reached, the instance is classified accordingly to the class that the leaf is assigned to [141].

In instance-based learning (KNN), each new instance is compared with all the classified dataset available and the instance closest by means of distance metrics is used to classify it which is the difference between the KNN algorithm and others. Different methods require training phases in order to be able to operate. Computing the distance between two instances is easy when assuming that all samples of the dataset have the same importance, which in most of the cases that is not true, and deciding which features are most important varies from the application. This problem is reflected in the distance metric by applying some attribute weighting which till this day is a significant problem instance-based learning even though is usually more robust than regular KNN. Since, for every instance that need to be classified, every sample of the dataset must be checked, not only the time but complexity of the algorithms increases proportionally to the dataset size [141].

5.3.5 Machine Learning approaches in Fall Detection

Xu et al. com [7], completed a survey regarding the new advances and challenges of FD systems where compared FD algorithms on the most cited works. As sensors development progresses, FD algorithms adjust with it. When comparing FD algorithms used in the most cited work before and after 2014, it was observed a trend by comparing the algorithms employed in the most cited work before and after 2014.

Concerning FD algorithms adopted before 2014, the accelerometer was a mainstream sensor employed by the FD system in early days. Considering the accelerometer can just record velocity and acceleration of a single part of the human body, thresholds-based methods became the chosen method. For FD algorithms adopted after 2014, machine learning-based FD algorithms became the preferred method. Considering that with the development of new types of sensors, they can discern further detail of human activities, the threshold-based algorithm became more inadequate to accomplish this goal. From the aspect of the specific type of algorithm, the support vector machine and the DT are the most employed algorithms with relatively high accuracies above 90%, ranging between 79.6% and 100% [7].

Chen et al.[64] developed an accelerometer-based FD algorithm using support vector machines for classifying the features (ADLs and falls). The model accuracy was the averaged after ten-fold CV. The average system accuracy was 94.58%. The sensitivity and specificity were 95.76% and 93.28%, respectively. Putra et al. [65] proposed an event-triggered machine learning strategy to classify ADLs and falls with accelerometery data. The proposed method aligns all fall stages so that the unique features each fall stage are more efficiently identified. Some of the used classifiers were the KNN and support vector machines. It was achieved an F-score of 98%. Liu et al. [66] applied support vector machines to accelerometery features in order to identify ADL and fall situations. The results revealed that the computed features had the highest accuracy with 99.1% and 98.4% in the training and testing, respectively. Finally, Shibuya et al. [142] used both acceleration and angular velocity to also classify balls and ADLs. Six features were extracted for fall classification using a support vector machines, achieving 98.8% and 98.7% fall classification accuracies of the data at the T4 and belt locations, sequentially.

5.4 Methods and Materials

5.4.1 Experimental Protocol

The system used to acquire the data was part of the one described in Chapter 4. For this experimental protocol, only the data from the MPU 9250 was necessary. A set of activities (Table 5.2 and Figure 5.5) was executed by eleven volunteers which ranged from 22 to 29 years (24.20 ±2.60 years), with a body mass between 52 and 80 kg (70.80 ± 8.23 Kg) and a height of 1.51 to 1.83 m (1.73 ± 0.09m). All participants provided their written consent. Each activity was performed three times. A total of 132 simulated falls were recorder with 66 combining the subject and cane (Table 5.2- Activities 6 and 7) and 66 only with the cane (Table 5.2 – Activities 4 and 5). Also, 99 ADL were registered (Table 5.2 – Activities 1, 2 and 3).

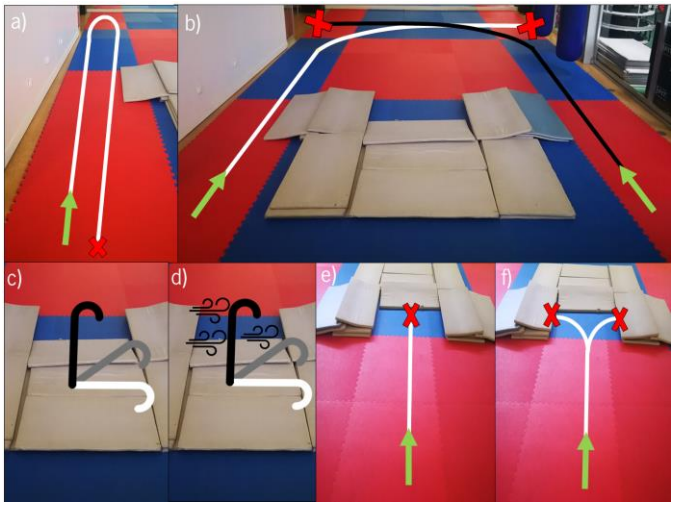

Figure 5.5: Activities performed for data acquisition: a) Activity 1; b) Activities 2 and 3; c) Activity 4; d)Activity 5; e)Activity 6; f)Activity 7.

Table 5.2: Activities simulated with the ASCane Prototype

Activity No.	Description
1	Walking at Normal Speed and 180° rotation (Subject + Cane)
2	Walk forward and turn right (Subject + Cane)
3	Walk forward and turn left (Subject + Cane)
4	Free Falling (Cane)
5	Thrown out (Cane)
6	Falling Forward (Subject + Cane)
7	Falling Sideways (Subject + Cane)

5.4.2 Strategy

The implemented strategy to uncover which FD algorithm is best suited to detect falls of a cane can be subdivided into four segments, as depicted in Figure 5.6. Three types of threshold-based algorithms found in the literature were implemented and tested. Namely, three fixed (Original Fixed Threshold Algorithms - Figure 5.6) one dynamic (Dynamic Threshold Algorithm - Figure 5.6) threshold algorithms found in the literature, as well as two improvements on the same algorithms (Modified Fixed Threshold Algorithms - Figure 5.6). Finally, a machine learning approach was also accomplished. Trough the conducted search, the computed features from the selected articles were extracted and are presented in Table 5.3 [64]–[66], [142]. Data were then divided into two different classes: Fall and ADL samples. Afterwards, 70% of each data were used to train the classifier and 30% to test it. The complete methodology for the development and testing of FD algorithms is depicted in Figure 5.6. All the algorithms were implemented offline using the Matlab 2018b version.

Different tests were accomplished by varying the kernel type and proportion of class samples in the support vector machine classifier. However, the best set of parameters was determined by enabling the "OptimizeHyperparameters" option in MATLAB. Features regarding ADL and falls were labelled using the parameter CVFast to mark the falling range [66]. The maximum CVFast of each fall trial was calculated and multiplied by 0.87. The samples higher than 0.87CVFast were considered a fall and labelled as 1.

Table 5.3: Summary of the features that may correlate with falls-risk in the selected FD algorithms [64]–[66], [142]

Study	Feature Name
Shibuya et al. [142]	Range of angular velocity for each individual axis
	Range of acceleration for each individual axis
Liu et al.[66]	SVM
	Fast Changed Vector
	Vertical Acceleration
Chen et al. [64]	SVM
	Rotation angle
	Slope
	The acceleration in the xy – plane
Putra et al. [65]	SVM
	Maximum Sum Vector Magnitude
	Minimum Sum Vector Magnitude
	Average Sum Vector Magnitude
	Root mean square of the acceleration vector magnitude
	Acceleration exponential moving average
	Signal magnitude area

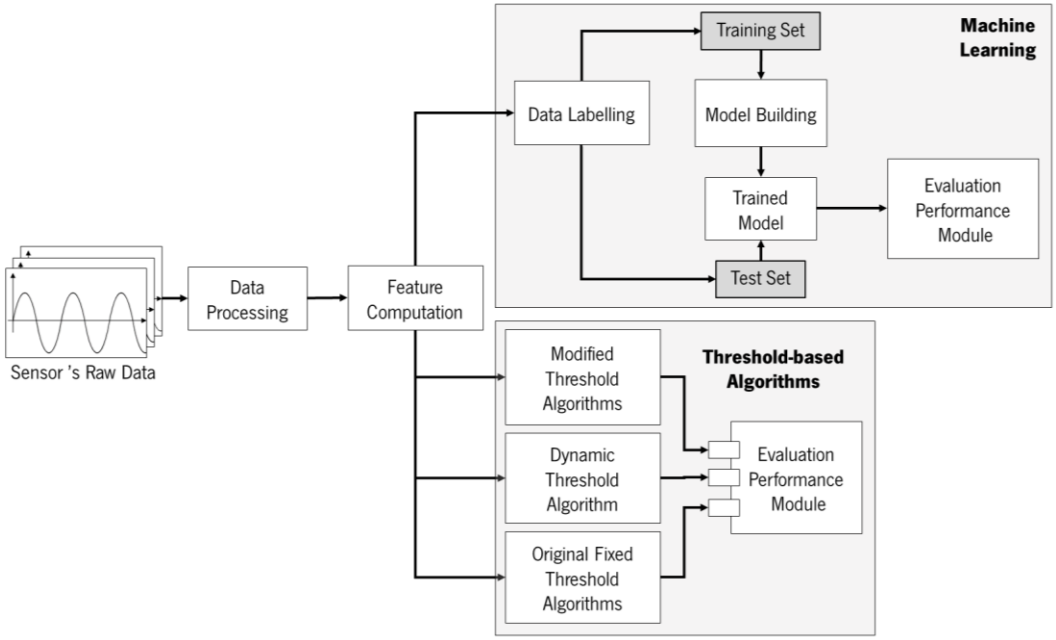

Figure 5.6: Schematic diagram of the implemented strategy for evaluation of different FD algorithms.

5.5 Results

5.5.1 Original Algorithms

The algorithms were tested with the acquired data on the aforementioned thresholds with their corresponding original thresholds. The results of the different performance indicators are summarized in Table 5.4.

Table 5.4: Performance Indicators of FD algorithms

Type	Study	Details	ACC	PREC	SENS	SPEC	MCC	KAPPA
Fixed Threshold	Bourke et al. [134]	[1]Trunk	0.5746	0.5708	1	0.0202	0.1074	0.023
		[1]Thigh	0.5658	0.5658	1	0	NaN[6]	0
	Bourke et al. [52]	[1]Trunk	**0.8114**	**0.9388**	**0.7132**	**0.9394**	**0.6534**	**0.6296**
	Kangas et al.[51]	[1]Waist	0.5789	0.5740	0.9922	0.0404	0.1105	0.0367
		[1]Head	0.5658	0.5658	1	0	NaN[6]	0
		[1]Wrist	0.5789	0.9714	0.2636	0.9899	0.3485	0.2282
Dynamic Threshold	Otanasap N. [135]	[2]0.0740	0.5658	0.5658	1	0	NaN[6]	0
Machine Learning	Support Vector Machine	[3]1:60 [4]RBF	0.9913	0.9744	0.4863	0.9998	0.6852	0.6449
		[3]1:1.6 [4]RBF	**0.9154**	**0.9390**	**0.8347**	**0.9660**	**0.8211**	**0.8178**
		[3]1:1.6 [4]Linear	0.9105	0.9329	0.8273	0.9627	0.8106	0.8070
		[3]1:1.6 [5]Optimized	0.9121	0.9358	0.8289	0.9643	0.8141	0.8105

[1]Location; [2]Fixed threshold Value; [3]ADL: Fall Proportion; [4]Kernel Function; [5]Optimized with MATLAB; [6]Not a Number

The algorithm introduced by Bourke et al. [134] presented similar results for the two sets of thresholds described (Table 5.4). It detected a fall in 100% of the cases. However, all or almost all the ADLs performed were also considered a fall with a SPEC of 0 and 2.02% for the thighs and trunk, respectively. With the method presented by Kangas et al. [51], the results are similar to the ones reached by Bourke et al. [134] in the three different sets of thresholds (Table 5.4). Nevertheless, while with the

waist and head thresholds a fall is detected in 99.22% and 100% of the cases, respectively, the thresholds for the wrist detected only 26.36% of falls. Using the algorithm from Bourke et al. [52], it resulted in overall higher performance compared to the remaining fixed threshold algorithms (Table 5.4), achieving an ACC of 81.14%. Like Bourke et al. [134] and Kangas et al. [51], with the dynamic algorithm proposed by Otanasap et al. [135], a fall was spotted 100% of the cases, yet, the entirely ADL dataset was also assessed as a fall (Table 5.4). With the machine learning approach, the best set of parameters achieved an ACC of 91.54 %, SENS of 83.47% and SPEC of 96.60%. The results for all accomplished tests are revealed in Table 5.4.

5.5.2 Modified Algorithms

Both falls and ADLs present a similar acceleration maximum as identified in Table 5.5 and Figure 5.7 a), which explains why the algorithm by Bourke et al. [134] was not able to detect ADLs. Thus, the algorithm was tested with a single lower threshold, Figure 5.7 b). The corresponding results are presented in Table 5.6. On the contrary, the ωres does not exhibit the same behaviour as the acceleration (Table 5.5). The maximum angular velocity achieved during an ADL is much lower than the one reached during a fall (3.5636 vs. 12.6706). Consequently, the first threshold of 3.1 rad/s (ωres) is hardly ever surpassed, as can be seen in Figure 5.8, on one trial.

Table 5.5: Maximum, minimum, mean and standard Deviation of the acceleration Sum Vector Magnitude and the angular velocity for the intentional falls and ADL trials

Feature	Type of Activity	Maximum	Minimum	Mean	Standard Deviation
SVM (g)	ADL	**13.8357**	0.1351	1.0557	0.3427
	Fall	**13.8980**	0.0681	3.8644	3.8296
ωres (rad/s)	ADL	**3.5636**	0	0.6711	0.5440
	Fall	**12.6706**	0	2.7512	1.89002

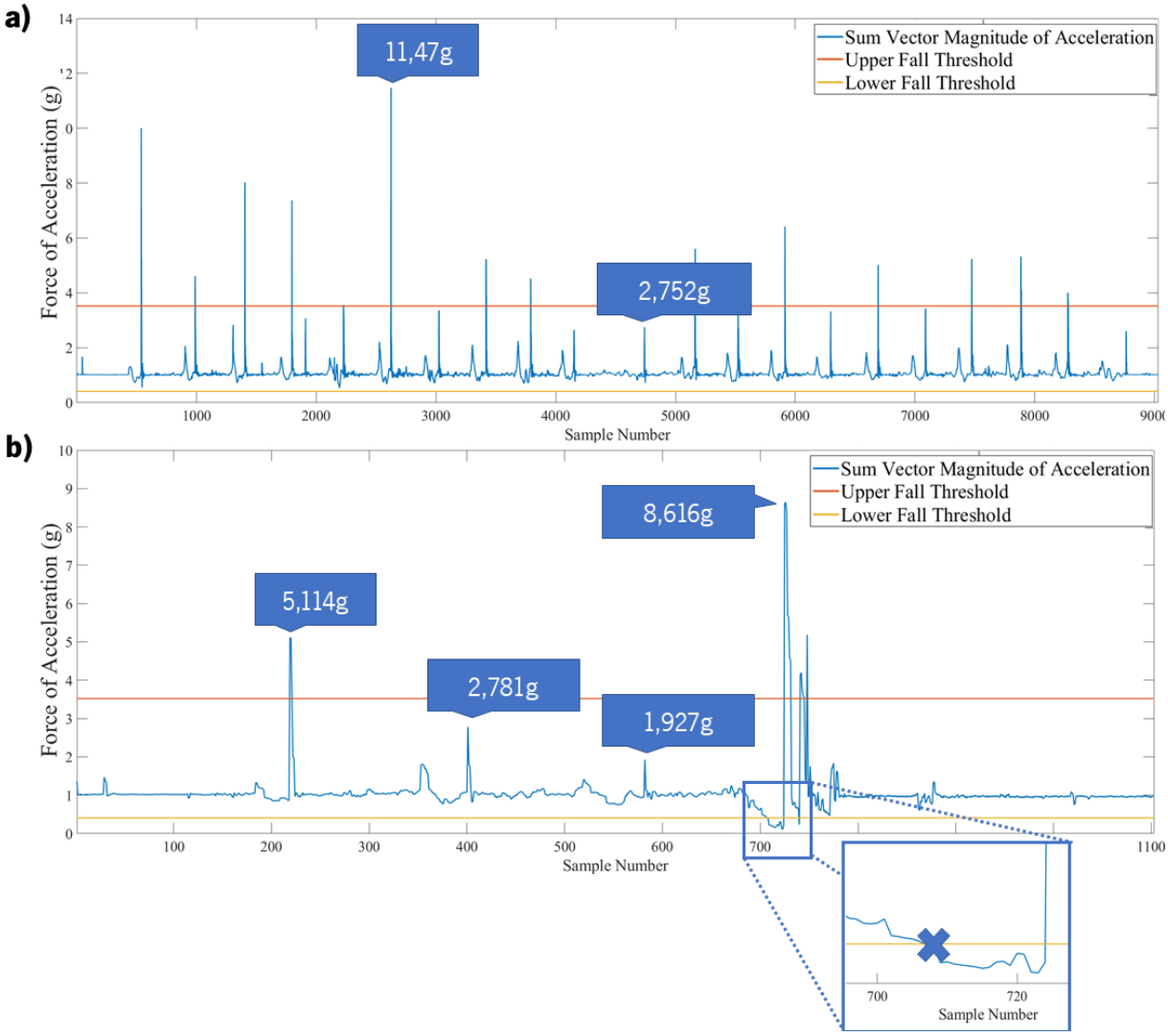

Figure 5.7: Sum Vector Magnitude for: a) One ADL trial; b) One intentional fall trial with the corresponding FD as a result of the lower threshold of 0.41g and the corresponding fall detection (blue X).

Table 5.6: Performance indicators of the FD algorithm proposed by Bourke et al. [134] tested only with a single lower threshold

Lower Threshold	ACC	PREC	SENS	SPEC	MCC	Kappa
0.41	0.9190	0.8815	0.9917	0.8222	0.8406	0.8312
0.2	**0.9781**	**0.9920**	**0.9690**	**0.9898**	**0.9559**	**0.9555**

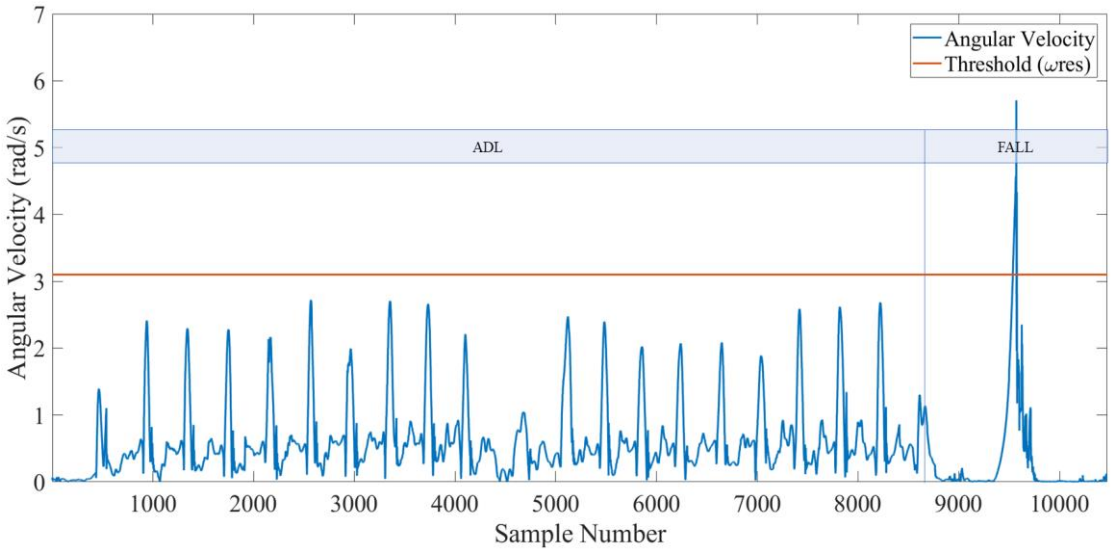

Figure 5.8: Angular Velocity of an ADL trial versus a simulated fall trial.

The algorithm present by Otanasap et al. [135], was also not able to detect ADLs. Consequently, an analysis of the feature's behaviour throughout the trials was accomplished (Figure 5.9) and the algorithm was tested with several different FT which results are indicated in Table 5.7.

Table 5.7: Performance Indicators of the FD algorithm proposed by Otanasap et al. [135] tested with different FT

FT	ACC	PREC	SENS	SPEC	MCC	KAPPA
7	0.8478	0.8444	0.9157	0.7455	0.6796	0.6756
7.2	0.8229	0.8488	0.9125	0.7679	0.6945	0.6914
7.4	0.8636	0.8750	0.8974	0.8148	0.7167	0.7163
7.6	**0.8837**	**0.9155**	**0.8784**	**0.8909**	**0.7648**	**0.7639**
7.8	0.8819	0.9104	0.8714	0.8947	0.7633	0.7624
8	0.8810	0.9206	0.8529	0.9138	0.7643	0.7619

5.6 Discussion

The algorithm introduced by Bourke et al. [134] considered a fall in almost all ADL trials, indicating that the original thresholds are not appropriate or adapted to canes considering that when the **cane hits the ground, there is a substantial increase in the SVM**, Figure 5.7 a), similarly to the trials of falls, Figure 5.7 b). Since the UFT is frequently surpassed when the cane hits the ground, contrarily to the LFT, Figure 5.7 a), the algorithm was tested with different lower thresholds. Consequently, the performance

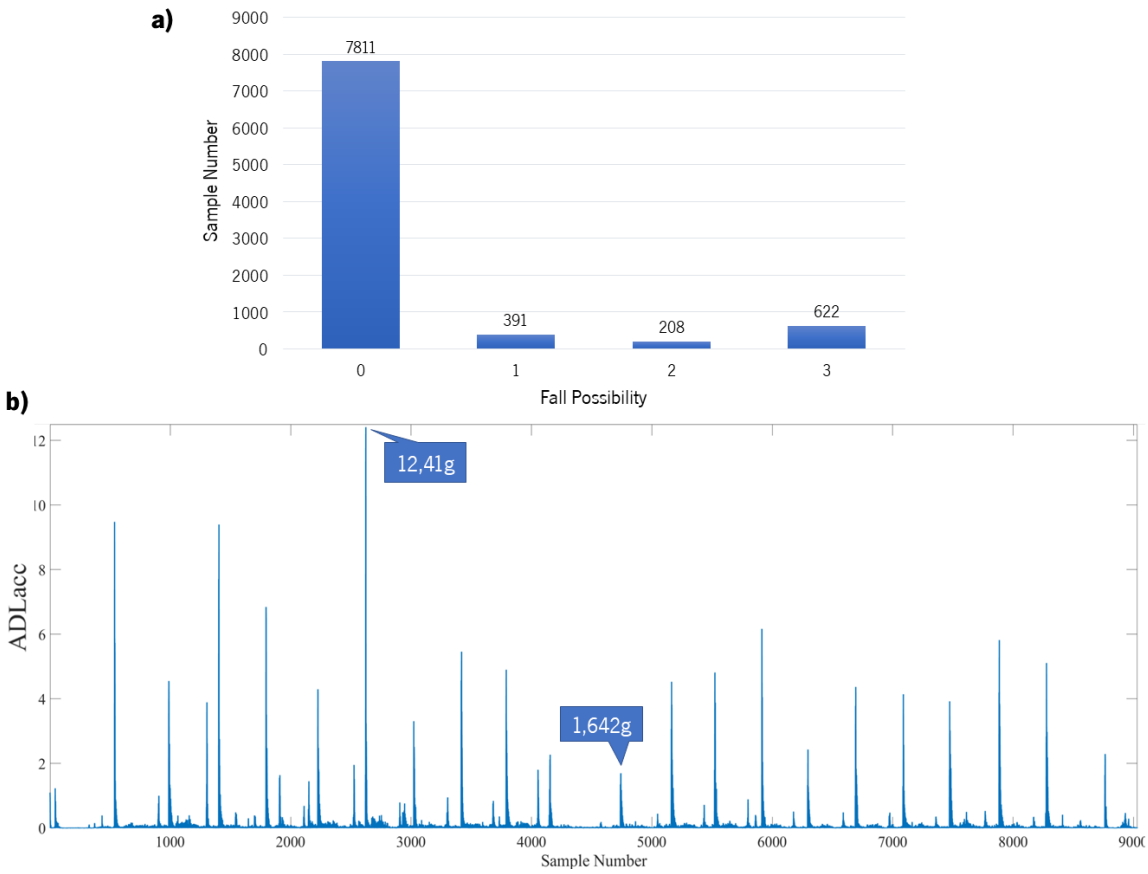

Figure 5.9: a) Fall possibility computed by the algorithm proposed by [170] during an ADL trial b) ADLacc of the same trial.

was significantly higher, in Table 5.6. Thus, the use of **UFTs with SVM on canes are not recommended** due to the problem mentioned above. This feature is directly related to the force applied to the cane for each strike with the floor, and it is different for every gait cycle (Figure 5.7 a)).

Regarding the study from Kangas et al. [51], none of the set of thresholds are suitable to canes. Both waist and head thresholds detect falls in almost ADL trials, and the wrist thresholds only detect a fall in 26% of the cases (Table 5.4). Considering that the five features used to evaluate the trial are accelerometery based, all of them will be affected when the cane hits the ground. Therefore, using this algorithm with the original thresholds is inefficient.

Since peak values of ωres for the recorded ADLs and falls are different (Table 5.5), the first threshold of 3.1 rad/s (ωres) is hardly ever surpassed, as can be seen in Figure 5.8, on one trial. Thus, the algorithm described by Bourke et al. [52] presented the best results among the fixed threshold FD algorithms. However, when **using a single lower acceleration threshold of 0.2g**, the ACC increased to **97.81%**, which is better than the results attained by the aforementioned algorithms.

Since the algorithm introduced by [135] is mainly based upon the ADLacc, it is expected a lower performance compared to the results stated in this study because this feature is accelerometery based.

As seen in Figure 5.9 b), during an ADL trial, the ADLacc surpasses the fixed threshold numerous times, as proven by the fall possibility computed and plotted in Figure 5.9 a). Thus, this method is not optimized for cane systems with the original FT. Consequently, the dynamic algorithm was tested with several different FT (Table 5.7). A new FT of **7.6g achieved the best performance**.

Class imbalance is a common problem faced in data mining due to imbalanced datasets [65]. In this situation, the number of samples from ADL is immensely more extensive than the number of fall samples with a proportion of 60:1. From Table 5.4, when the classifier was trained with an imbalanced dataset, it achieved an ACC of 99.13%. However, the classifier is overfitting the data. Afterwards, when the classifier was trained with a proportion of 1:1.6 (Table 5.4), the SENS improved by almost 40% in the three other cases. However, when using the RBF (Radial Basis Kernel) kernel, the best result in this domain was achieved with a SPEC and SENS of 96.60% and 83.47%, respectively. Comparing the MCC and KAPPA values from the implemented algorithms, the embedment of a single LFT of 0.2g is more desirable (MCC = 95.59%; KAPPA = 95.55%). This method surpasses the values of the machine learning implementation which has a range of MCC between 0.68 and 0.82 and a KAPPA between 0.69 and 0.82.

However, the best performance was achieved by the algorithm proposed by Bourke et al. [134] that was modified. With a single lower threshold of 0.2g, values of SENS, SPEC and MCC were 96.90%, 98.98% and 95.59%, respectively. Results obtained from the machine learning classifier were lower when compared to the proposed method likely because of the sample labelling method used, the CVFast. This method could be inappropriate for data acquired with a cane and may need to be improved. Thus, the proposed FD method is rather simple, with only a single lower threshold, which is suitable where restricted computational power will be available in the ASCane. Furthermore, it has been proven that ωres can also be an excellent variable to distinguish fall from ADLs. Although it was not evaluated, **coupling a ωres threshold with the 0.2 g lower threshold appears to be the best strategy regarding FD** since only the lower threshold may not be sufficient for a robust algorithm. Hence the need to be accompanied by another variable.

6. ASCane Event Detection in Controlled and Real-Life Situations

The main goal of this chapter is to **detect six cane phases through the ASCane during assisted walking**. A cane event detection system will be implemented and tested by comparing data acquired from an IMU attached to a cane and a ground truth.

This chapter will be subdivided into six major parts: i) Examination of how the cane's gait is related to the user's gait; ii) The human gait event detection algorithm found in literature; iii) Data collection from sensing devices through trials in healthy young people and feature computation; iv) Comparison between the detected cane events and the developed ground truth system; v) Comparison between the ground truth and several different combinations of machine learning classifiers and feature selection methods; vi) Post-processing algorithm for increased performance.

6.1 Relationship between gait assessment and fall risk

Using a cane is intended to help the user. However, research has shown this is not always the situation. Liu et al. [143] assess the usage of canes by older adults in senior living communities and revealed that **patients still fall**, **despite the help of their device**. Also, the research team revealed five significant problems that should be approached by the medical community: the need for medical consultation for device selection/use, the incorrect cane height/maintenance, the use of a cane in the wrong hand, the inability to sustain the proper gait pattern, and inaccurate posture during locomotion, which can improve the fall risk [144]. Furthermore, the use of an assistive device alters the users' spatiotemporal parameters, such as cadence, steps/min, step length, step time, stance and swing percentage [144].

Consequently, a **gait assessment describing cane usage while walking can provide valuable information** not only to the user, but also the medical professionals. This evaluation might be **capable of enhancing the capability of cane usage** for older cane users. Therefore, **reducing the possibility of possible falls** amongst them. Moreover, gait event detection can possibly be used in the rehabilitation domain, specifically, in the **design of personalized gait therapies** that tune therapeutic assistance in accordance to the patient-specific demands and strive to promote a more effective functional motor recovery. Several motion capture systems have been employed to evaluate human gait events. Most generally, this analysis is conducted in a motion analysis laboratory with force platforms and optical motion systems. Nonetheless, these motion capture systems are non-portable and are operated only in controlled environments. They are not optimized for the analysis of continuous gait cycles for long-term mobility situations. Thus, **embedding the detection of the different events into a cane is optimal** [145]–[147].

Before examining gait with a walking aid, it is necessary to understand the mechanics of what is perceived as a "gait cycle." The human gait is a rhythmic and standardised sequence of movements that end in a displacement of the person's COG [33]. A gait cycle can be described as a period separating the

initial contact of the foot with the floor until the instant that happens again. The human gait cycle can be divided into two different phases: stance and swing. The stance phase corresponds to the period in which the foot is in contact with the floor.

In contrast, the swing phase coincides with the time in which the foot is not on the floor [94]. However, the human gait cycle can be divided into several more phases. In the following, it is presented the description of all gait phases considered and are depicted in Figure 6.1 [1].

- Heel-Strike (HS): the event which equals to the first ground contact of the leading limb. By definition, a gait cycle ends and begins with the HS;
- Foot-Flat (FF): when the plantar surface of the foot contacts with the ground, thus, the leading limb can take over the bodyweight;
- Middle Mid-Stance (MMST): begins when the opposing foot elevates and continues till the bodyweight is aligned over the forefoot;
- Heel-Off (HO): the moment which the heel lifts from the ground;
- Toe-Off (TO): corresponds to the moment in time that the foot leaves the ground;
- Middle Mid-Swing (MMSW): phase in which the swinging limb passes the opposite stance limb.

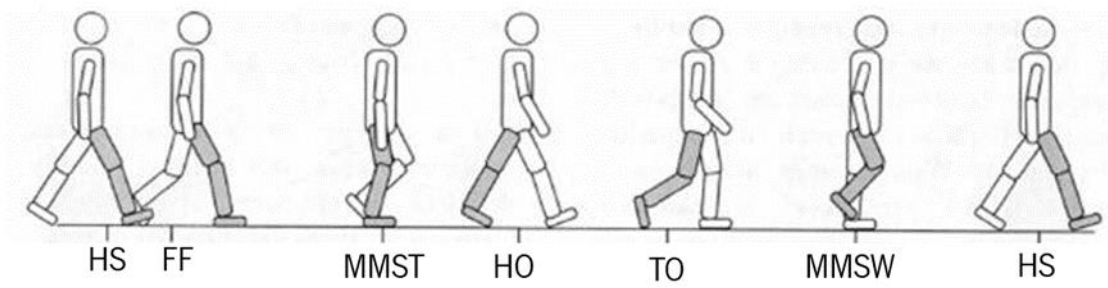

Figure 6.1: Human gait phases and corresponding events during one gait cycle.

6.2 Ambulation with a cane

For proper locomotion with a cane, the device must be used on the opposing side of the affected leg and in tandem with it to simulate normal gait and to improve balance. Moreover, there are two ways of walking with a cane, two and three-point gate [148]. The sequential moves of two-point gait are listed below, and their representation is portrayed in Figure 6.2.

1. Balance the body weight onto the healthy or unaffected leg (Figure 6.2 - Stage 1);
2. Move the cane and the affected leg forward in unison, keeping the cane near the body to prevent leaning to the side (Figure 6.2 - Stage 2);

3. Transfer the bodyweight forward to the cane and move the unaffected leg forward (Figure 6.2 - Stage 3).

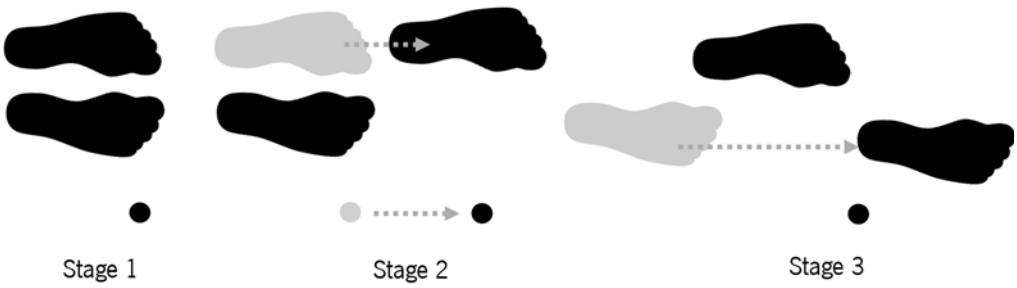

Figure 6.2: Representation of Two-Point Gait with a cane.

The consecutive movements of three-point gait are depicted in Figure 6.3 and are as follows:

1. Balance the body-weight on the strong or unaffected limb (Figure 6.3 - Stage 1).
2. Move the cane forward, assuring the cane is close to the body (Figure 6.3 - Stage 2).
3. Move the weak or affected foot forward (Figure 6.3 - Stage 3).
4. Transfer the weight from the unaffected foot to the affected foot and cane, and then brings the unaffected foot forward to join the affected foot (Figure 6.3 - Stage 4).

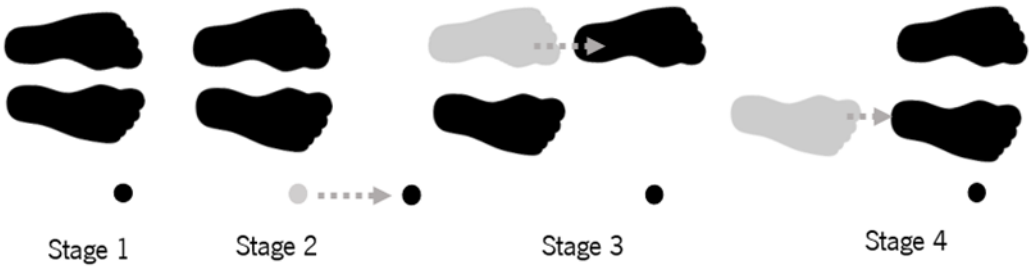

Figure 6.3: Representation of Three-Point Gait with a cane.

Ambulating with two-point gait, the cane accompanies the opposite leg movement. Consequently, both gait events (foot and cane) occur approximately at the same time. Following, the six different cane events are described and matched to the human gait cycle phases previously described in Section 6.1, as seen in Figure 6.4.

- First Ground Contact (FGC): the event which equals to the first ground contact of the cane. Similar to the human gait cycle, the cane gait cycle ends and begins with the FGC;
- Full Base Contact (FBC): when the cane base is in complete contact with the ground;
- Maximum Support Moment (MSM): begins when the cane is in full support of the subject's body weight;
- Partial Cane Off (PCO): the moment which the cane lifts from the ground;

- Full Cane Off (FCO): corresponds to the moment in time that the cane base lifts entirely from the ground;
- Cane MidSwing (CMSW): phase in which the swinging cane passes the opposite stance limb.

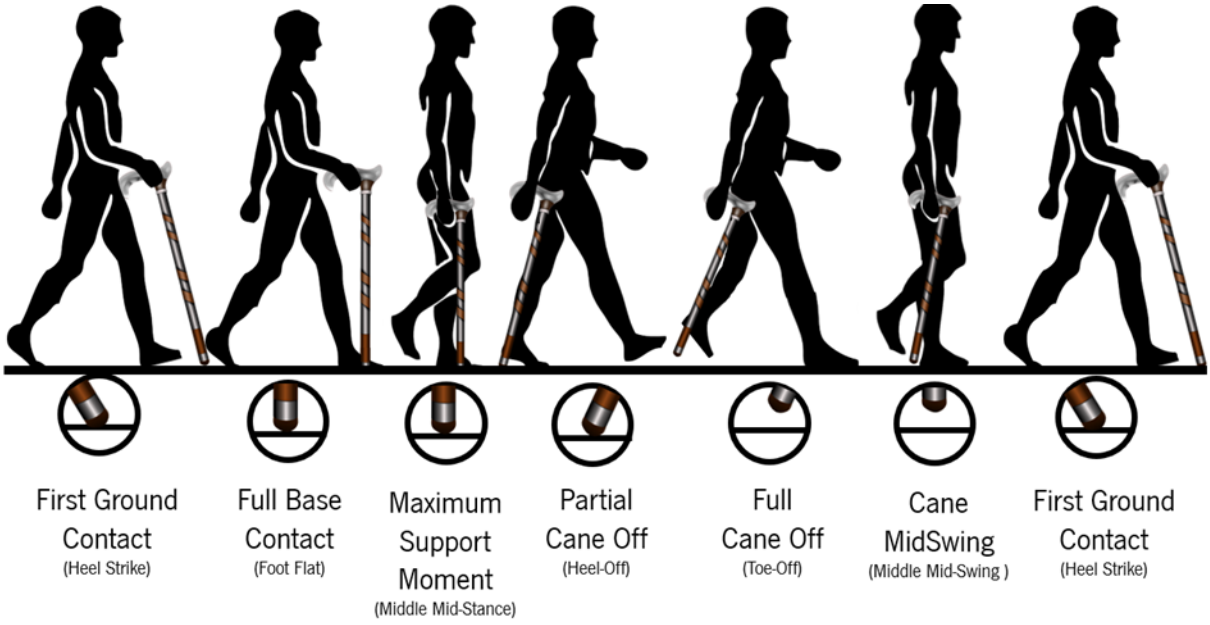

Figure 6.4: Human gait phases matched to the respective cane phases during one gait cycle.

6.3 Real-time gait event detection

The difficulty of gait detection is the development of algorithms that can detect gait events while the subject is walking (real-time detection). Various sensor arrangements have been employed for gait detection in ambulatory settings, including single and multiple sensor arrangements. Three types of measurements are found in the literature for gait event detection: force, angular rate and accelerometery based measurements [1].

Regarding force-based measurements, the single possible location for these types of sensors is between the sole and the ground. Regarding cane event detection, the placement of the sensor is in the tip of the cane, which has a minimal surface area. Thus, just one sensor could be installed, and only the stance and swing phases could be determined. Typically, these types of systems provide adequate results. Still, they present a few disadvantages. For example, specifying load changes produced during walking from those created by weight shifting is not possible. Nevertheless, force-based event detection either

with sensors attached to the foot or even with force plates is yet part of the ground truth system for computation of the accuracy of gait event detection in newly developed methods [1][149].

Usually, the use of accelerometers entails extra signal processing techniques and compensation regarding the influence of gravity. Additional drift problems can be present due to the integration of the acquired data. The corresponding attachment of the sensors can also be a difficulty considering muscle movement while walking, appearing as a high-frequency error in the data [1][150][151].

Most of the algorithms using angular rate measurements use the same one-dimensional angular rate sensor in a single sensor solution. The significant advantage of using gyroscopes as motion analysis systems is that it is not affected by the gravitational component as the accelerometery based systems. Additionally, the vibration subjected by the sensors through the heel strike does not alter the gyroscope output since they are less susceptible to their position as a result of their measurement principle. They can be anyplace on the same plane giving nearly an equal signal output. Besides, movements in other planes are not taken, e.g. change in walking direction [1][149].

For real-time human gait event detection through the foot angular velocity, it is possible to detect the previous gait events described. In Figure 6.5 is presented the angular velocity of the foot through one gait cycle with the corresponding gait events delimited [152].

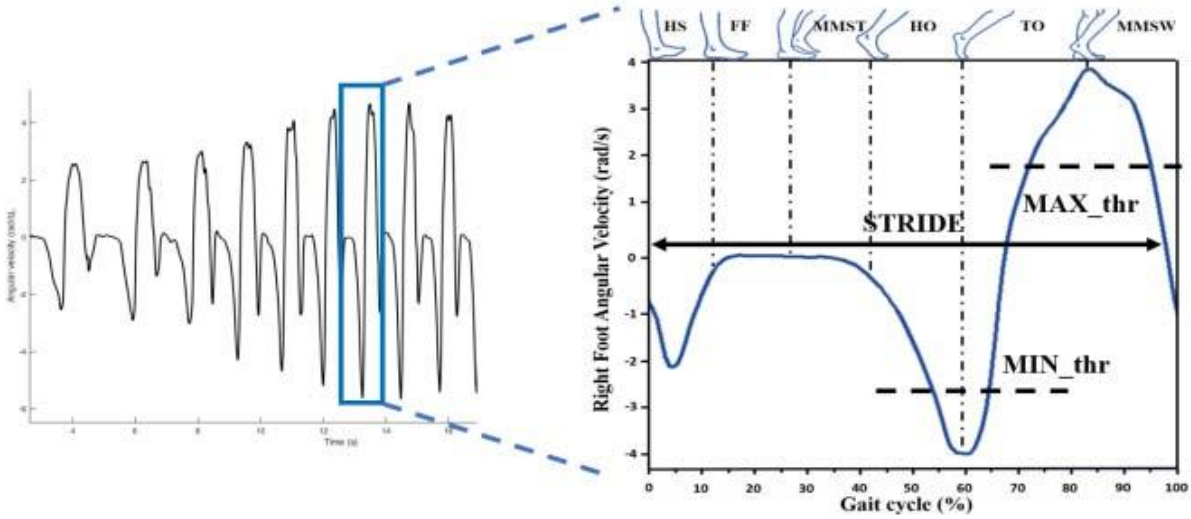

Figure 6.5: Angular velocity of the right foot along the sagittal plane (sensor's z-axis) (continuous line) and representation of six human gait events (HS, FF, MMST, HO, TO, and MMSW) during one gait cycle performed by a healthy subject, taken from [152].

Figueiredo et al. [152] developed an **adaptive rule-based FSM for human gait event detection in controlled and real-life situations** that can operate at various gait speeds and relies only on the **angular velocity of the sagittal plane**. The proposed method was proven to be an accurate (ACC > 90.12%), time-effective (delay detection < 30.53 ± 9.88 ms and advanced detections <

15.31 ± 5,52 ms), low-cost, wearable, and with a low-computation power towards real-time gait analysis. Therefore, it can be used either in rehabilitation tasks and gait assessment [152]. Based on curve tracing techniques, threshold crossing, local extrema and signal derivatives evaluation, the authors established decision rules for gait events transitions. The flowchart of the abovementioned algorithm is presented in Figure 6.6.

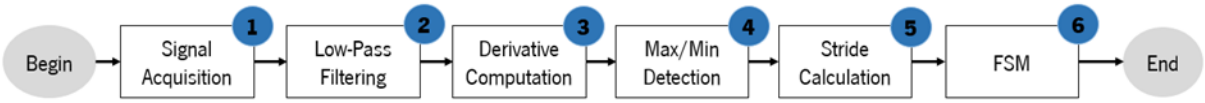

Figure 6.6: Flow chart of the proposed algorithm to detect the gait events

After the signal acquisition and respective filtration (First and second stages, Figure 6.6), the first derivative is computed which enables the detection of velocity increases (positive signal), decreases (negative signal) or constant velocity (approximately zero). To detect only the significant variations (that usually are correlated with the local peaks), derivatives under a threshold (near zero) are fixed to zero, reducing the signal noise (Stage 3 – Figure 6.6). The minimum/maximum calculation stage (Stage 4 – Figure 6.6) is utilised to recognise HS, MMSW, FF, and TO, given their dependence to the local extrema. The 5th stage computes the given steps step calculation using the last three valid steps, which enables the algorithm to be sensitive to changes in the pattern. The last stage implements the FSM that changes states per defined decision rules.

6.4 Methods And Materials

6.4.1 General Overview

The proposed methodology used for recognition of cane's events during gait is comprised of several steps. A schematic overview of the accomplished approach is highlighted in Figure 6.7. After the experimental trials and manual segmentation per pre-defined conditions, this chapter is subdivided into two sections. Firstly, the **modification of an adaptive state-of-the-art FSM human gait event detector** to detect the six cane gait events was accomplished. Secondly, a **machine learning study** was performed to find which are the best set of features and machine learning classifier to segment a cane stride in six phases. In the following subsections, a full description of each module is given, together with the explanation of the work developed.

6.4.2 Experimental Protocol

To collect sensor data during locomotion, experimental procedures were conducted, following a designed protocol. The system used to collect the data was part of the one described in Chapter 4. Since the algorithm designed by Figueiredo et al. [152] used angular velocity from the foot, an IMU was also placed in that same location.

Furthermore, to achieve a complete study of cane ambulation and to link the different gait phases with the recorded angular velocity and acceleration, another inertial measurement system was coupled, the MTw Awinda (Xsens Netherlands). The developed system (without Xsens) is depicted in Figure 6.8

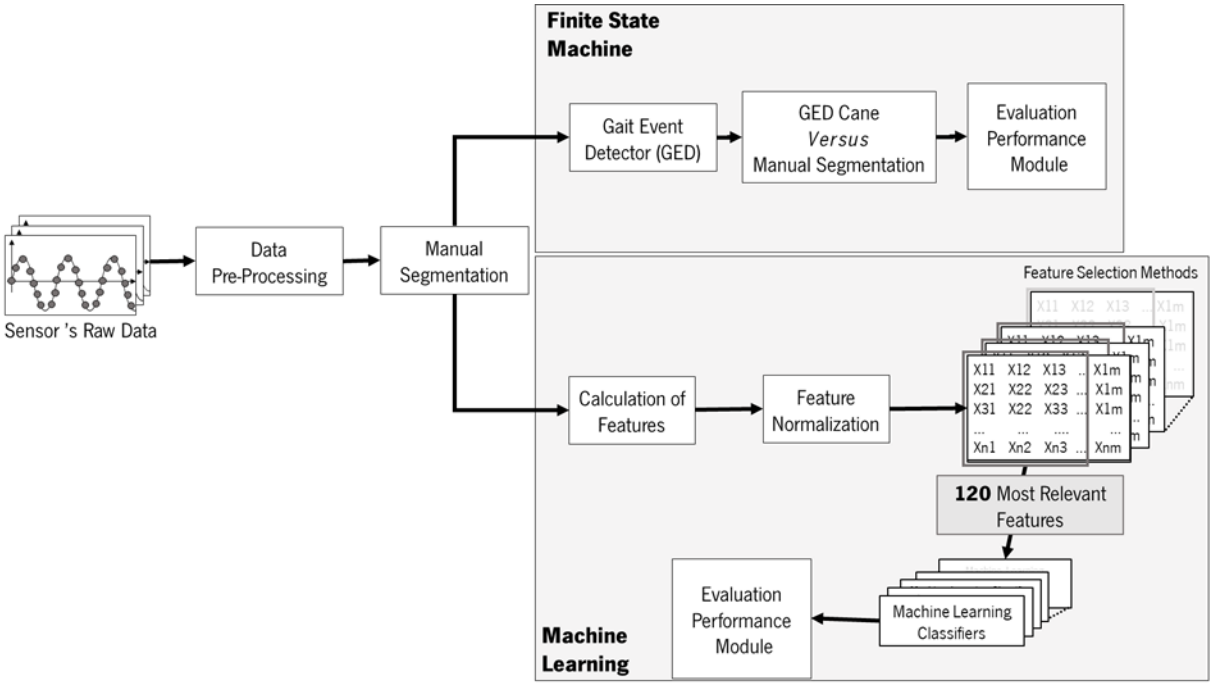

Figure 6.7: General Overview of the carried-out methodology for the detection of canes gait events

For the validation of the gait event detector, it was used repeated measures of healthy gait patterns recorded in controlled and real-life situations, as portrayed in Figure 6.9. Fourteen subjects were included in two protocols, one for each condition. The subjects approved to participate in this study and were randomly distributed within the two protocols.

Considering the **controlled walking situations**, to validate cane event detection and to test the effect of variations in the ground surface and gait speed it was included seven healthy volunteers (five males and two females). The subjects presented an age which ranged from 22 to 25 years (23.29 ±1.16 years), with a body mass between 52 and 81 kg (69.57 ± 9.06 Kg) and a height of 1.51 to 1.81 m (1.70 ± 0.09m). The participants carried walking experiments on an instrumented split-belt treadmill at different speeds (1.0 and 1.5 km/h) and slopes (0%, and 10%). Three gait trials were randomly conducted for the

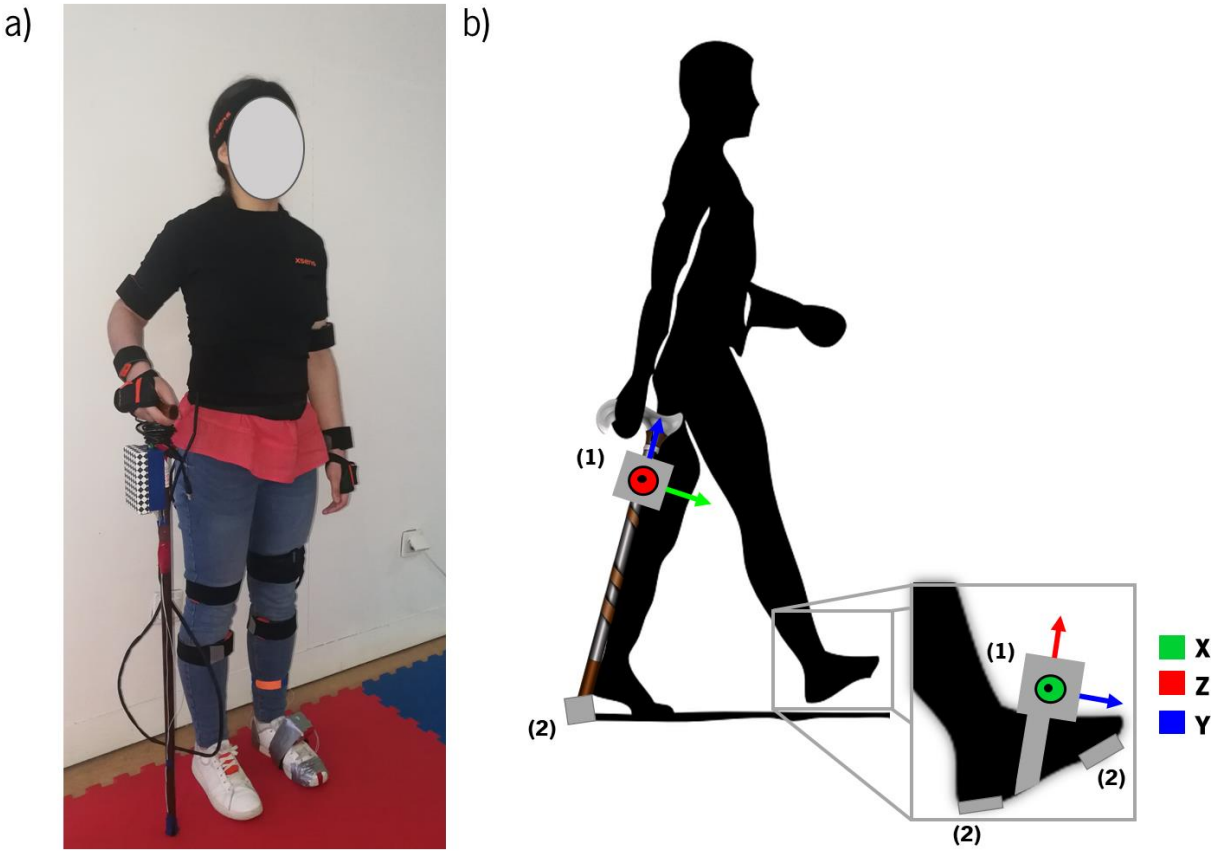

Figure 6.8: A) Subject equipped with all systems B) Developed system used during data acquisition (1) IMUs; (2) FSRs.

following scenarios: 30 seconds walking without inclination and speed of 1.0 km/h and 30 seconds walking with an inclination of 10° and speed of 1.0 km/h. Besides, the participants were told to carry walking trials at changeable speeds to approximate a real-life environment. In this case, the subjects walked for 60 seconds and changed gait speed every 20 seconds according to the provided instructions (increasing from 1.0 km/h to 1.5 km/h and decreasing from 1.5 km/h to 1.0km/h). To give reliable results, the acceleration period was not admitted in the detection of gait events, except for the trials where the speed was variable.

Real-Life Walking Situations were also considered to assess human locomotion in various conditions. For this matter, it was included seven healthy subjects (five males and two females), who used their sports-shoes). The subjects presented an age which ranged from 23 to 25 years (24.14 ±0.83 years), with a body mass between 61 and 75 kg (70.85 ± 5.25 Kg) and a height of 1.70 to 1.81 m (1.75 ± 0.04m). Since human gait is very dynamic in the real-world frequently, including different gait speeds, surfaces and surface inclinations, the recommended computational method was verified in uncontrolled indoor and outdoor conditions. Three gait trials were randomly conducted for the following scenarios, which are shown in Figure 6.9: forward level-ground walking on a 20 m flat surface; forward level-ground

walking on a rough surface (urban ground) along 30 m; descending and ascending an inclined ground (approximately 10°) and a 10 m rough surface, and climbing a staircase of 8 steps with standard dimensions (a height of 17 cm, depth of 31 cm, and step width of 110 cm). For each condition, the participants were asked to walk at a comfortable speed to achieve proper ambulation with a cane.

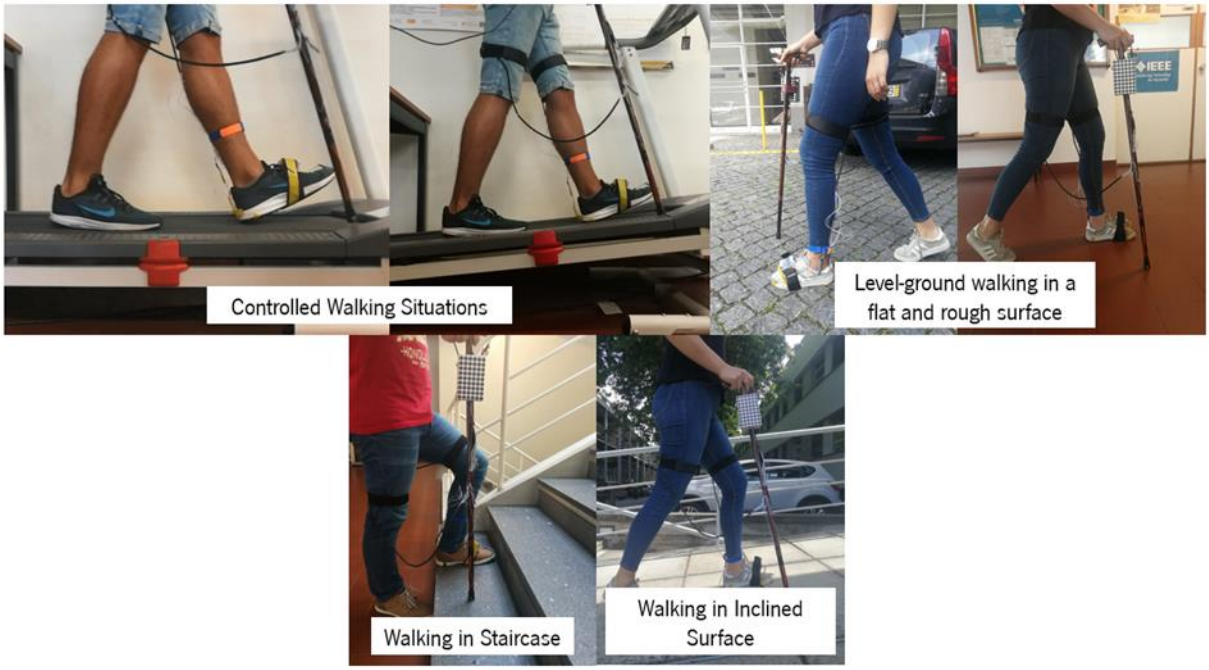

Figure 6.9: Validation of the gait event detection system under controlled and real-life walking conditions (flat and rough level-ground, inclined surfaces and staircases).

6.4.3 Data Labelling

The gait event detection algorithm developed by Figueiredo et al. [152] relies only on the foot angular velocity. Comparing the mean and mean plus/minus standard deviation of the cane and foot angular velocity of all collected strides (for controlled situations), as depicted in Figure 6.10, it is possible to conclude that the **waveform of the signals throughout the stride presents several key differences**. The two minimums, Figure 6.10 a) and c), which are used to detect the HS, MMSW, FF and TO events, are not as significant (FGC, CMSW, FBC and FCO for the cane events, respectively). The angular velocity reached by the ASCane, Figure 6.10 b) is not as steady at 0°/s as the one achieved by the foot, which is part of the decision rules for FF and MMST detection. Furthermore, the peak value in the gyroscope signal, which happens at the moment of MMSW, is also not as high as the one achieved by the foot, Figure 6.10 d). Consequently, **to accomplish precise data labelling, additional signals and/or features are needed**. To keep the segmentation as simple as possible, only the raw signals collected from the ASCane were used.

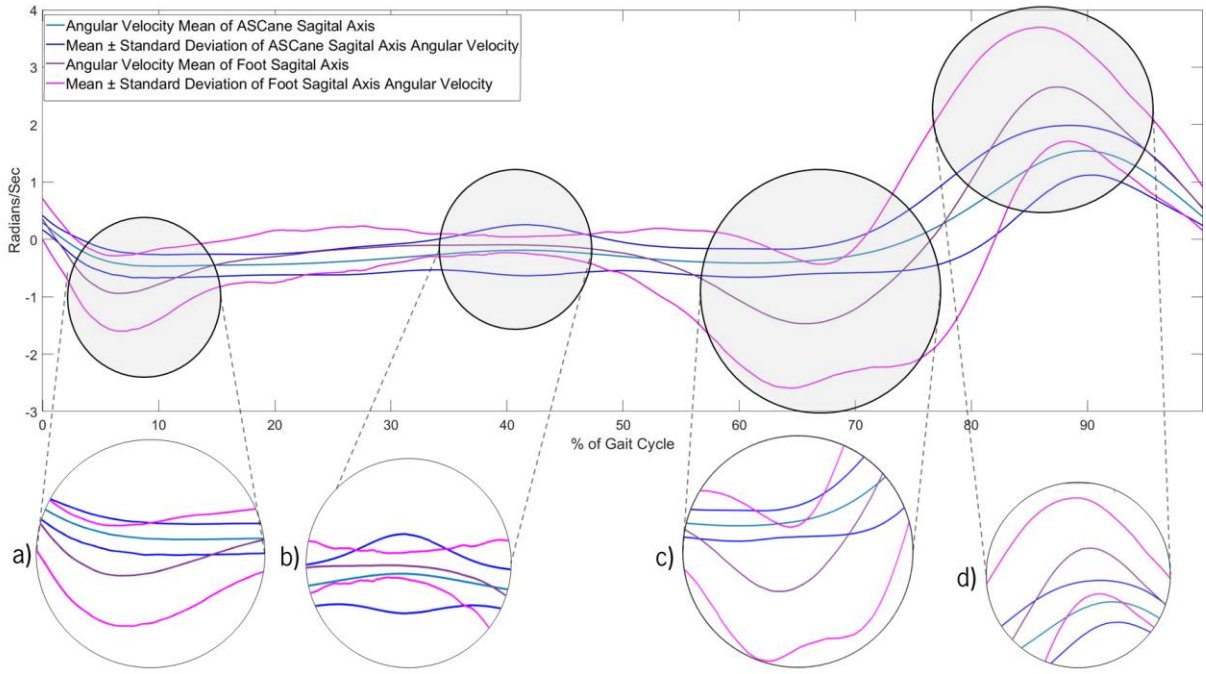

Figure 6.10: Cane angular velocity along the sensor's z-axis (moves relatively to the sagittal plane) mean, and plus/minus its standard deviation of all collected strides measured at controlled situations.

The Xsens company developed a robust software engine using a biomechanical model of the human body to estimate human motion in real-time accurately. The biomechanical model, Figure 6.11, is composed by 23 segments: pelvis, L5, L3, T12, T8, neck, head, right and left shoulder, upper arms, forearms, hands, upper legs, lower legs, feet and toes. Moreover, for the segments where no sensor is attached, the kinematics are determined based on the biomechanical model combining stiffness parameters between connecting segments. In addition to the standard configuration abovementioned, additional motion trackers can be added to items to be included in the trial, for example, a walking stick, as shown in Figure 6.11.

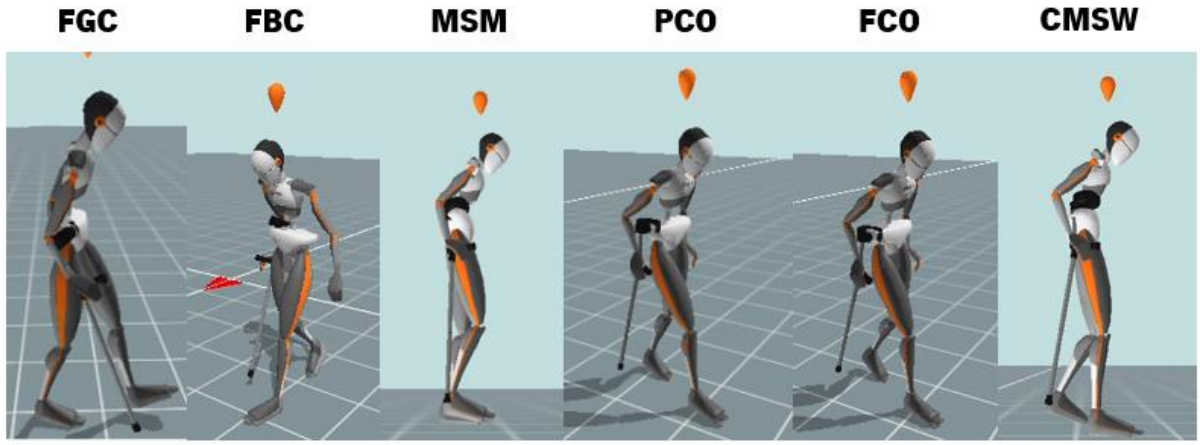

Figure 6.11: Biomechanical model of human body ambulation with a cane through the different gait phases.

To properly segment gait events, **the algorithm must incorporate the acceleration and FSR signals**. In Figure 6.12 and 6.13 are portrayed the mean, and the mean plus/minus the standard deviation of the ASCane FSR and acceleration (transverse plane) signal for the four different walking situations assessed, respectively. It is verified that both acceleration and FSR signals **present a constant waveform on level-ground, inclined surfaces and staircases**.

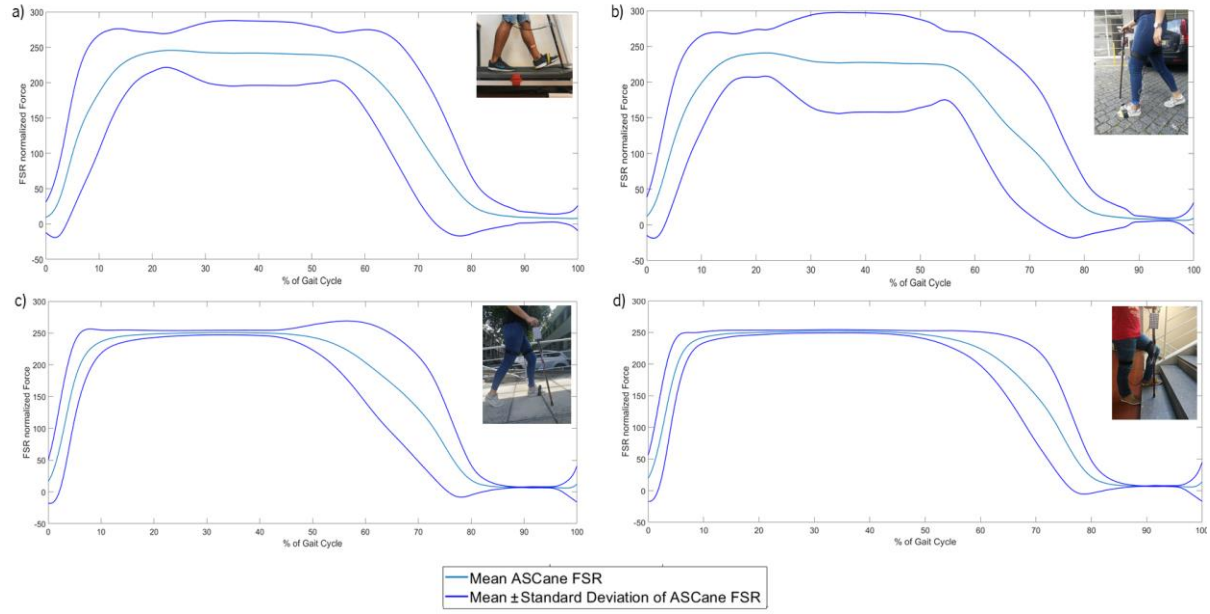

Figure 6.12: ASCane FSR reading along the sensor's z-axis (moves relatively to the sagittal plane) mean, and plus/minus its standard deviation of all collected strides measured at different ground facets: A) controlled situations, B) level-ground, C) inclined surface (10°), D) staircase.

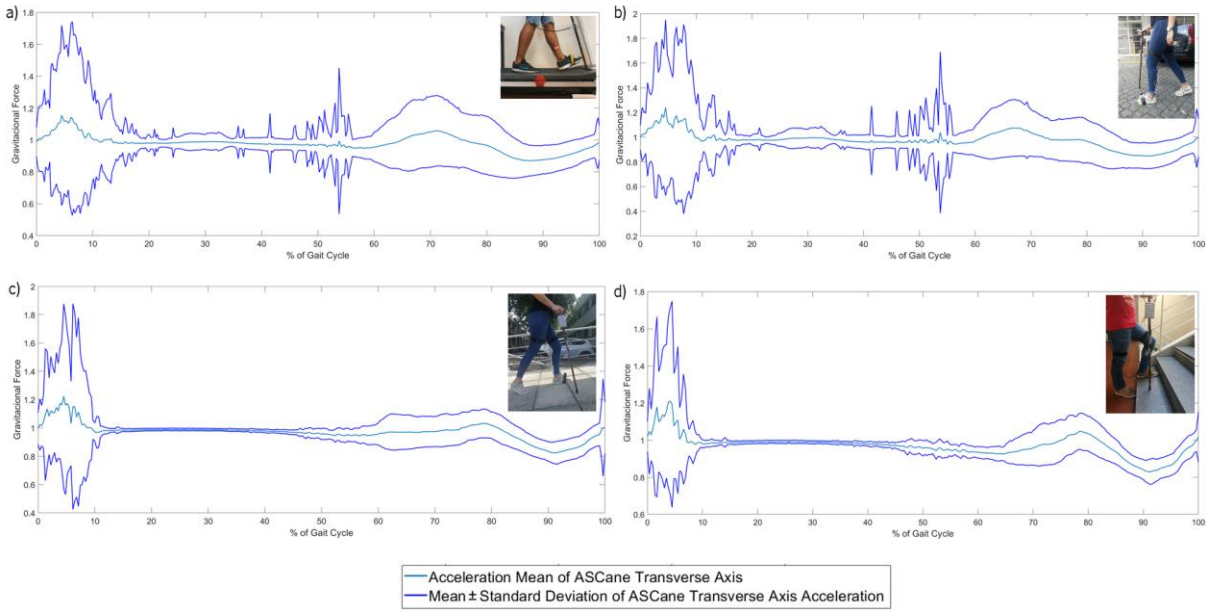

Figure 6.13: ASCane acceleration along the sensor's Y-axis (moves relatively to the transverse plane) mean, and plus/minus its standard deviation of all collected strides measured at different ground facets: A) controlled situations, B) level-ground, C) inclined surface (10°), D) staircase.

After an extensive analysis of all the seven signals acquired, it was possible to achieve the decision rules for the ground truth of all the 1620 steps taken. More specifically, 962 controlled steps, 234 steps on a flat surface, 161 steps on rough ground, 151 steps on inclined terrain, and 112 steps on staircases.

First, it was verified that the cane acceleration and **angular velocity presented a constant waveform on level-ground, inclined surfaces and staircases** (Figure 6.14). Therefore, the same heuristic rules can be established for all different scenarios.

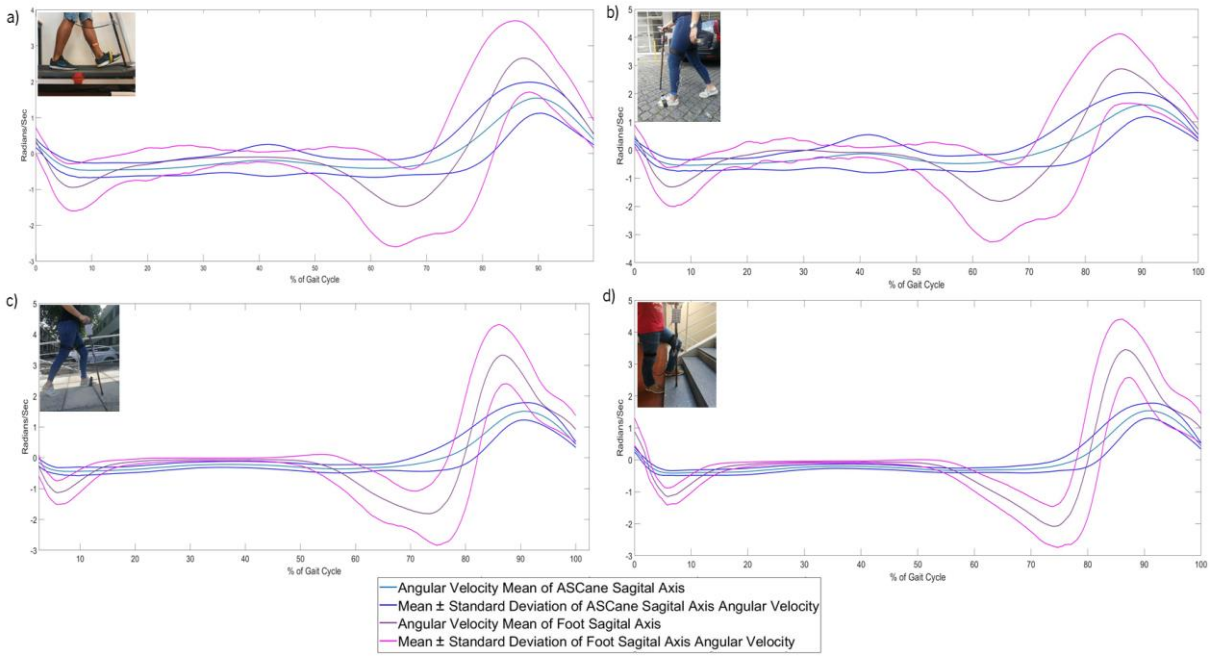

Figure 6.14: Cane angular velocity along the sensor's Z-axis (moves relatively to the sagittal plane) mean, and plus/minus its standard deviation of all collected strides measured at different ground facets: A) controlled situations, B) level-ground, C) inclined surface (10°), D) staircase.

When the cane impacts with the ground, an intense polarity inversion of the acceleration vector is detected as well as an increase in the FSR reading, which is used to determine the exact moment of the FGC. FBC is set at the moment were the FSR reading stabilizes at is maximum. The ground truth for the MSM event was set when the acceleration oscillates, and the data from the ASCane FSR remains at is maximum, which corresponds to the moment where the subject transfers his bodyweight to the cane and moves the unaffected leg. PCO and FCO events, the user is lifting the cane to move it along with the affected leg. Therefore, for the PCO, the FSR signals starts decreasing. Concerning the FCO, the FSR signal continues decreasing until zero and, the acceleration increases due to the cane is beginning to swing. The CMSW is determined as the maximum angular velocity detected in the stride after the FCO detection. A complete segmentation of a stride with all the features used is exposed in Figure 6.15.

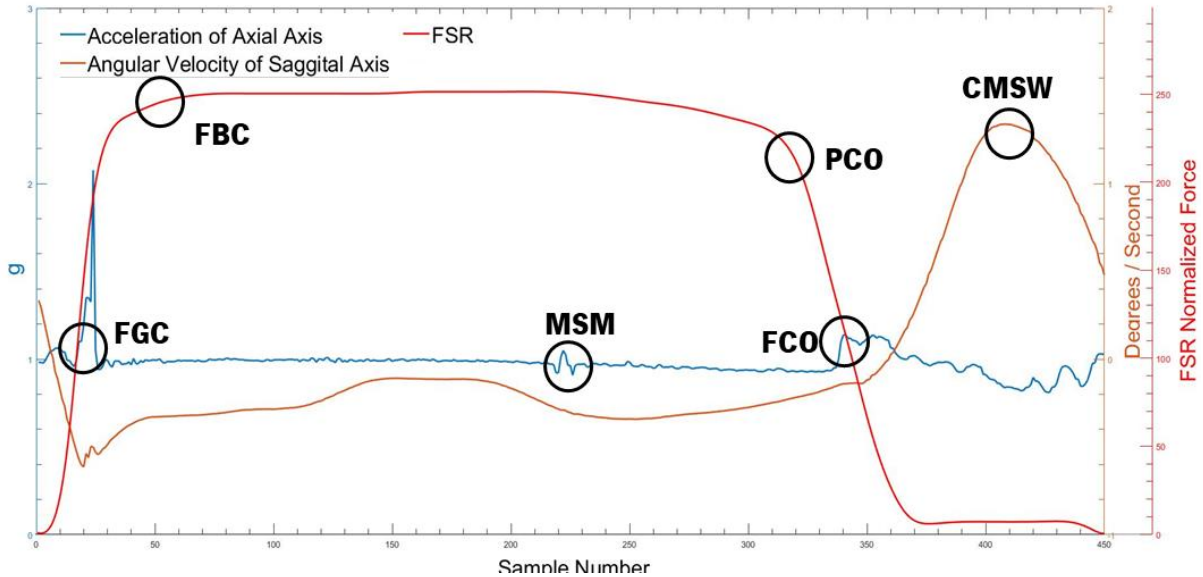

Figure 6.15: Acceleration (moves relatively to the transverse plane), angular velocity (moves relatively to the sagittal plane) and FSR signals of a full cane stride with corresponding gait events manually segmented per pre-defined conditions.

6.4.4 Finite-State-Machine Framework

As stated, the cane angular velocity throughout a stride is less prominent than the one from the foot. Nevertheless, the algorithm was tested with the data acquired with the cane. However, after an extensive inspection of the algorithm decision rules and signal processing techniques, **two modifications were accomplished**.

Figueiredo et al.[152] use two distinct thresholds as a part of the decision rules to detect the TO and MMSW event, *MINthr* and *MAXthr*, respectively. The *MINthr* corresponds to an adaptive threshold used for the detection of the second minimum. Contrarily, the *MAXthr* is used to determine the maximum angular velocity reached during the stride. In the original algorithm, both these thresholds are defined as 60% of the mean value of the three previous detected minima and maxima, respectively. Since the new signal is not as distinctive, **the condition was updated for 40%**. As asserted, the algorithm also relies upon signal derivatives. A pre-processing technique in which if the signal first derivative is lower than 0.01, the derivative is considered null was accomplished Figueiredo et al. [152]. To increase the efficiency of the algorithm, and since the FS of the ASCane signal is much higher, this **pre-processing technique was discarded**.

6.4.5 Machine Learning Framework

In this stage, the pre-processing techniques are applied to the unprocessed acquired data to maximize model performance and decrease its training time. The pre-processing methods used involve **data normalization and feature selection**.

The computation of features is not only required for the creation of machine learning models but also for future online classification. In fact, after gathering all the sensor data from the ASCane, it is essential to create a vector of features for every time window of the measured signals. They should be significant and representative of the data to have the needed information for correct classification, which is disclosed in chapter 2. All the computed features are listed in Table XXIV – Appendix 3. This module converts the input data to an output feature vector containing 288 features (Figure 6.16).

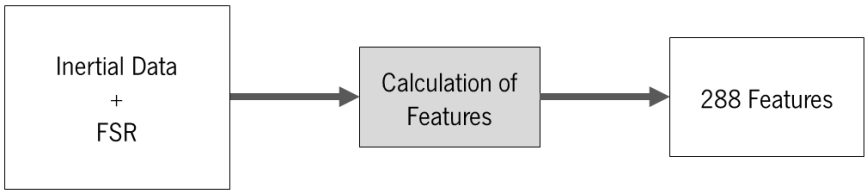

Figure 6.16: Inputs and outputs of the feature computing module

Throughout data normalization, features are treated using the **min-max scaling method**, as illustrated in Figure 6.17. This process intends to convert all metrics to a standard range such that features with a higher value range do not decrease the significance of features with smaller ranges. It changes the values of each feature, which means that the data is centered in 0.5 and is limited to **vary between 0 and 1.**

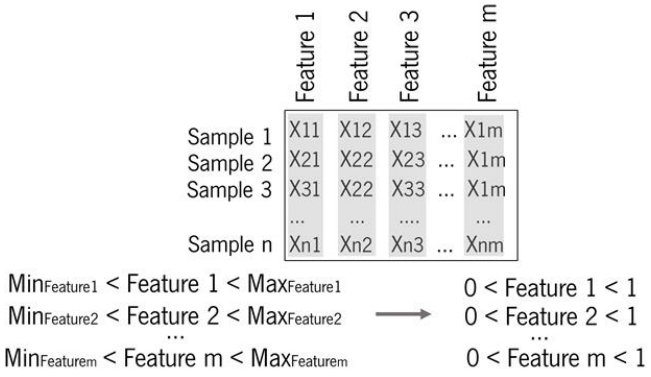

Figure 6.17: Feature normalization method used.

The selection of an optimal subset of features is an essential step in every classification challenge. Often, a considerable number of features are computed to represent the target concept better. Given this set of **288 features**, the problem is to select the subset of size *x* (with *x* being the number of features)

that maximizes a scoring function of a given classifier. Since the classification of six different gait phases of a cane was never accomplished, the best subset of features is yet to be uncovered. Thus, **8 feature selection methods were used**: Correlation Based Feature Selection (CFS), Relief, Unsupervised Discriminative Feature Selection (UDFS), Principal Component Analysis (PCA), Least Absolute Shrinkage and Selection Operator (LASSO), Laplacian Score, Unsupervised Feature Selection with Ordinal Locality (UFSOL) and Local Learning-Based Clustering Feature Selection (LLCFS), as seen in Fig 6.18.

Various classification algorithms in machine learning have been used to predict and classify different human gait phases in recent research. Yet, none of them is applied to canes. Building an accurate classifier is challenging for several reasons. If the training set is small, then it is less feasible to understand the underlying distribution of the data.

Another problem is the complexity of the model and its generalizing abilities. If the classifier is too dull, it may fail to seize the underlying structure of the data. However, if the classifier is too elaborate and there are too many free parameters, it may include noise in the model, which leads to overfitting performing poorly on test samples. The **9 machine learning classifiers** used were the KNN, with an equal, inverse and squared inverse distance weighting function; Discriminant Analysis Classification with linear and quadratic discriminant function; Ensemble Learning; Decision Tree and Regression Model with linear and pure quadratic terms.

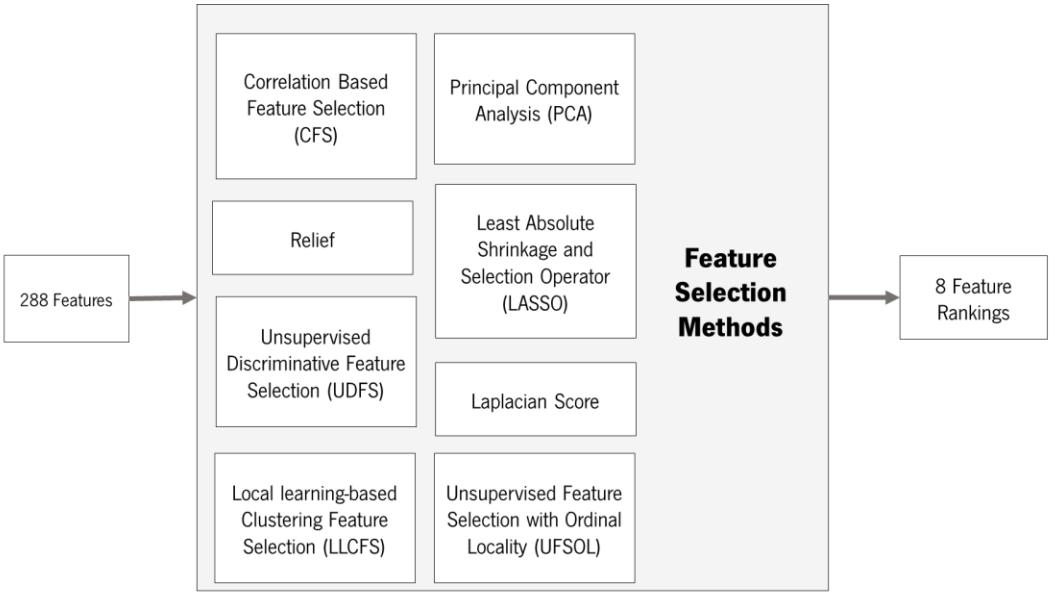

Figure 6.18: Inputs, outputs and the different feature selection methods used in the feature selection module.

To cover all possible scenarios, a **3-stage process was achieved**. With the first stage, an incremental feature method **combining all feature selection methods and machine learning**

classifier scenarios was performed. For example, with PCA as the feature selection method, and ensemble learning as the classifier, the machine learning model was built and tested with one up to the 120 most discriminate features. For the second stage, the two most suitable combinations were tested once again, this time with **increased j-k-fold CV**. The machine learning models presented in this work were built and tested offline using Matlab® (2018b, The Mathworks, Natick, USA). Nevertheless, their implementation in a microcontroller will be discussed in future challenges. Both studies are depicted in Figure 6.19.

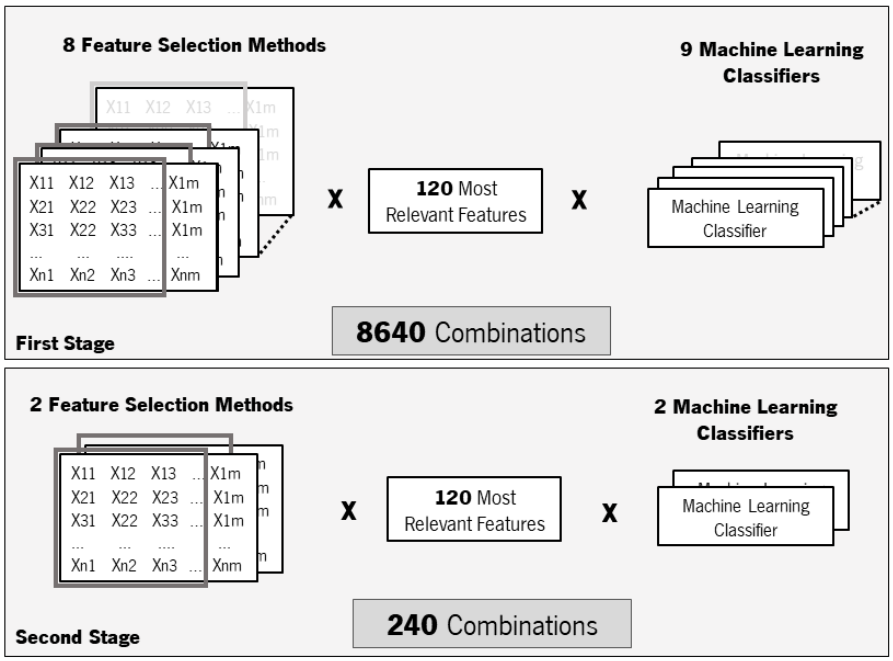

Figure 6.19: The different combinations of feature selection methods, number of features and classifier tested for the first and second stage.

The third and last stage involved **an online post-processing algorithm** of the machine learning classifier results (Figure 6.20). Firstly, the classifier was **tested with unseen data** to test its predictive power, more specifically, 9 full trials (3 of controlled situations and 2 of each remaining walking condition). Secondly, a post-processing algorithm was applied to the same results and benchmarked against the classifier results.

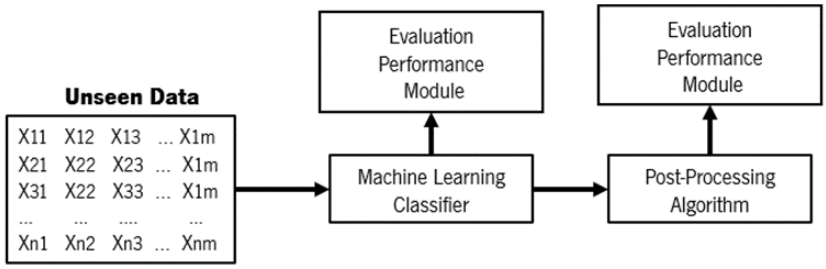

Figure 6.20: Completed methodology for the third stage.

Firstly, all the gait event transitions are found. The algorithm starts by detection the first transition from first ground contact (phase 1) and will iteratively find the next ones. In case a transition is not found, the algorithm will try to find a transition overleaping the one not detected. It will always verify if the new found transition occurs after the last one identified. In the end, a gait event detection transition list is exhibited, and the signal samples between them are set. Which means, for example, that the samples between the transition MSM (phase 3) to PCO (phase 4) and PCO (phase 4) to FCO (phase 5) are set as PCO. The algorithms flowchart is presented in Figure 6.21.

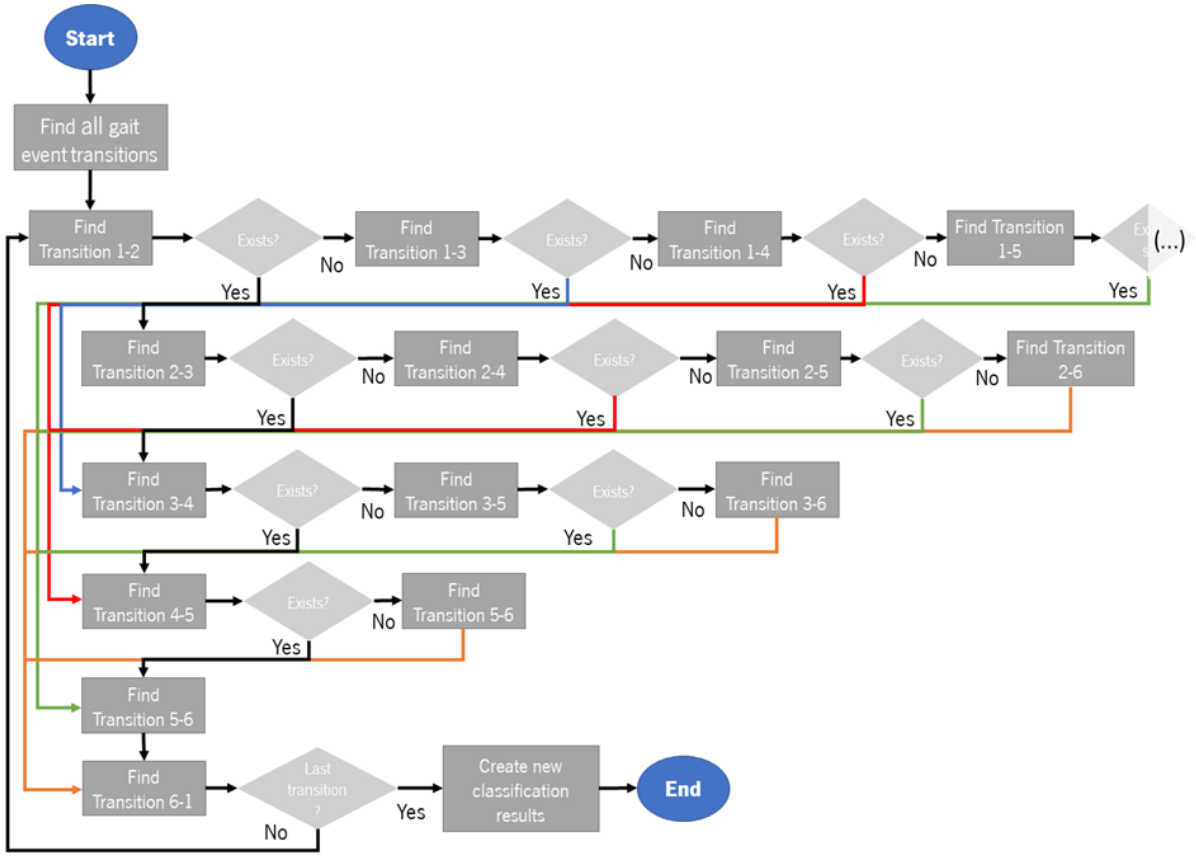

Figure 6.21: Flowchart of the post-processing algorithm developed for increasing the performance of gait event detection.

After the model building, its **performance is evaluated utilising CV**. The evaluation procedure is used for analysing models with varying input parameters such as their hyperparameters or feature combinations. The evaluation is especially essential to conclude the classification performance of unseen data, to use a limited number of samples to estimate how the model is expected to perform when used to make predictions of unseen data through its training. In the first stage, only **5-fold CV** was performed due to the high number of combinations to evaluate. In the second stage, each model's performance is evaluated using **10-5–fold CV**. To assess the classification results, nine different metrics were used previously described in Chapter 2, namely, MCC, ACC, SENS, SPEC, PREC and F1S.

6.5 Results

6.5.1 Finite-State Machine Algorithm

It was examined the ACC, the percentage of occurrence and duration of delays and advances in controlled and real-life scenarios to evaluate the versatility and time-effectiveness of the algorithm. Furthermore, the time-effectiveness was just inspected for accurate detections. A misdetection was considered for timing error higher than 100ms, which is considered a critical duration for motor rehabilitation purposes.

By analysing Table I in Appendix 1, it is verified that the **CMS and FGC** events exhibited the **highest ACC** (98.51% and 83.92%, respectively). On the other hand, the **MSM event and PCO were not detected** (0.74% and 0.96%, respectively). The findings of the controlled situations also indicate that the **FBC and FCO have a higher occurrence of delayed detections** (43.25% and 34.91%), being detected with a mean delay of 55.32±27.90ms and 51.42±16.85ms, respectively. **Advanced detections were mainly observed for the PCO** (77.78ms) and **MSM** (71.43).

The results throughout the different gait phases for the remaining walking situations are consistent with the ones achieved for controlled situations, although with lower accuracies Tables II to IV in Appendix 1. **The FGC was the most accurately detected gait event** (ACC > 52.78%) while the **MSM was the least detected phase** (ACC < 11.11%). Delayed detections were more common than advanced ones ranging between 0% to 32.43% and 0% to 95.41%.

In controlled situations, the algorithm did not detect, on average, 1.11% of each gait event, followed by 4.52%, 8.96% and 27.38% for level-ground surfaces, inclined surfaces and stairs, sequentially. It is crucial to disclose that the timing errors revealed in Tables I, II, III and VI do not comprehend the algorithm latency of 10ms due to the filtering process.

6.5.2 Machine Learning Framework

To determine which are the best set of features and machine learning classifier for the ASCane gait event recognition, three studies were conducted. The first stage aimed to evaluate which were the two combinations of classifier and feature selection method that provided the best overall results. It is crucial to disclose that the evaluation metrics presented in this first stage are the mean between the six different classes.

The results comparing the different feature selection methods and classifiers are presented from Tables V to XII in Appendix 1. Through direct observation, it is possible to acknowledge that the **ensemble**

learning classifier is the one that **achieved the best results** amongst all feature selection methods (ACC > 93.17%, SENS > 92.86 %, SPEC > 98.62%, PREC> 93.26%, MCC > 91.68%, F1S > 93.03%). On the other hand, both **regression models** tested (linear and pure quadratic) presented the **lowest performance** (ACC > 40.60%, SENS > 40.02%, SPEC > 88.61%, PREC > 44.28%, MCC > 28.69%, F1S > 37.06%). It is also verified that the number of features used to train the classifier, which results in the best overall performance, relates to the feature selection method used. For each feature selection method tested, curiously, the three KNN classifiers performed the same, even with different distance weight functions (Squared Inverse, Equal and Inverse). The two best combinations were chosen based on two criteria: the classifier must be different and have the best overall performance amongst all computed evaluation metrics. Consequently, two combinations resulted from these criteria: **LLCFS with Ensemble Learning** and **UDFS with KNN** (Squared Inverse as distance weight function), which results are exposed in Table 6.1.

Table 6.1: Overall ACC, SENS, SPEC, PREC, MCC and F1S of the two best combinations of feature selection methods, classifiers and number of features in the first stage.

Feature Selection Method	Classifier	Number of Features	Overall Performance					
			ACC	SENS	SPEC	PREC	MCC	F1S
UDFS	KNN Squared Inverse	20	94.49	94.51	98.90	94.24	93.26	94.36
LLCFS	Ensemble Learning	118	96.10	96.03	99.22	96..06	95.26	96.02

The second stage intended to estimate the real performance of the selected machine learning classifiers and choose the one who performed the best. Consequently, the chosen combinations were tested once again with a 10-5-fold CV, instead of 1-5-fold CV. For both combinations, all the evaluation metrics increased, as seen in Table XIII from Appendix 1. Moreover, in Figure 6.22 is represented the evaluation performance of the KNN model with UDFS as feature selection method trained with 1 up to 120 features. Contrarily, in Figure 6.23 is represented the evaluation performance of the ensemble learning model with LLCFS as feature selection method trained with 1 up to 120 features.

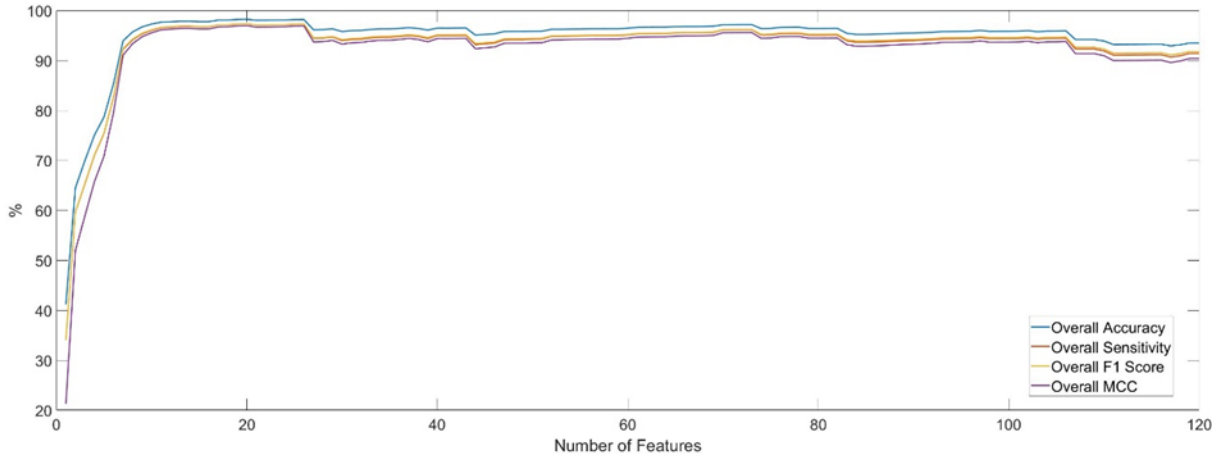

Figure 6.22: Overall ACC, SENS, F1S and MCC obtained with the KNN model trained from 1 up to the 120 most significant features computed by the UDFS feature selection method.

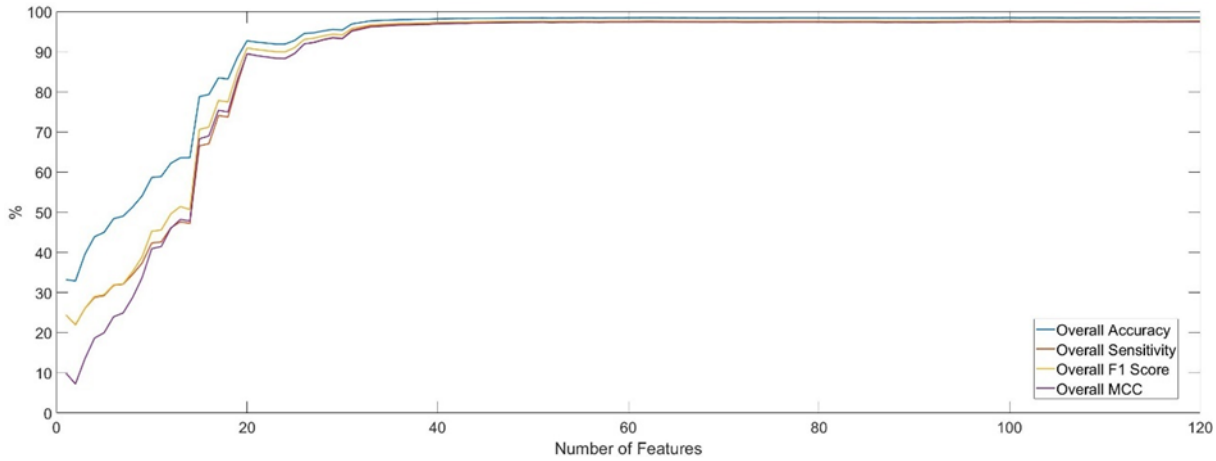

Figure 6.23: Overall ACC, SENS, F1S and MCC obtained with the ensemble learning model trained from 1 up to the 120 most significant features computed by the LLCFS feature selection method.

For the KNN classifier, the ACC increased by 3.73% (reaching 98.22%), the SENS improved by 2.83% (97.34%), and the SPEC, PREC, MCC and F1S reached 99.63%, 97.33 %, 97.33% and 96.97%, respectively. Regarding the Ensemble Learning model, the results improved similarly. The resultant ACC raised 2.36% (matching 98.46%), the SENS increased 1.60% (97.63%), and the SPEC, PREC, MCC and F1S reached 99.68%, 97.87%, 97.75% and 97.43%, respectively.

The classifier was chosen considering the existing trade-off between the evaluation metrics, computational power and number of features needed. Therefore, the combination of the 20 most significant features through the **UDFS method with the KNN algorithm** as classifier was chosen. In Table XIV from Appendix 1, the different evaluation performance metrics for each gait event are presented. The PCO was the gait event that presented the lowest detection with an ACC and SENS of 92.87% and 92.86% while the FBC presented the highest with 98.88% and 98.87%, respectively. The 20 most significant features (through the UDFS) for cane event classification are listed in Table 6.2.

Table 6.2: The 20 most significant features by the feature selection method UDFS for the detection of six cane gait events

Feature Ranking	Feature	Description
1	'High_Pass_Filter_Acc_X'	Acceleration along the X-axis plane High-Pass filtered with cut-off frequency of 0.1Hz
2	'High_Pass_Filter_Acc_Z'	Acceleration along the Z-axis plane High-Pass filtered with cut-off frequency of 0.1Hz
3	'Acc_Z_Raw'	Raw acceleration along the Z axis
4	'Acc_X_Raw'	Raw acceleration along the X axis
5	'GC_Acc_X'	Gravity Component along the X-axis
6	'GC_Acc_Z'	Gravity Component along the Z-axis
7	'Displacement_X'	Displacement along the X axis
8	'Velocity_Y'	Velocity along the Y axis
9	'Velocity_Z'	Velocity along the Z axis
10	'Quaternion4'	Fourth element of quaternion vector
11	'Pitch'	Euler Angle - Pitch
12	'Quaternion3'	Third element of quaternion vector
13	'Yaw'	Euler Angle - Yaw
14	'SVM_Gyr_Band_Pass'	Sum Vector Magnitude of the angular velocity Band-Pass filtered with cut-off frequencies of 0.1Hz and 90Hz
15	'SVM_Gyr_High_Pass'	Sum Vector Magnitude of the angular velocity High-Pass filtered with a cut-off frequency of 0.1Hz
16	'GC_Acc_Y'	Gravity Component along the Y-axis
17	'High_Pass_Filter_Gyr_Z'	Angular Velocity along the Z-axis plane High-Pass filtered with cut-off frequency of 0.1Hz
18	'Gyr_Z_Raw'	Raw Angular velocity along the Z axis
19	'Quaternion2'	Second element of quaternion vector
20	'Roll'	Euler Angle - Roll

The use of a post-processing algorithm intended to **increase the performance metrics and remove outliers** from the resultant signal. The comparison between the use and non-use of the

algorithm is represented in Table 6.3. It is verified that all evaluation metrics slightly increase apart of the SENS, SPEC and F1S in staircase climbing, which decreased by 0.71% (90.29%), 0.03% (98.66%), and 0.61% (90.46%), respectively. The ACC increased by 0.16% (98.32%), 0.24% (94.02%), 0.42% (96.72%) and 0.13% (93.72%) in controlled situations, inclined surfaces, level ground and staircase walking, accordingly.

Table 6.3: Comparison between the ACC, SENS, SPEC and PREC before and after the application of the post-processing algorithm in the four different walking scenarios.

Walking Situations	ACC		SENS		SPEC		PREC	
	Before	After	Before	After	Before	After	Before	After
Controlled Situations	98.16	98.32	97.78	97.90	99.63	99.66	97.61	97.92
Inclined Surfaces	93.78	94.02	91.90	91.96	98.75	98.81	90.93	91.19
Level Ground It is	96.30	96.72	90.33	90.81	99.28	99.37	93.55	94.72
Stairs	93.59	93.72	91.00	90.29	98.69	98.66	89.43	91.16

In Figure 6.24 is depicted a comparison between the ground truth with the output of the best machine learning model with unseen data. Following, in Figure 6.25 is portrayed a comparison between the output of the best machine learning model with unseen data and the post-processing algorithm results. Finally, to contrast the use and non-use of the post-processing algorithm, in Figure 6.26 is pictured the comparison between the output of the post-processing algorithm and the output of the best machine learning model with unseen data.

6.6 Discussion

A real-time and adaptive computational method for assessing human gait events in controlled and real-life walking situations using repeated measures of healthy gait patterns was modified to account for the cane angular velocity signal differences of the sagittal plane.

Even though the angular velocity signal in the sagittal plane of a cane presents similar shape as the one recorded for the foot, it is not as distinctive. Therefore, the segmentation of gait events becomes more challenging. In Figure 6.14, is portrayed the mean, and the mean plus/minus the standard deviation of the foot and cane angular velocity on the sagittal plane for the four different walking situations assessed throughout a gait cycle. In all four cases, the amplitude of the foot signal is much higher, both in the maximum, first and the second minimum, which is used to identify the MMSW, FF and TO events.

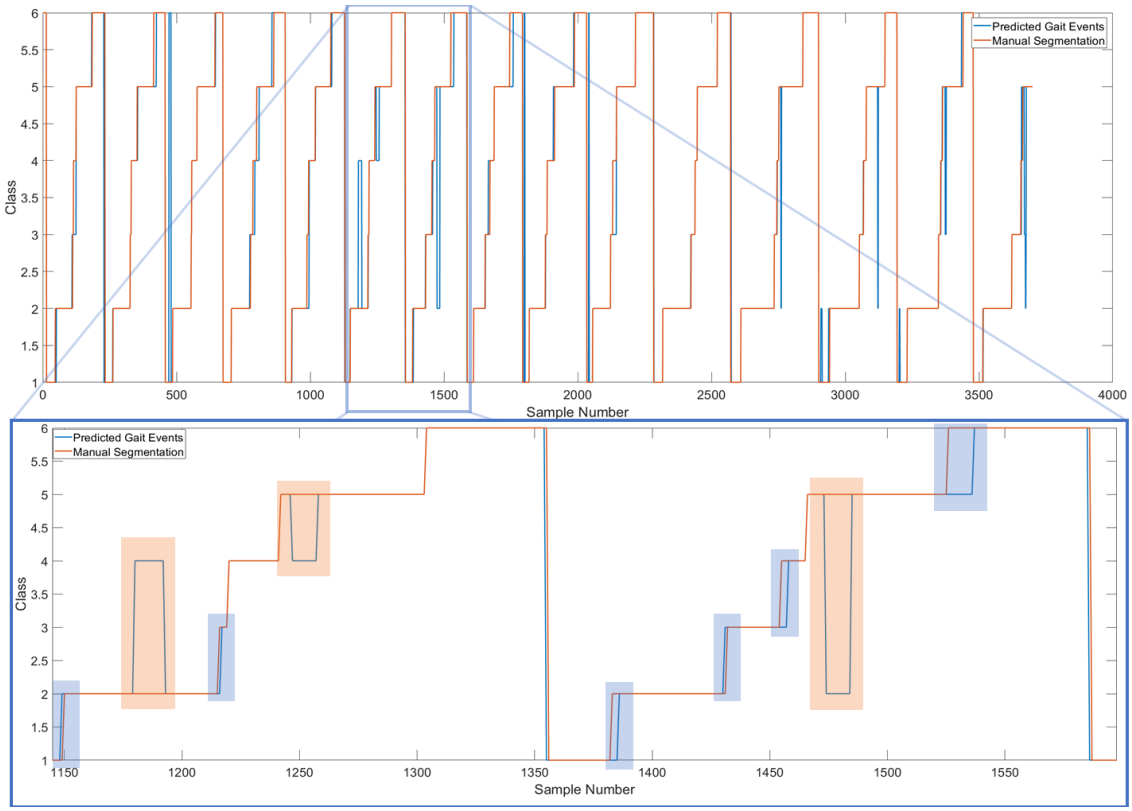

Figure 6.24: Comparison between the ground truth (orange) with the output of the best machine learning model with unseen data (blue) for a full trial.

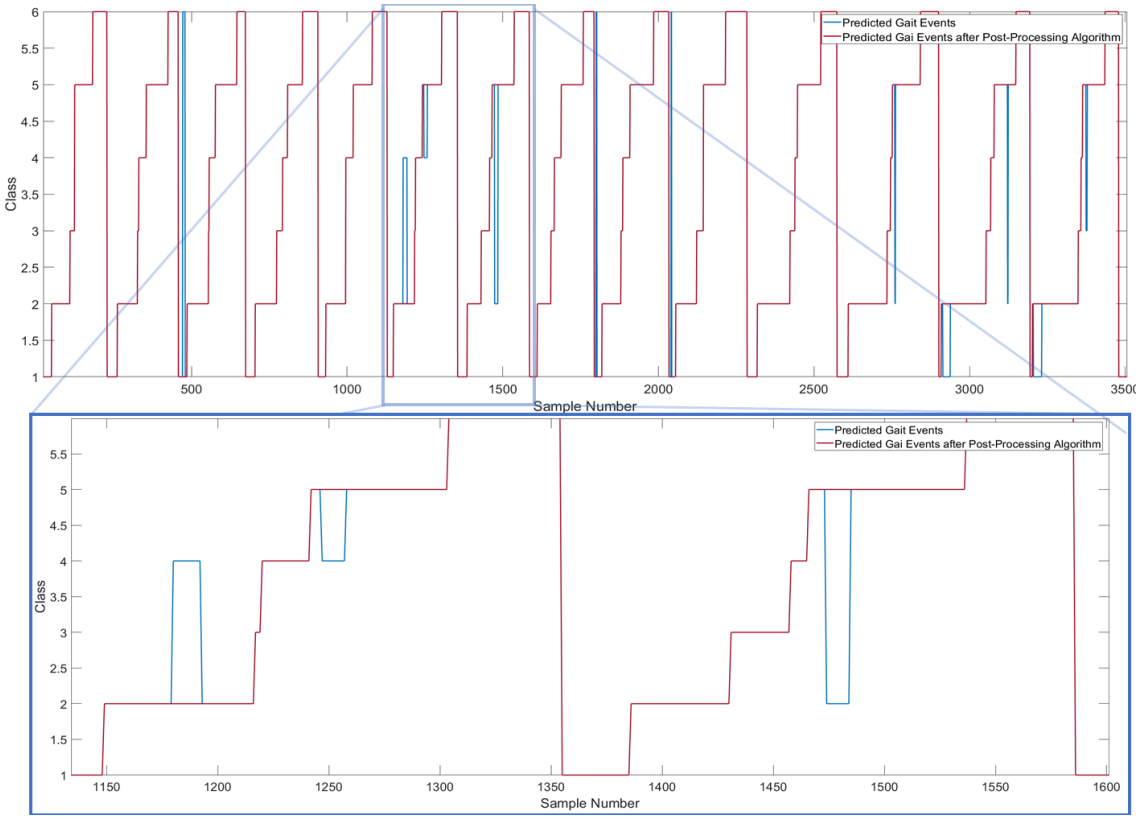

Figure 6.25: Comparison between the use (red) and non-use (blue) of the post-processing algorithm for a full trial.

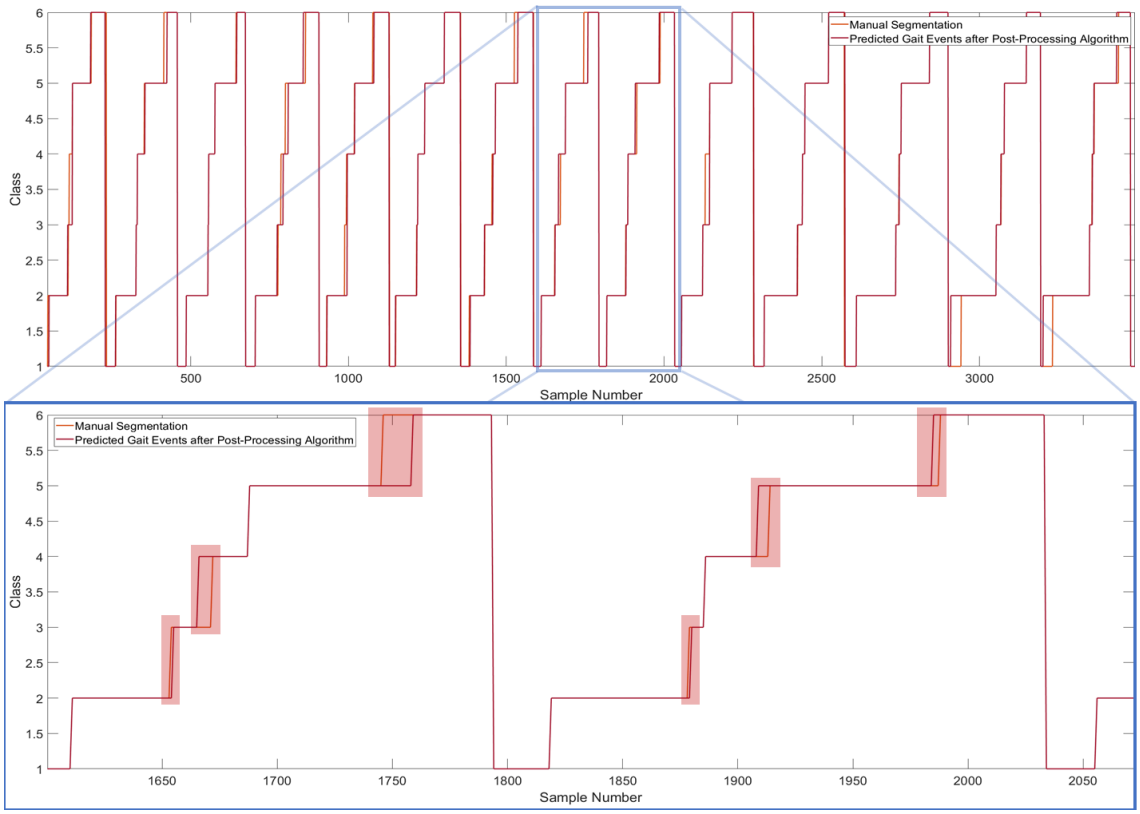

Figure 6.26: Comparison between the output of the post-processing algorithm (red) and the ground truth (orange) for a full trial.

The FGC was the second most detected event with ACC ranging between 52.78% and 83.92% for climbing stairs and controlled situations, respectively. Advanced detections were highly observed (between 69.36% and 96.94%). Even with trial and error thresholds adjustments after an empirical analysis, both the ACC and time advance in detection did not improve significantly.

Throughout the different walking conditions, the **MSM was the least detected event** inside the time range, with ACC between 0.74% and 11.11%. In the algorithm, human MMST was established as *n* samples after FF occurred, where *n* corresponds to the duration of the last valid MMST. In contrast, the cane MSM is the moment where the subjects transfer his weight to the cane, which can occur at a different time throughout several strides and the angular velocity signal cannot represent that moment, while the acceleration values can.

The average human foot area is much larger than the base area of a cane. Thus, the time interval between PCO and FCO is much smaller than the one between HO and TO, happening almost instantaneously, as seen in Figure 6.14. Consequently, the segmentation of the phases can be challenging for a finite-state-machine algorithm, with ACC lower than 46.54% and a high number of advanced and delayed detections.

Moreover, the **CMSW was the most accurately detected event** (ACC > 77.36%). The highest time advance and delay percentages were 1.50% and 0.95%, respectively. Hence, if the algorithm identified the CMSW event, it would accurately be segmented with sample PREC 98.50% of the times. The algorithm decision rules depend on stride time, which sets adaptative periods where the events shall occur, and the stride time calculation considers rising or declining periods (which are not as significant in data acquired through the ASCane. Consequently, the stride time is easily miscomputed, decreasing the detection rate of all gait events

The results prove that the **modified algorithm cannot be directly applied to the detection of cane events without further modifications**. The single axis of a gyroscope located on the top of the cane does not provide enough information for the segmentation of a cane gait events at these conditions. The implementation of the ground truth decision rules into the literature algorithm is discussed in future work.

To estimate the real performance of machine learning classifiers, J-K-fold CV was performed in all studies and combinations. In the first stage, due to time constraints, only a 1-5-K-fold CV was accomplished. According to [153] if K > 3, to guarantee overlapping training sets, it is possible to have comparable variance across K. Meaning that the only reliable reason to increase K is to reduce bias.

In contrast, increasing J does not affect bias but does significantly decrease the internal variability. The authors also concluded that the ACC of the model tuned by 1-10-fold CV is not stable enough to enable the comparison with other models of close performance. To be capable of distinguishing between the trained models with close performance differing, it requires higher choices of J. Also, based on a study by Kohavi et al. [154], using K=5 or k=10 produces a reasonable trade-off between bias and variance. Consequently, a 10-5–fold CV was chosen for the second stage.

From Figure 6.22, which represents the evaluation performance of the KNN model with UDFS as feature selection method from 1 to 120 features in the training dataset, the model, with only 10 features, already presents overall performance above 90%, contrarily to the ensemble learning model with LLCFS as a feature selection method, Figure 6.23. The highest overall performance of the KNN classifier was with only 20 features, which was the model chosen to the third stage. With the same number of features, the ensemble learning model presents lower performance, 5.51% in ACC, 7.84% in SENS, 1.27% in SPEC and 4.77%, 6.42%, 7.52% in PREC, F1S and MCC, respectively. Moreover, the computational power required for an ensemble learning model is much higher than the one needed for a KNN model.

After testing the model with unseen data, even though the performance was high, occasionally the model misclassified samples, resulting in outliers, as seen in Figure 6.24 (orange boxes).

Furthermore, the model misclassified samples right after a gait event transition, as also seen in Figure 6.24 (blue boxes). The developed algorithm aimed **only at removing the outliers of the signal**, since there is not possible, with a pre-processing technique, to suppress the advanced of delayed detections in gait event transitions. The algorithm result for a full trial is depicted in Figure 6.25, as seen, **all the outliers for the trial were removed** and replaced with the correct gait event. Only a small increase in performance was expected since the **presence of outliers was low when compared to the number of times the model considered a transition delayed or advanced in time**. Lastly, in Figure 6.26 it is possible to compare the true labels with the algorithm results, as seen, **the only difference between both signals is the sample in which the transition between the gait event happens** (Figure 6.26 (red boxes)).

7. ASCane Pre-Fall Step Detection System

One of the primary goals of this thesis was to be capable of estimating a fall through an ordinary cane system. According to the literature, **fall and pre-fall states are considered relevant to be detected**. Subsequently, this chapter aims at developing a classifier fitted of **distinguishing normal gait and PFS situations**, using ASCane gait parameters through an IMU-based system throughout ADLs. This chapter will be divided into three major arts: i) System setup, data collection from sensing devices through trials in healthy young people, and computation of metrics; ii) Selection of the most relevant metrics through several feature selection methods; iii) Training and testing of different machine learning classifiers with the most suitable set of metrics.

The scientific literature regarding fall-related systems installed into a cane is very focused on FD systems which employ threshold or multi-threshold algorithms. FD systems are often based on impact detection [94], [95], [105], [155]. Nevertheless, some canes embed systems which try to avoid falls or imbalances, but they are embedded in a robotic system with a wheele based [100]–[103], [156]. Besides up to our knowledge, **there is still no cane system proposed regarding PFS detection using IMUs**. Hence it is necessary to establish a framework that takes advantage of the perceptual information to monitor the subject movement execution and, in the most undesirable case, use it to prevent fall situations.

Ribeiro et al. [157] developed a strategy to predict a fall only using wearable sensors attached to the subjects' lower back, thighs and feet. It was considered four different locomotion modes to be classified: fall, pre-fall (Gait cycle before the fall's situation), walk forward, and global (including walking

in circle and walk forward, bypassing an obstacle). Using convolutional neural networks based on deep learning, PFS were identified with a success rate of 88.24%, whereas fall and walk forward plus global locomotion modes presented accuracies of 100% and 93.26%, respectively. Consequently, the pre-fall step presents key differences from normal steps. Based on these achieved results, it is possible to establish **the hypothesis that the inertial data acquired from a cane from the last step before a fall might be different from data of standard steps.**

7.1 Methods and Materials

7.1.1 General Overview

The proposed methodology used for detecting PFS situations is very similar to the one achieved in Chapter 6. A schematic overview of the completed strategy is highlighted in Figure 7.1. After the experimental trials and segmentation of the last complete valid step before a fall, a machine learning study was performed to find which are the best set of features and machine learning classifier to identify PFS situations. In the following subchapters, a brief description of each module is given, together with the explanation of the work developed.

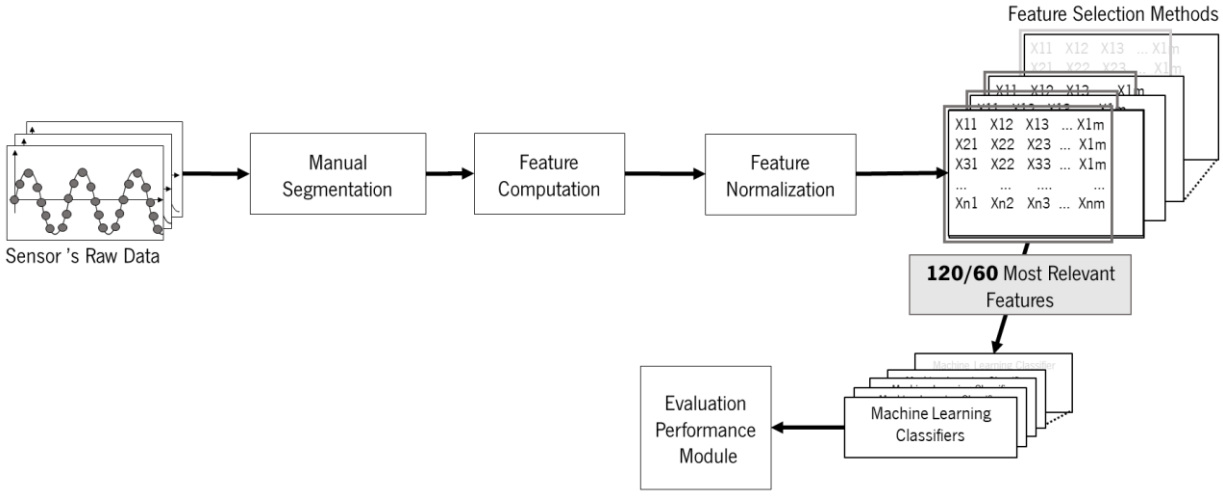

Figure 7.1: General Overview of the carried-out methodology for the detection of pre-fall situations.

7.1.2 Experimental Protocol

All trials were performed at the gymnasium and data from four different fall directions were collected (front, backward, right and left), as portrayed in Figure. 7.2. The falls were executed by ten volunteers which ranged from 22 to 25 years (23.6 ± 1.02 years), with a body mass between 52 and 80 kg (67.80 ± 7.88 Kg) and a height of 1.51 to 1.81 m (1.71 ± 0.83 m). All participants provided their written consent, and each fall direction was performed a total three times per subject with a total of 120

simulated falls. Figure 7.3 a) depicts the ASCane and Figure 7.3b) illustrates the ASCane system with the sensors location and their corresponding orientation.

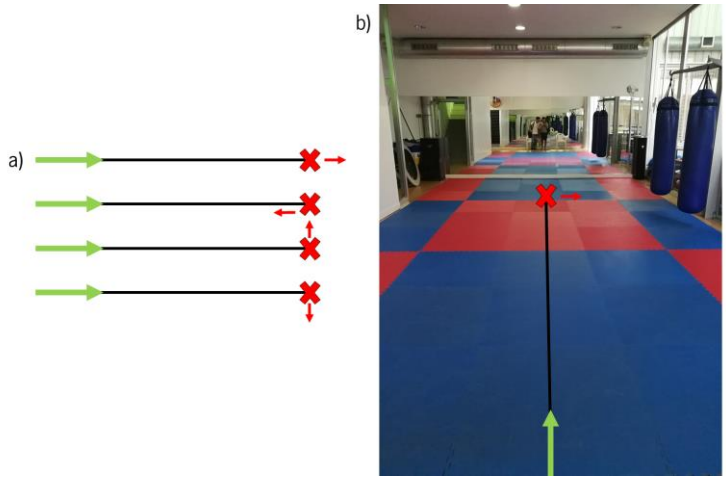

Figure 7.2: a) Fall scenarios mimicked - Subjects starts walking (green arrow) and Falls (red X) to the red arrow direction; b) Example of a fall to the right in the gymnasium.

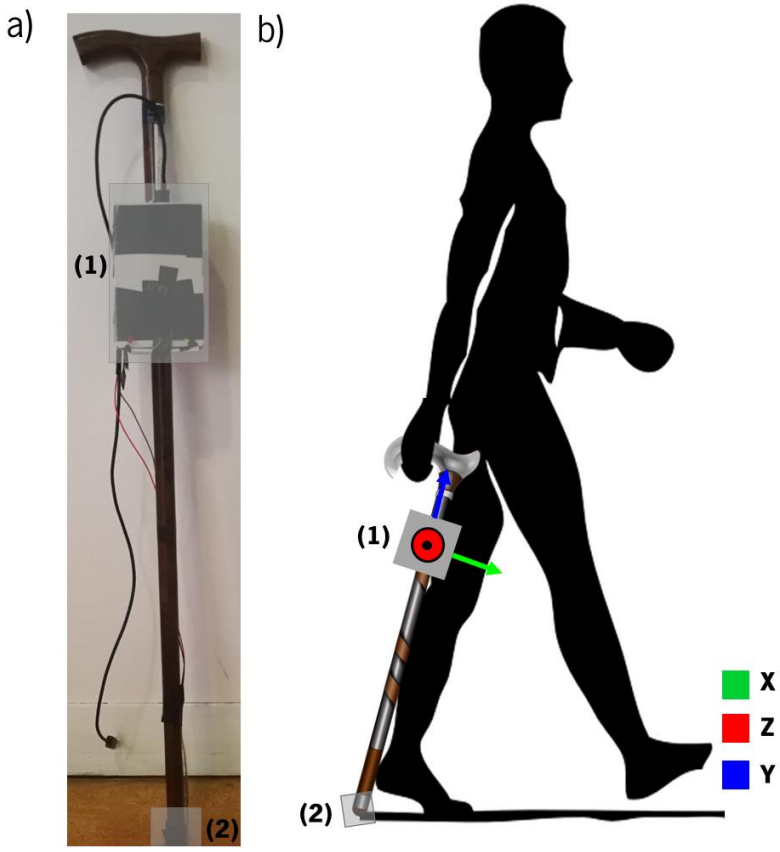

Figure 7.3: a) ASCane; b) ASCane system during data acquisition (1) IMU; (2) FSR.

7.1.3 Machine Learning Framework

Since the data acquired was equal as Chapter 6 (ASCane acceleration, angular velocity and FSR), the computed features were the same (Table XXIV – Appendix 3). Consequently, feature computation and

normalization were equal for both sections, resulting in 288 features normalized between 0 and 1. Regarding **feature selection methods**, the **same ones were used** to rank the features for the predictive model, with exception of PCA, which was not able to rank the features. Therefore, the feature selection methods used were: CFS, Relieff, UDFS, LASSO, Laplacian Score, UFSOL and LLC.

Considering this is a binary classification, support vector machines can be directly applied to the dataset. For PFS detection, **it was used support vector machines** using three different kernels: linear, gaussian and polynomial. Moreover, **the machine learning classifiers previously used were also implemented** for PFS detection, namely: KNN, with an equal, inverse and squared inverse distance weighting function; DA with linear and quadratic discriminant function; Ensemble Learning; Decision Trees and Regression Model with linear and pure quadratic terms. The support vector machines were only built and tested with up to 60 most discriminative features (instead of the 120) due to time-constrains since, for each model, the computation time was approximately 1 hour.

The goal was to find the beast combination of classifier and features to maximize performance. To do so, a three-stage study was accomplished. Similar to the previous chapter, all possible combination of machine learning classifiers and features resulting from several feature selection methods were tested and evaluated. Secondly, the two most suitable combinations were tested once again, this time with **increased j-k-fold CV**, both stages are depicted in Figure 7.4.

The third and last stage involved the development of an **online post-processing filtering** to reduce the false-positive rate. The classifier was tested with unseen data to test its predictive power, more precisely, 6 full trials from different subjects with random fall direction and 9 full trials of ADLs (the same walking activities tested in Chapter 6). Subsequently, the developed post-processing online filter was applied to the same results and benchmarked against the classifier results. The algorithms flowchart is presented in Figure 7.5. Initially, all the samples inside the pre-defined window of the sample (i) with length ($window\_size$) are selected, and the number of positive detections (N) is calculated. A positive detection is considered a sample of a PFS. At this point, four different scenarios are possible:

- The number of positive detections (N) can be equal or superior to the number of positive detections threshold ($sample\_thr$), and the sample (i) is classified as a normal step, in which the sample (i) remains a normal step.
- The number of positive detections (N) can be equal or superior to the number of positive detections threshold ($sample\_thr$), and the sample (i) is classified as a PFS. Consequently, the sample (i) remains classified as a PFS.

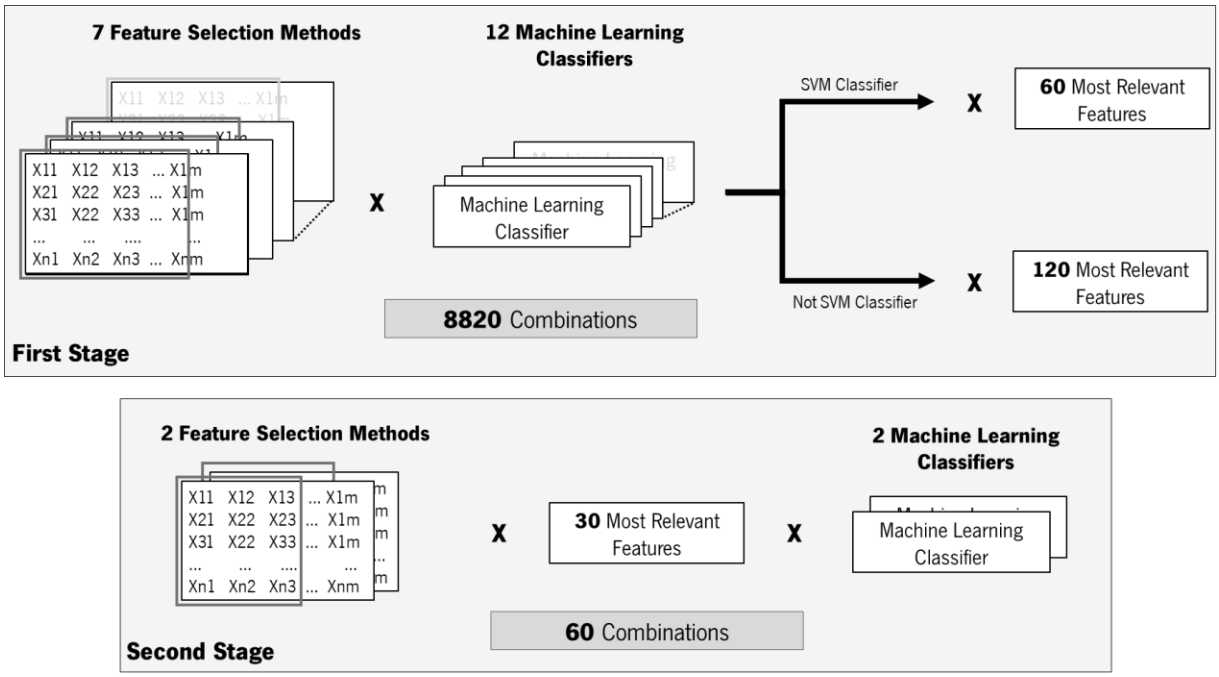

Figure 7.4: The different combinations of feature selection methods, number of features and classifier tested for the first and second stage.

- The number of positive detections (*N*) can be inferior to the number of positive detections threshold (*sample_thr*), and the sample (i) is classified as a PFS. Thus, the sample (*i*) is overridden as a normal step.
- The number of positive detections (*N*) can be inferior to the number of positive detections threshold (*sample_thr*), and the sample (*i*) is classified as a normal step. Hence, the sample (*i*) remains classified as a normal step.

This decision process continues for each sample (*i*) until the end of the given trial. It is crucial to disclose that *N* is independent of *i*, meaning that instead of modifying the original results of the machine learning model, **the post-processing algorithm creates a new result vector**. To achieve the highest performance, this filter was iteratively tested with every combination of *sample_thr* and *window_size* from 1 up to 100, which performs a total of 10 000 different combinations. Lastly, a **study regarding the detection time was conducted** with the filtered classification to uncover how much time in delay the cane detects the PFS as well as the time difference between the PFS detection and the impact with the ground/end of the PFS. To evaluate all possible combinations, six metrics were computed, specifically: MCC, ACC, SENS; SPEC, PREC and F1S, the same as Chapter 6.

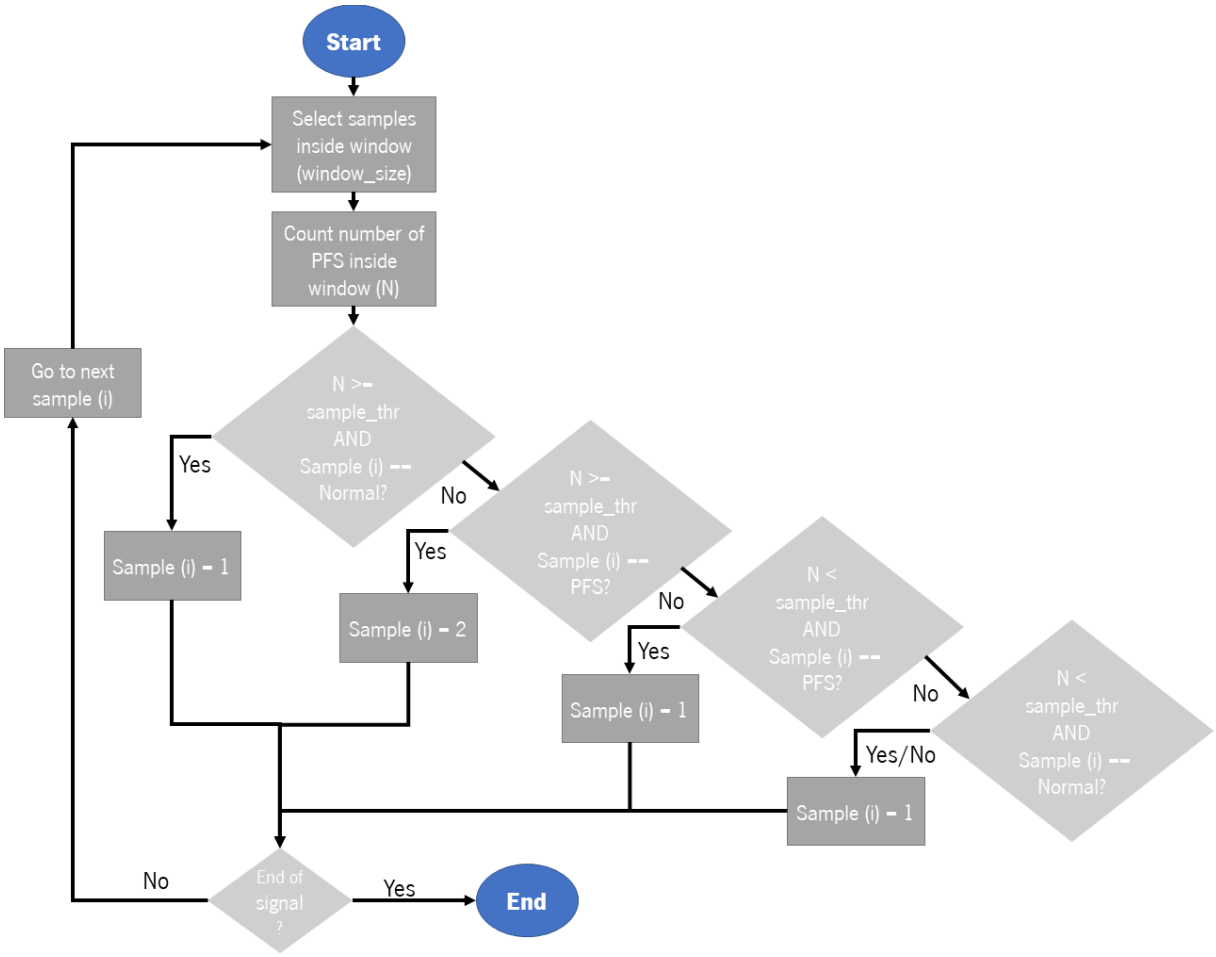

Figure 7.5: Flowchart of the post-processing filter developed for increasing the performance of PFS detection and elimination of PF detections.

7.2 Results

The first stage conducted for PFS detection intended at assessing which were the two best combinations of machine learning classifiers and feature selection methods that provided the best overall performance, with the least number of features. The results comparing the best combinations of performances are presented from Tables XV to XXI in Appendix 2. The number of features selected was the one that achieved the best ACC. **The Laplacian Score and Relieff feature selection methods produced the best overall performance**. While the Relief method performed slightly better, considering the trade-off within performance, number of features required and model size, the Laplacian Score is the most fitting feature selection method (ACC> 89.89%, SENS>91.92%, SPEC>80.97%, PREC>95.43%, MCC>67.74%, F1S>93.66%). Concerning the application of the different classifiers with the Laplacian Score, it is possible to acknowledge that the **KNN classifier and support vector machines with a polynomial kernel attained the best outcomes** (ACC> 98.85%, SENS>99.29%, SPEC>96.97%, PREC>99.30%, MCC>96.25%, F1S>99.29%). On the other hand, **both DA tested** (linear

and quadratic) **presented the lowest performance** (ACC> 80.97%%, SENS>91.92%, SPEC> 80.97%, PREC> 95.43%, MCC > 67.74%, F1S > 93.66%).

The two best combinations were chosen based on two criteria: the classifier must be different and needs to have the best trade-off between performance and number of features necessary. Consequently, two combinations resulted from these criteria: **Laplacian Score with support vector machines (polynomial kernel) and KNN (squared inverse as distance weight function)**, which results are exposed in Table 7.1.

Table 7.1: Overall ACC, SENS, SPEC, PREC, MCC and F1S of the two best combinations of feature selection method, classifiers and number of features in the first stage accomplished for PFS detection

Feature Selection Method	Classifier	Number of Features	Overall Performance					
			ACC	SENS	SPEC	PREC	MCC	F1S
Laplacian	KNN Squared Inverse	12	98.85	99.29	96.97	99.30	99.29	96.25
	Support Vector Machines - Polynomial	51	99.89	99.92	99.78	99.95	99.93	99.67

The second stage was designed to estimate the real performance of the selected machine learning classifiers and choose the one who performed the best. Consequently, the chosen combinations were **tested once again with a 10-5-fold CV**, instead of 1-5-fold CV. With increased J-K-fold, the training time of the classifier increases proportionally. Since for each iteration, the support vector machines training time was approximately 39 hours, due to time constraints, only the first 30 iterations of both classifiers were conducted for their comparison.

Regarding the KNN classifier, **all the evaluation metrics increased**, as seen in Table XXII from Appendix 2. The ACC increased by 0.23% (reaching 99.08%), the SENS improved by 0.1% (99.39%), and the SPEC, PREC, MCC and F1S reached 97.72%, 99.47%, 99.43%, 97.00, respectively. The comparison between the results from the first and second stage are exhibited in Table 7.2 and the evaluation performance of the KNN classifier trained with 1 up to the 30 most significant features is represented in Figure 7.6.

Table 7.2: Comparison between the first and second stage results (ACC, SENS, SPEC, F1S and MCC) of the KNN model (Squared Inverse as distance weight function) trained with the 12 most significant features resulted from the Laplacian Score Feature Selection method

ACC		SENS		SPEC		PREC		F1S		MCC	
1st	2nd	1st	2nd	1st	2nd	1st	2nd	1st	2nd	1st	2nd
98.85	99.08	99.29	99.39	96.97	97.72	99.30	99.47	99.29	99.43	96.25	97.00

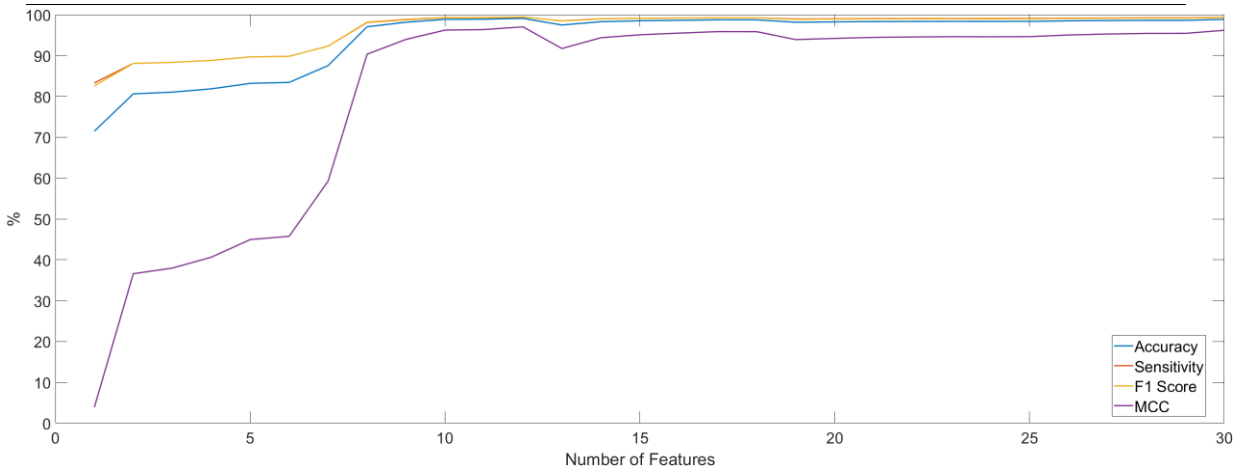

Figure 7.6: Overall ACC, SENS, F1S and MCC obtained with the KNN model trained from 1 up to the 30 most significant features computed by the Laplacian Score feature selection method.

Concerning the application of support vector machines, **the results decreased slightly**. The resultant ACC lowered 0.8% (matching 99.09%), the SENS dropped 1.00% (98.92%), and the SPEC, PREC, MCC and F1S reached 98.63%, 99.91%, 99.92% and 99.58%, respectively. The comparison between the results from the first and second stage are exhibited in Table 7.3. and the evaluation performance of the support vector machines trained with 1 up to the 30 most significant features is represented in Figure 7.7.

Table 7.3: Comparison between the first and second stage results (ACC, SENS, SPEC, F1S and MCC) of the support vector machines model (polynomial kernel) trained with the 12 most significant features resulted from the Laplacian Score Feature Selection method

ACC		SENS		SPEC		PREC		F1S		MCC	
1st	2nd	1st	2nd	1st	2nd	1st	2nd	1st	2nd	1st	2nd
99.89	99.09	99.92	98.92	99.78	98.63	99.95	99.91	99.93	99.92	99.67	99.58

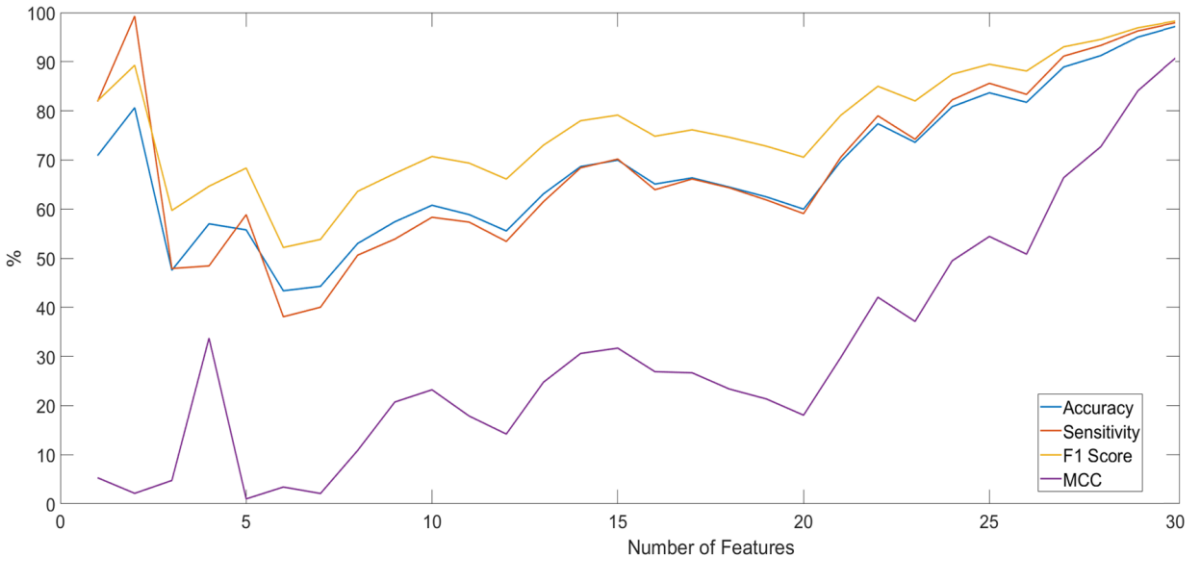

Figure 7.7: Overall ACC, SENS, F1S and MCC obtained with support vector machines (polynomial kernel) model trained from 1 up to the 30 most significant features computed by the Laplacian Score feature selection method.

Once again, the classifier was chosen considering the existing trade-off between the evaluation metrics, computational power and number of features needed**. The KNN classifier performance was superior** to the one reached by the support vector machines, and the difference between the number of features is significantly (approximately 40). Therefore, the combination of the 12 most significant features through the Laplacian Score method with the KNN algorithm as classifier was chosen to continue to the next and final stage, the 12 most significant features are listed in Table 7.4.

Table 7.4: The 12 most significant features by the Laplacian Score for the detection of PFSs in a cane.

Feature Ranking	Feature	Description
1	'FSR'	ASCane FSR
2	'Quaternion1'	First element of quaternion vector
3	'Correlation - Gyr X – Z'	Correlation Between Angular Velocity X and Z axis
4	'MAD'	Magnitude of Angular Displacement
5	'Quaternion2'	Second element of quaternion vector
6	'Roll'	Roll (Madgwick Sensor-Fusion Algorithm)
7	'Max_Gyr_Z'	Maximum Angular Velocity (Z axis)
8	'Displacement_Y'	Displacement (Y axis)
9	'RAC - Y'	Resultant of Average Acceleration (Y axis)

Feature Ranking	Feature	Description
10	'Yaw'	Yaw (Madgwick Sensor-Fusion Algorithm)
11	'RAC SVM'	SVM of Resultant of Average Acceleration
12	'RAC - X'	Resultant of Average Acceleration (X axis)

The use of a post-processing algorithm intended to **increase the performance metrics and remove PF from the resultant signal**. The comparison between the use and non-use of the algorithm for different windows sizes and sample numbers are presented in Table XXIII in Appendix 2. It is verified that ACC, SENS F1S and MCC increase while SPEC and PREC decreased. As we increase *window_size*, the ACC rises until it peaks (ACC = 99.76%) with a *window_size* of 20 and *sample_thr* of 20 (Figure 7.8 - grey X). Yet, PF detections are still detected (SENS = 99.93%). With a *window_size* of **39** and *sample_thr* of **39** (Figure 7.8 - blue X), **all the PF are eliminated**, resulting in an ACC of 99.65% (1.5% increase), SENS of 100% (1.89% increase), SPEC of 84.44% (decrease of 15.56%), PREC of 99.64%(decrease of 0.39%) and F1S and MCC of 99.82% and 91.73% (increase of 0.78% and 18.58%) respectively. Increasing the *window_size* to 100, PF detections start to appear again (SENS = 99.73%). The comparison between the use and non-use of the post-processing algorithm with a *window_size* of 39 and *sample_thr* of 39 for all tested trials is depicted in Figure 7.9.

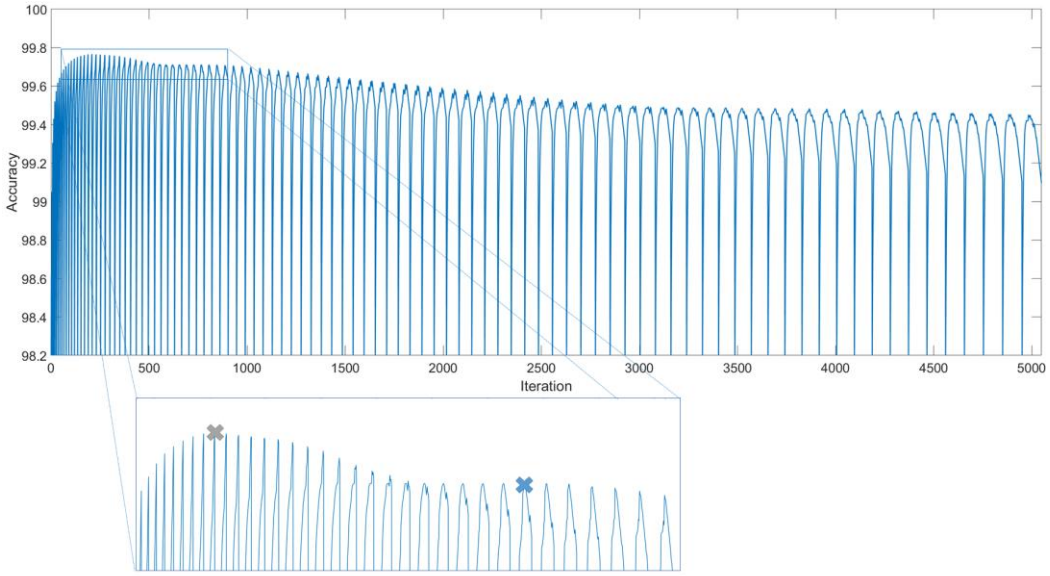

Figure 7.8: ACC of all tested combinations (sample_thr and window_size) from 1 up to 100 (each) of the post-processing algorithm where the combination with the highest achieved ACC is marked with grey and the chosen combination market at blue.

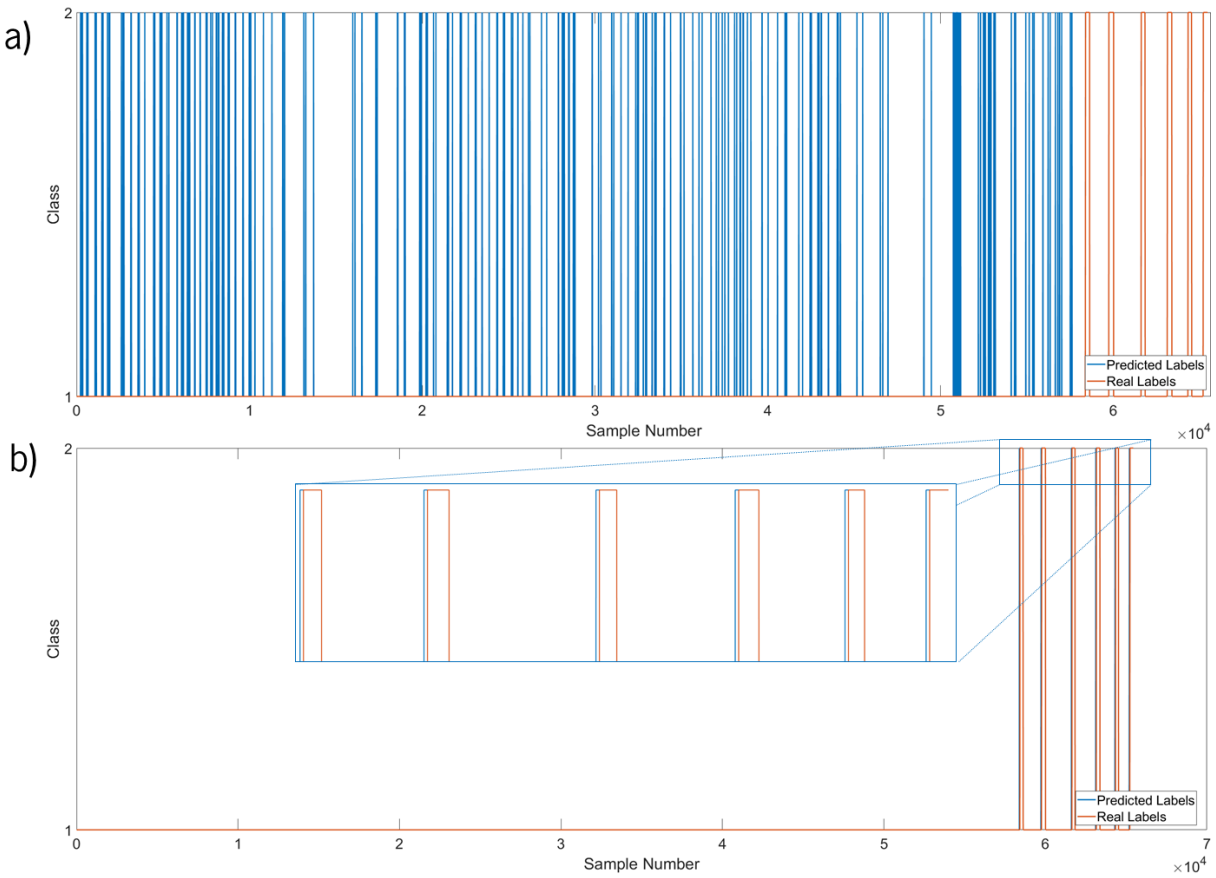

Figure 7.9: Comparison between the non-use (a) and use (b) of the post-processing filter with *sample_thr* and *window_size* of 39.

With the use of the post-processing filter, the detection of a PFS is delayed 0.191±0.011s (Table 7.5), detected **1.019±0.11s** (Table 7.6) before the end of the respective step and **2.009±0.628s** (Table 7.7) before the impact with the ground. Without the use of the filter, the PFS is detected **1.22±0.11s** (Table 7.6) before the end of the respective step and **2.107±0.635s** (Table 7.7) before the impact with the ground. The use of the post-processing filter results in a delayed impact detection of 0.098s.

Table 7.5: Comparison between the Mean and Standard Deviation of the time difference between the detection of the PFS (with and without the use of the post-processing filter) and the real labels

	Without Filter		**With Filter: Window Size / Number of Samples**					
			20/20		39/39		100/33	
	Samples	**Time(s)**	**Samples**	**Time(s)**	**Samples**	**Time(s)**	**Samples**	**Time(s)**
Mean	-0.333	-0,002	18.83	0,094	38.33	**0,191**	31.83	0,159
Standard Deviation	0.516	0,003	0.752	0,003	2.338	**0,011**	0.752	0,003

Table 7.6: Comparison between the Mean and Standard Deviation of the time difference between the detection of the PFS (with and without the use of the post-processing filter) and the end of the PFS

	Without Filter		**With Filter: Window Size / Number of Samples**					
			20/20		39/39		100/33	
	Samples	**Time(s)**	**Samples**	**Time(s)**	**Samples**	**Time(s)**	**Samples**	**Time(s)**
Mean	242.5	1.215	223.33	1,117	203.83	**1,019**	210.33	1,052
Standard Deviation	21.95	0.109	22.214	0,111	22.0410	**0,110**	21.805	0,109

Table 7.7: Comparison between the Mean and Standard Deviation of the time difference between the detection of the PFS (with and without the use of the post-processing filter) and the impact with the ground

	Without Filter		**With Filter: Window Size / Number of Samples**					
			20/20		39/39		100/33	
	Samples	**Time(s)**	**Samples**	**Time(s)**	**Samples**	**Time(s)**	**Samples**	**Time(s)**
Mean	440.5	2.20	421.33	2,107	401.83	**2,009**	408.33	2,042
Standard Deviation	126.92	0.63	127.19	0,636	125.57	**0,628**	126.98	0,635

For example, in Figure 7.10, a fall trial is depicted with all events marker with an X. The beginning of the PFS is marked at orange, the detection of the PFS with the post-processing algorithm (*window_size* of 39 and *sample_thr* of 39) labelled at green (1.675s and 1.025 before impact and end of the PFS, respectively), the end of the PFS indicated at grey and the impact at yellow.

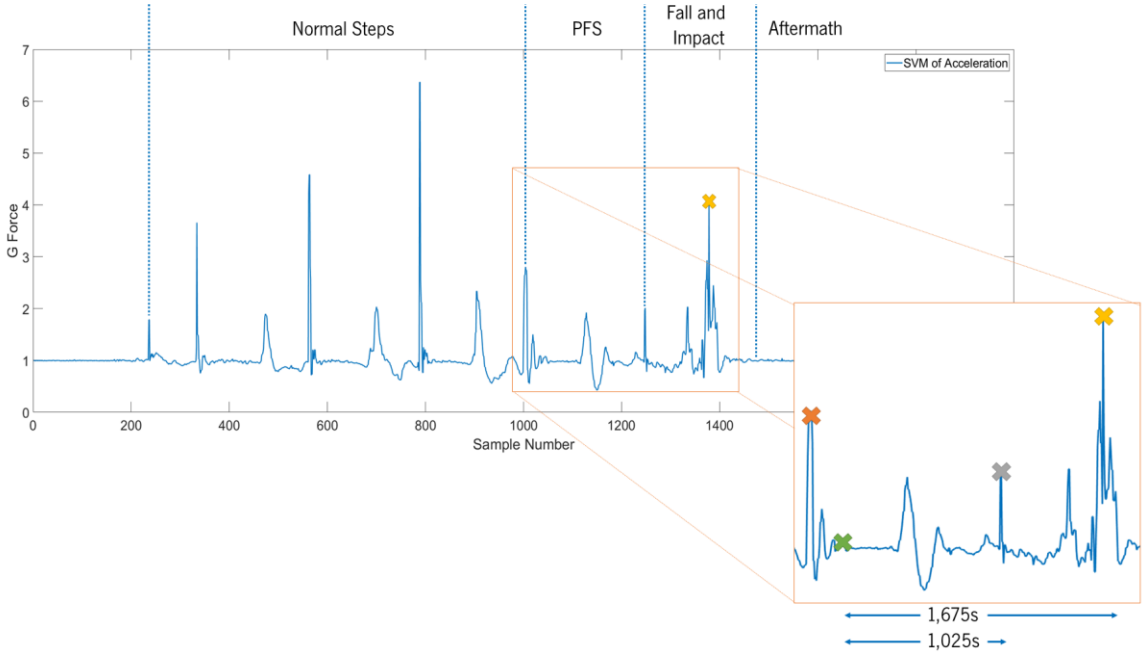

Figure 7.10: PFS detection of a trial with all events marker with an X, PFS (marked at orange), detection of the PFS with the post-processing algorithm (window_size of 39 and sample_thr of 39 marked at green), the end of the PFS (marked at grey) and the impact (marked at yellow).

7.3 Discussion

From Figure 7.6, which represents the evaluation performance of the KNN model with Laplacian Score as feature selection method from 1 to 30 features in the training dataset, the model, with only 10 features, already presents overall performance above 98%. Contrarily, the support vector machines model, Figure 7.7, demands more than 25 features to achieve performance above 90%.

Moreover, starting at 12 features until 30, the performance of the model prevails constant, and slightly decreasing at some iterations. **The highest overall performance of the KNN classifier was with 12 features**, which was the model chosen to the third stage. With the same number of features, the support vector machines present much lower performance, 45.66% in ACC, 45.98% in SENS, 32.98% in SPEC and 12.66%, 33.32%, 82.88% in PREC, F1S and MCC, respectively.

After testing the model with unseen data, even though the performance was high, occasionally the model misclassified samples, resulting in false positive detections, as seen in Figure 7.9 a). **The elimination of PF was imperative** admitting that if a PFS system was installed into the ASCane, it would be activated several times during ADLs.

The developed post-processing filter aimed only at excluding the false positives of the signal. In Figure 7.9 b) it is possible to observe that the **post-processing filter in the unseen data eliminated all PF detections**. However, by applying a *sample_thr* of 39, the PFS will be detected with a delay of 39 samples, which translated to a 0.195s mean delay, as seen in Figure 7.9 b) (zoomed area). To guarantee that a fall is prevented, the system needs to act during PFS. By Table 7.6, with the use of a *window_size* of 39 and *sample_thr* of 39, the **PFS is detected 1.019s before the end of the corresponding PFS and 2.009s before impact**, Table 7.7, which is a significant amount of time for an actuator.

8. Conclusions

Throughout this master thesis, the author realized that the occurrence of falls amongst the elderly is a significant risk that can lead to fatal or non-fatal falls, and present high costs. As a result, it is imperative to achieve efficient methodologies to counteract the stated problem, and any attempt to avoid or prevent a fall can save multiple lives. According to the state-of-the-art, research groups and commercial brands are more focused on fall detection systems embedding IMUs. Nevertheless, only detecting falls is not enough to prevent or save lives. Thus, PFS detection systems are crucial devices that can save lives by detecting a fall before it happens, giving more time to actuate.

Although several steps have already been taken in this direction, one of the conclusions reached is that wearable systems, even with their advantages, still are rejected by patients since the proposed systems required to be attached to the subject's body, which weighs on the individual and constrains his movements. Therefore, embedding sensors into a cane can be the best choice since these assistive devices are widely used amongst the geriatric community and the number of prescriptions is increasing due to gait/balance disorders and lower limbs weakness. Furthermore, an evaluation of the canes gait can be capable of enhancing the ability of cane usage, also reducing the possibility of possible falls amongst them. The work carried out in this dissertation addresses the use of a cane system not only for fall and pre-fall detection but also for the segmentation of a cane stride into six different gait phases.

Chapter 4 addresses the development of the ASCane system. The result is a light and small system, that is easily installed into any ordinary cane. The use of the IMU for the acquisition of kinematics and the FSR limits the number of sensors embedded into the cane, increasing the system simplicity, which facilitates its setup.

Concerning the detection of falls in Chapter 5, typically, FD strategies can be divided into three categories: fixed threshold, adaptive threshold and machine learning. With the application of support vector machines, it was achieved good results (SENS = 83.47%), (SPEC = 96.60%) and (MCC = 82.11%). However, the best performance was achieved with a single lower threshold of 0.2g, (SENS = 96.90%), (SPEC = 98.98%) and (MCC = 95.59%) which decreases the computational power required by the microprocessor used.

Regarding machine learning in this dissertation, the classification of PFS and cane events was established using a min-max scaling procedure [0,1] to normalize the data features, followed by a combination of different machine learning classifiers and feature selection methods. The selected classification algorithm for building the final machine learning model was then optimized with post-processing algorithms and filters.

For the classification of cane events, which is disclosed in Chapter 6, detailed comparisons were evaluated due to the implementation of two different approaches: a finite-state-machine algorithm present in the literature, and a machine learning study to uncover which set of features and classifier better distinguish the six different gait phases of a cane. From these results, it was concluded that, for the time being, the machine learning approach with a post-processing algorithm is more suitable to be embedded into the cane system while the state-of-the-art algorithm is not improved to account for the inertial differences of data acquired in the cane. For the different walking scenarios tested, it was achieved an

overall high performance (ACC = 95.70%, SENS =92.74 %, SPEC =99.13%, PREC = 93.74%) considering the misdetections existed only in the gait event transitions.

The results for PFS detection, the same machine learning approach was conducted, and it was concluded that the combination of the 12 most relevant features from the Laplacian score feature selection methods combined with the KNN (Squared Inverse) as the machine learning classifier provided the best results, followed by an online post-processing filter to remove false positive detections. It was achieved great performance (ACC = 99.65%, SENS =100 %, SPEC =84.44%, PREC = 99.64%) detecting the PFS 1.019s ± 0.110 before its end and 2.009 ± 0.628 before impact.

The work herein presented enables to answer the RQs outlined in Chapter 1.

- **RQ1:** Which is the best fall detection strategy to be implemented in a cane? This RQ is addressed in Chapter 5

  The best fall detection strategy that can be implemented into a cane is a single lower threshold of 0.2g. However, for increased robustness, the use of another threshold, ωres is indicated.

- **RQ2:** Which are the features and machine learning classifier with greater potential to distinguish between the different human gait events in the implemented classifiers? This RQ is addressed in Chapter 6.

  The 20 most significant features resulting from the UDFS combined with the KNN machine learning classifier (followed by and post-processing algorithm) achieved the highest overall performance amongst all combinations tested (Table 6.2). More specifically the Acceleration along the X-axis plane High-Pass filtered with cut-off frequency of 0.1Hz; Acceleration along the Z-axis plane High-Pass filtered with cut-off frequency of 0.1Hz; Raw acceleration along the Z axis; Raw acceleration along the X axis; Gravity Component along the X-axis; Gravity Component along the Z-axis; Displacement along the X axis; Velocity along the Y axis; Velocity along the Z axis; Fourth element of quaternion vector; Euler Angle - Pitch; Third element of quaternion vector; Euler Angle - Yaw; SVM of the angular velocity Band-Pass filtered with cut-off frequencies of 0.1Hz and 90Hz; SVM of the angular velocity High-Pass filtered with a cut-off frequency of 0.1Hz ; Gravity Component along the Y-axis; Angular Velocity along the Z-axis plane High-Pass filtered with cut-off frequency of 0.1Hz; Raw Angular velocity along the Z axis; Second element of quaternion vector and the Euler Angle – Roll. With a 10-5-Fold CV it was

achieved 99.08%, 99.39%, 97.72%, 99.47%, 99.43%, and 97.00% for ACC, SENS, SPEC, PREC, F1S and MCC, respectively. When testing the trained model with unseen data it was achieved an ACC, SENS, SPEC, PREC, F1S and MCC of 99.65%, 100%, 84.44%,99.64%, 99.82% and 91.73%, sequentially.

- **RQ3:** Which are the features and machine learning classifier with greater potential to distinguish between normal gait and pre-fall situations in data acquired from a cane? This RQ is addressed in Chapter 7.

  The 12 most significant features resulting from the Laplacian Score feature selection methods combined with the KNN machine learning classifier (followed by and post-processing filter) achieved the highest overall performance amongst all combinations tested (Table XXII – Appendix 2). More specifically the ASCane FSR; First element of quaternion vector; Correlation Between Angular Velocity X and Z axis; Magnitude of Angular Displacement; Second element of quaternion vector; Roll (Madgwick Sensor-Fusion Algorithm); Maximum Angular Velocity (Z axis); Displacement (Y axis); Resultant of Average Acceleration (Y axis); Yaw (Madgwick Sensor-Fusion Algorithm); SVM of Resultant of Average Acceleration; Resultant of Average Acceleration (X axis); With a 10-5-Fold CV it was achieved 98.85%, 99.29%, 96.97%, 99.30%, 99.29% and 96.25% for ACC, SENS, SPEC, PREC, F1S, and MCC, respectively. When testing the trained model with unseen data it was achieved an ACC, SENS, SPEC, PREC, F1S and MCC of 98.15%, 98.11%, 100%, 100%, 99.04% and 73.15%, sequentially.

8.1 Future Work

As future work, the ASCane system should be improved with some changes at the hardware level. Firstly, the system implementation should be accomplished in a printed circuit board instead of a breadboard since the cane is continuously subjected to falls, the internal circuits can be jeopardised. Secondly, a rechargeable battery should be installed since the ASCane must be connected to a USB power supply (e.g. computer) to operate. Furthermore, interoperability is a subject that needs to be studied regarding the developed system in order to different information systems (e.g. desktop and mobile apps) be able to access, exchange, integrate and cooperatively use data in a coordinated manner. Thus, providing timely and seamless portability of information regarding the health of individuals and populations globally.

Regarding the developed FD strategies (Chapter 5), the addition of the ωres feature into the single LFT algorithm must be tested to perceive if the extra feature increases the overall performance of the developed algorithm. Moreover, it would improve its robustness since it was proved that ωres presents significant differences between fall and ADL situations. Moreover, different labelling methods should be studied regarding the machine learning approach taken since the used method (CVFast) may not be the most suitable for a cane.

The implementation of the newly discovered conditions in the finite-state-machine algorithm for cane event segmentation is mandatory (Chapter 6). Subsequently, a comparison with the attained results from the most suited machine learning model needs to be completed to decide which methodology should be implemented into the microcontroller of the ASCane, enabling real-time testing.

It is also critical to study feature redundancy, both in Chapter 6 and 7, since some of the selected features are highly correlated, offering small training "value" considering that the presence/state of one value (e.g. filtered signal) can always (or almost always) be used to determine the presence/state of the other (e.g. raw signal). Performing a hyperparameter optimisation in the best obtained model is essential since all models in this thesis were trained with the default parameters. Additionally, the construction and use of associative skill memories and convolutional neural networks based on deep learning as tools for locomotion mode recognition (standard steps, PFS and falls) and cane event recognition (FGC, FBC, MSM, PCO, FCO, CMSW) should be completed since are innovative concepts used within the context of human fall prediction and gait analysis. Applying the results from the cane event machine learning model (Chapter 6) as input for the machine learning model, which predicts PFS is also proposed.

In addition, it is required to surmount the considerable small number of samples acquired in Chapters 5, 6 and 7. It would be crucial building such a database with relevant gait parameters obtained from not only healthy but also elderly and impaired subjects during walking over different conditions of speed and ground, using the ASCane system. Consequently, it would be possible to determine if the ASCane is capable of accurately detecting its gait phases, as well as fall and PFS situations.

REFERENCES

[1] J. Rueterbories, E. G. Spaich, B. Larsen, and O. K. Andersen, "Methods for gait event detection and analysis in ambulatory systems," *Med. Eng. Phys.*, vol. 32, no. 6, pp. 545–552, 2010.

[2] M. Yang, H. Zheng, H. Wang, and S. McClean, "Feature selection and construction for the discrimination of neurodegenerative diseases based on gait analysis," *2009 3rd Int. Conf. Pervasive Comput. Technol. Healthc. - Pervasive Heal. 2009, PCTHealth 2009*, 2009.

[3] World Health Organization, "Falls," 2018. [Online]. Available: https://www.who.int/news-room/fact-sheets/detail/falls. [Accessed: 01-Feb-2019].

[4] E. R. Burns, J. A. Stevens, and R. Lee, "The direct costs of fatal and non-fatal falls among older adults — United States," *J. Safety Res.*, vol. 58, pp. 99–103, 2016.

[5] Y. S. Delahoz and M. A. Labrador, "Survey on fall detection and fall prevention using wearable and external sensors," *Sensors (Switzerland)*, vol. 14, no. 10, pp. 19806–19842, 2014.

[6] G. C. Chen, C. N. Huang, C. Y. Chiang, C. J. Hsieh, and C. T. Chan, "A reliable fall detection system based on wearable sensor and signal magnitude area for elderly residents," *Lect. Notes Comput. Sci. (including Subser. Lect. Notes Artif. Intell. Lect. Notes Bioinformatics)*, vol. 6159 LNCS, pp. 267–270, 2010.

[7] T. Xu, Y. Zhou, and J. Zhu, "New advances and challenges of fall detection systems: A survey," *Appl. Sci.*, vol. 8, no. 3, p. 418, 2018.

[8] S. Yusif, J. Soar, and A. Hafeez-Baig, "Older people, assistive technologies, and the barriers to adoption: A systematic review," *Int. J. Med. Inform.*, vol. 94, pp. 112–116, 2016.

[9] N. Noury, P. Rumeau, A. K. Bourke, G. ÓLaighin, and J. E. Lundy, "A proposal for the classification and evaluation of fall detectors," *Irbm*, vol. 29, no. 6, pp. 340–349, 2008.

[10] C. Y. Hsieh, K. C. Liu, C. N. Huang, W. C. Chu, and C. T. Chan, "Novel hierarchical fall detection algorithm using a multiphase fall model," *Sensors (Switzerland)*, vol. 17, no. 2, 2017.

[11] J. Dai, X. Bai, Z. Yang, Z. Shen, and D. Xuan, "PerFallD: A pervasive fall detection system using mobile phones," *2010 8th IEEE Int. Conf. Pervasive Comput. Commun. Work. PERCOM Work. 2010*, pp. 292–297, 2010.

[12] A. Lachtar, T. Val, and A. Kachouri, "3DCane: a monitoring system for the elderly using a connected walking stick," *Int. J. Comput. Sci. Inf. Secur.*, vol. 14, no. 8, pp. 1–8, 2016.

[13] A. J. Campbell, M. J. Borrie, G. F. Spears, S. L. Jackson, J. S. Brown, and J. L. Fitzgerald, "Circumstances and consequences of falls experienced by a community population 70 years and over during a prospective study," *Age Ageing*, vol. 19, no. 2, pp. 136–141, 1990.

[14] C. Becker *et al.*, "Proposal for a multiphase fall model based on real-world fall recordings with body-fixed sensors," *Z. Gerontol. Geriatr.*, vol. 45, no. 8, pp. 707–715, 2012.

[15] Y. W. Bai, S. C. Wu, and C. H. Yu, "Recognition of direction of fall by smartphone," *Can. Conf. Electr. Comput. Eng.*, no. 1, 2013.

[16] M. Kangas, I. Vikman, J. Wiklander, P. Lindgren, L. Nyberg, and T. Jämsä, "Sensitivity and specificity of fall detection in people aged 40 years and over," *Gait Posture*, vol. 29, no. 4, pp. 571–574, 2009.

[17] W. S. Baek, D. M. Kim, F. Bashir, and J. Y. Pyun, "Real life applicable fall detection system based on wireless body area network," *2013 IEEE 10th Consum. Commun. Netw. Conf. CCNC 2013*, pp. 62–67, 2013.

[18] M. V. Albert, K. Kording, M. Herrmann, and A. Jayaraman, "Fall classification by machine learning using mobile phones," *PLoS One*, vol. 7, no. 5, pp. 205–212, 2012.

[19] J. Jacob *et al.*, "A fall detection study on the sensors placement location and a rule-based multi-thresholds algorithm using both accelerometer and gyroscopes," *IEEE Int. Conf. Fuzzy Syst.*, pp. 666–671, 2011.

[20] R. Y. W. Lee and A. J. Carlisle, "Detection of falls using accelerometers and mobile phone technology," *Age Ageing*, vol. 40, no. 6, pp. 690–696, 2011.
[21] M. Mubashir, L. Shao, and L. Seed, "A survey on fall detection: Principles and approaches," *Neurocomputing*, vol. 100, pp. 144–152, 2013.
[22] C. Smeesters, W. C. Hayes, and T. A. McMahon, "Disturbance type and gait speed affect fall direction and impact location," *J. Biomech.*, vol. 34, no. 3, pp. 309–317, 2001.
[23] U. Laessoe, H. C. Hoeck, O. Simonsen, T. Sinkjaer, and M. Voigt, "Fall risk in an active elderly population - Can it be assessed?," *J. Negat. Results Biomed.*, vol. 6, no. 1, p. 2, 2007.
[24] D. Skelton and C. Todd, "What are the main risk factors for falls among older people and what are the most effective interventions to prevent these falls?," *WHO Regional Office for Europe (Health Evidence Network report)*, 2004. [Online]. Available: http://www.euro.who.int/document/E82552.pdf. [Accessed: 05-Oct-2018].
[25] H. Stolze, S. Klebe, C. Zechlin, C. Baecker, L. Friege, and G. Deuschl, "Falls in frequent neurological diseases: Prevalence, risk factors and aetiology," *J. Neurol.*, vol. 251, no. 1, pp. 79–84, 2004.
[26] F. ETO, "Causes of Falls in the Elderly," *J. Japan Med. Assoc.*, vol. 122, no. 13, pp. 1950–1954, 1999.
[27] World Health Organization, "A Global Report on Falls Prevention : Epidemiology of Falls," *WHO Rep.*, pp. 1–32, 2007.
[28] E. Anena and E. Muchane, "A general perspective of falls amongst the elderly. A Literature review study," p. 79, 2012.
[29] M. A. Abdal Qader, R. M. Amin, S. A. Shah, Z. M. Isa, K. A. Latif, and H. F. Ghazi, "Psychological risk factors associated with falls among elderly people in Baghdad city, Iraq," *Open J. Prev. Med.*, vol. 03, no. 07, pp. 441–445, 2013.
[30] A. Lee, K. W. Lee, and P. Khang, "Preventing falls in the geriatric population.," *Perm. J.*, vol. 17, no. 4, pp. 37–39, 2013.
[31] L. Z. Rubenstein and K. R. Josephson, "The epidemiology of falls and syncope," *Clin. Geriatr. Med.*, vol. 18, no. 2, pp. 141–158, 2002.
[32] M. Thibaud *et al.*, "Impact of physical activity and sedentary behaviour on fall risks in older people: A systematic review and meta-analysis of observational studies," *Eur. Rev. Aging Phys. Act.*, vol. 9, no. 1, pp. 5–15, 2012.
[33] B. Homann *et al.*, "The impact of neurological disorders on the risk for falls in the community dwelling elderly: a case-controlled study," *BMJ Open*, vol. 3, no. 11, pp. 1–9, 2013.
[34] V. Weerdesteyn, M. De Niet, H. J. R. Van Duijnhoven, and A. C. H. Geurts, "Falls in individuals with stroke," *J. Rehabil. Res. Dev.*, vol. 45, no. 8, pp. 1195–1214, 2008.
[35] J. Youn, Y. Okuma, M. Hwang, D. Kim, and J. W. Cho, "Falling Direction can Predict the Mechanism of Recurrent Falls in Advanced Parkinson's Disease," *Sci. Rep.*, vol. 7, no. 1, pp. 1–6, 2017.
[36] N. E. Allen, A. K. Schwarzel, and C. G. Canning, "Recurrent falls in parkinson's disease: A systematic review," *Parkinsons. Dis.*, vol. 2013, 2013.
[37] J. D. Schaafsma, N. Giladi, Y. Balash, A. L. Bartels, T. Gurevich, and J. M. Hausdorff, "Gait dynamics in Parkinson's disease: Relationship to Parkinsonian features, falls and response to levodopa," *J. Neurol. Sci.*, vol. 212, no. 1–2, pp. 47–53, 2003.
[38] J. M. Baker, "Gait Disorders," *Am. J. Med.*, vol. 131, no. 6, pp. 602–607, 2018.
[39] Roné Grobbellaar, "COMPARISON BETWEEN FORWARD AND BACKWARD GAIT RETRAINING FOR MOBILITY IN INDIVIDUALS WITH MILD TO MODERATE PARKINSON ' S DISEASE," Stellenbosch University, 2017.
[40] L. Kalilani, M. Asgharnejad, T. Palokangas, and T. Durgin, "Comparing the Incidence of

Falls/Fractures in Parkinson's Disease Patients in the US Population Linda," *PLoS One*, vol. 11, no. 9, pp. 1–11, 2016.
[41] F. E. Shaw, "Falls in cognitive impairment and dementia," *Clin. Geriatr. Med.*, vol. 18, no. 2, pp. 159–173, 2002.
[42] N. Kanemura *et al.*, "Analysis of Risk Factors for Falls in the Elderly with Dementia.," *J. Phys. Ther. Sci.*, vol. 12, no. 1, pp. 27–31, 2000.
[43] L. Gitlin, R. Schemm, L. Landsbergs, and D. Burgh, "Factors predicting Assistive Device use in the Home by Older People Following Rehabilitation," *J. ageing Heal.*, vol. 8, no. 4, pp. 554–575, 1996.
[44] A. M. Hill *et al.*, "Falls after discharge from hospital: Is there a gap between older peoples' knowledge about falls prevention strategies and the research evidence?," *Gerontologist*, vol. 51, no. 5, pp. 653–662, 2011.
[45] C. Luz, T. Bush, X. Shen, and R. Pruchno, "Do canes or walkers make any difference? nonuse and fall injuries," *Gerontologist*, vol. 57, no. 2, pp. 211–218, 2017.
[46] S. C. Coelho Fabrício, R. A. Partezani Rodrigues, and M. Lobo da Costa, "Falls among older adults seen at a São Paulo State public hospital: Causes and consequences," *Rev. Saude Publica*, vol. 38, no. 1, pp. 93–99, 2004.
[47] R. Rajagopalan, I. Litvan, and T. P. Jung, "Fall prediction and prevention systems: Recent trends, challenges, and future research directions," *Sensors (Switzerland)*, vol. 17, no. 11, pp. 1–17, 2017.
[48] E. E. Stone and M. Skubic, "Fall detection in homes of older adults using the microsoft kinect," *IEEE J. Biomed. Heal. Informatics*, vol. 19, no. 1, pp. 290–301, 2015.
[49] K. Chaccour, R. Darazi, A. H. El Hassani, and E. Andres, "From Fall Detection to Fall Prevention: A Generic Classification of Fall-Related Systems," *IEEE Sens. J.*, vol. 17, no. 3, pp. 812–822, 2017.
[50] K. M. Culhane, M. O'Connor, D. Lyons, and G. M. Lyons, "Accelerometers in rehabilitation medicine for older adults," *Age Ageing*, vol. 34, no. 6, pp. 556–560, 2005.
[51] M. Kangas, A. Konttila, P. Lindgren, I. Winblad, and T. Jämsä, "Comparison of low-complexity fall detection algorithms for body attached accelerometers," *Gait Posture*, vol. 28, no. 2, pp. 285–291, 2008.
[52] A. K. Bourke and G. M. Lyons, "A threshold-based fall-detection algorithm using a bi-axial gyroscope sensor," *Med. Eng. Phys.*, vol. 30, no. 1, pp. 84–90, 2008.
[53] S. H. Fang, Y. C. Liang, and K. M. Chiu, "Developing a mobile phone-based fall detection system on android platform," *2012 Comput. Commun. Appl. Conf. ComComAp 2012*, pp. 143–146, 2012.
[54] N. Pannurat, S. Thiemjarus, and E. Nantajeewarawat, "Automatic fall monitoring: A review," *Sensors (Switzerland)*, vol. 14, no. 7, pp. 12900–12936, 2014.
[55] J. T. Perry, S. Kellog, S. M. Vaidya, J. H. Youn, H. Ali, and H. Sharif, "Survey and evaluation of real-time fall detection approaches," *6th Int. Symp. High Capacit. Opt. Networks Enabling Technol. HONET '09*, pp. 158–164, 2009.
[56] L. Liu, M. Popescu, M. Rantz, and M. Skubic, "Fall detection using doppler radar and classifier fusion," *Proc. - IEEE-EMBS Int. Conf. Biomed. Heal. Informatics Glob. Gd. Chall. Heal. Informatics, BHI 2012*, vol. 25, no. Bhi, pp. 180–183, 2012.
[57] S. Hwang and M. Ryu, "Fall Detection with Three-Axis Accelerometer and Magnetometer in a Smartphone," *Proc. Int. Conf. Comput. Sci. Technol.*, pp. 65–70, 2012.
[58] M. Kangas, A. Konttila, I. Winblad, and T. Jämsä, "Determination of simple thresholds for accelerometry-based parameters for fall detection," *Annu. Int. Conf. IEEE Eng. Med. Biol. - Proc.*, vol. 2007, pp. 1367–1370, 2007.

[59] F. Wu, H. Zhao, Y. Zhao, and H. Zhong, “Development of a wearable-sensor-based fall detection system,” *Int. J. Telemed. Appl.*, vol. 2015, p. e576364, 2015.

[60] C. F. Lai, S. Y. Chang, H. C. Chao, and Y. M. Huang, “Detection of cognitive injured body region using multiple triaxial accelerometers for elderly falling,” *IEEE Sens. J.*, vol. 11, no. 3, pp. 763–770, 2011.

[61] F. Bianchi, S. J. Redmond, M. R. Narayanan, S. Cerutti, and N. H. Lovell, “Barometric pressure and triaxial accelerometry-based falls event detection,” *IEEE Trans. Neural Syst. Rehabil. Eng.*, vol. 18, no. 6, pp. 619–627, 2010.

[62] A. Raj, K. Gandhi, B. T. Nalla, and N. K. Verma, *Human Fall Detection System over IMU Sensors Using Triaxial Accelerometer*, vol. II. Springer Singapore, 2018.

[63] W. Engel and W. Ding, “Reliable and practical fall prediction using artificial neural network,” *ICNC-FSKD 2017 - 13th Int. Conf. Nat. Comput. Fuzzy Syst. Knowl. Discov.*, pp. 1867–1871, 2018.

[64] K.-H. Chen, J.-J. Yang, and F.-S. Jaw, “Accelerometer-based fall detection using feature extraction and support vector machine algorithms,” *Instrum. Sci. Technol.*, vol. 44, no. 4, pp. 333–342, Jul. 2016.

[65] I. Putra, J. Brusey, E. Gaura, and R. Vesilo, “An Event-Triggered Machine Learning Approach for Accelerometer-Based Fall Detection,” *Sensors*, vol. 18, no. 2, p. 20, Dec. 2017.

[66] S.-H. Liu and W.-C. Cheng, “Fall Detection with the Support Vector Machine during Scripted and Continuous Unscripted Activities,” *Sensors*, vol. 12, no. 9, pp. 12301–12316, Sep. 2012.

[67] A. T. Özdemir and B. Barshan, “Detecting falls with wearable sensors using machine learning techniques,” *Sensors (Switzerland)*, vol. 14, no. 6, pp. 10691–10708, 2014.

[68] Y. Tao, H. Qian, M. Chen, X. Shi, and Y. Xu, “A Real-time intelligent shoe system for fall detection,” *2011 IEEE Int. Conf. Robot. Biomimetics, ROBIO 2011*, pp. 2253–2258, 2011.

[69] Y. Angal and A. Jagtap, “Fall detection system for older adults,” *2016 IEEE Int. Conf. Adv. Electron. Commun. Comput. Technol. ICAECCT 2016*, pp. 262–266, 2017.

[70] S. Zhao, W. Li, W. Niu, R. Gravina, and G. Fortino, “Recognition of Human Fall Events Based on Single Tri-axial Gyroscope,” 2018.

[71] K. L. Perell, A. Nelson, R. L. Goldman, S. L. Luter, N. Prieto-Lewis, and L. Z. Rubenstein, “Fall risk assessment measures: An analytic review,” *Journals Gerontol. - Ser. A Biol. Sci. Med. Sci.*, vol. 56, no. 12, pp. 761–766, 2001.

[72] J. Silva and I. Sousa, “Instrumented timed up and go: Fall risk assessment based on inertial wearable sensors,” *2016 IEEE Int. Symp. Med. Meas. Appl. MeMeA 2016 - Proc.*, vol. 2020, 2016.

[73] T. Tamura, T. Yoshimura, M. Sekine, M. Uchida, and O. Tanaka, “A wearable airbag to prevent fall injuries,” *IEEE Trans. Inf. Technol. Biomed.*, vol. 13, no. 6, pp. 910–914, 2009.

[74] National Center for Chronic Disease Prevention and Health, “The state of aging and health in America 2007,” 2013. [Online]. Available: https://www.cdc.gov/aging/pdf/state-aging-health-in-america-2013.pdf. [Accessed: 05-Aug-2019].

[75] J. Liu, X. Zhang, and T. E. Lockhart, “Fall risk assessments based on postural and dynamic stability using inertial measurement unit,” *Saf. Health Work*, vol. 3, no. 3, pp. 192–198, 2012.

[76] T. R. Burchfield and S. Venkatesan, “Accelerometer-based human abnormal movement detection in wireless sensor networks,” *Heal. Proc. 1st ACM SIGMOBILE Int. Work. Syst. Netw. Support Healthc. Assist. Living Environ.*, pp. 67–69, 2007.

[77] T. E. Lockhart and J. Liu, “Differentiating fall-prone and healthy adults using local dynamic stability,” *Ergonomics*, vol. 51, no. 12, pp. 1860–1872, 2008.

[78] G. Shi, Y. Zou, Y. Jin, X. Cui, and W. J. Li, “Towards HMM based human motion recognition using MEMS inertial sensors,” *2008 IEEE Int. Conf. Robot. Biomimetics, ROBIO 2008*, pp.

1762–1766, 2008.
[79] Y. Liu *et al.*, "Validation of an accelerometer-based fall prediction model," *2014 36th Annu. Int. Conf. IEEE Eng. Med. Biol. Soc. EMBC 2014*, pp. 4531–4534, 2014.
[80] A. González, M. Hayashibe, V. Bonnet, and P. Fraisse, "Whole body center of mass estimation with portable sensors: Using the statically equivalent serial chain and a kinect," *Sensors (Switzerland)*, vol. 14, no. 9, pp. 16955–16971, 2014.
[81] E. P. Doheny *et al.*, "Displacement of centre of mass during quiet standing assessed using accelerometry in older fallers and non-fallers," pp. 3300–3303, 2012.
[82] F. R. Allen, E. Ambikairajah, N. H. Lovell, and B. G. Celler, "An adapted Gaussian mixture model approach to accelerometry-based movement classification using time-domain features," *Annu. Int. Conf. IEEE Eng. Med. Biol. - Proc.*, pp. 3600–3603, 2006.
[83] I. Cleland *et al.*, "Optimal placement of accelerometers for the detection of everyday activities.," *Sensors (Basel).*, vol. 13, no. 7, pp. 9183–9200, 2013.
[84] B. Cates, T. Sim, H. M. Heo, B. Kim, H. Kim, and J. H. Mun, "A novel detection model and its optimal features to classify falls from low- and high-acceleration activities of daily life using an insole sensor system," *Sensors (Switzerland)*, vol. 18, no. 4, 2018.
[85] J. J. Kavanagh and H. B. Menz, "Accelerometry: A technique for quantifying movement patterns during walking," *Gait Posture*, vol. 28, no. 1, pp. 1–15, 2008.
[86] Ning Wang, E. Ambikairajah, N. H. Lovell, and B. G. Celler, "Accelerometry Based Classification of Walking Patterns Using Time-frequency Analysis Ning," 2007.
[87] M. Iosa, T. Marro, S. Paolucci, and D. Morelli, "Stability and harmony of gait in children with cerebral palsy," *Res. Dev. Disabil.*, vol. 33, no. 1, pp. 129–135, 2012.
[88] L. Z. Rubenstein and K. R. Josephson, "Falls and Their Prevention in Elderly People: What Does the Evidence Show?," *Med. Clin. North Am.*, vol. 90, no. 5, pp. 807–824, 2006.
[89] World Health Organization, "WHo Global report on falls Prevention in older Age," 2007. [Online]. Available: https://www.who.int/ageing/publications/Falls_prevention7March.pdf. [Accessed: 06-Jun-2019].
[90] B. J. Kercher and L. Z. Rubenstein, "Home-Safety Checklists for Elders in Print and on the Internet," *Generations*, vol. 26, no. 4, pp. 69–74, 2002.
[91] B. Aguiar, T. Rocha, J. Silva, and I. Sousa, "Accelerometer-based fall detection for smartphones," *IEEE MeMeA 2014 - IEEE Int. Symp. Med. Meas. Appl. Proc.*, 2014.
[92] P. Pierleoni, A. Belli, L. Palma, M. Pellegrini, L. Pernini, and S. Valenti, "A High Reliability Wearable Device for Elderly Fall Detection," *IEEE Sens. J.*, vol. 15, no. 8, pp. 4544–4553, 2015.
[93] G. Shi, C. S. Chan, W. J. Li, K. S. Leung, Y. Zou, and Y. Jin, "Mobile human airbag system for fall protection using mems sensors and embedded SVM classifier," *IEEE Sens. J.*, vol. 9, no. 5, pp. 495–503, 2009.
[94] W. Wu *et al.*, "The SmartCane System: An Assistive Device for Geriatrics," in *Proceedings of the 3rd International ICST Conference on Body Area Networks*, 2008, no. June, pp. 0–3.
[95] M. Lan, A. Nahapetian, A. Vahdatpour, L. Au, W. Kaiser, and M. Sarrafzadeh, "SmartFall: An automatic fall detection system based on subsequence matching for the smartcane," *BODYNETS 2009 - 4th Int. ICST Conf. Body Area Networks*, p. 8, 2011.
[96] H. Bateni and B. E. Maki, "Assistive devices for balance and mobility: Benefits, demands, and adverse consequences," *Arch. Phys. Med. Rehabil.*, vol. 86, no. 1, pp. 134–145, 2005.
[97] C. Sadowski and A. Jones, "Ambulatory assistive devices. How to appropriately measure and use canes, crutches and walkers," *Pharm. Pract. (Granada).*, 2014.
[98] O. Almeida, M. Zhang, and J. C. Liu, "Dynamic fall detection and pace measurement in walking sticks," *Proc. - 2007 Jt. Work. High Confid. Med. Devices, Software, Syst. Med. Device*

Plug-and-Play Interoperability, HCMDSS/MDPnP 2007, pp. 204–206, 2007.
[99] Y. Hui-Ching, "Elderly People's Use of and Attitudes towards Assistive Devices," Queensland University of Technology, 2009.
[100] P. Di *et al.*, "Fall detection and prevention control using walking-aid cane robot," *IEEE/ASME Trans. Mechatronics*, vol. 21, no. 2, pp. 625–637, 2016.
[101] P. Di, J. Huang, S. Nakagawa, K. Sekiyama, and T. Fukuda, "Fall detection and prevention in the elderly based on the ZMP stability control," *Proc. IEEE Work. Adv. Robot. its Soc. Impacts, ARSO*, pp. 82–87, 2013.
[102] P. Di, J. Huang, S. Nakagawa, K. Sekiyama, and T. Fukuda, "Fall detection for the elderly using a cane robot based on ZMP estimation," *2013 Int. Symp. Micro-NanoMechatronics Hum. Sci. MHS 2013*, 2013.
[103] P. Di, J. Huang, K. Sekiyama, and T. Fukuda, "Motion control of intelligent cane robot under normal and abnormal walking condition," *Proc. - IEEE Int. Work. Robot Hum. Interact. Commun.*, pp. 497–502, 2011.
[104] Q. Yan, J. Huang, and Z. Luo, "Human-robot coordination stability for fall detection and prevention using cane robot," *2016 Int. Symp. Micro-NanoMechatronics Hum. Sci. MHS 2016*, no. 1, 2017.
[105] P. H. Chen, Y. H. Li, C. W. Chiou, C. Y. Lee, and J. M. Lin, "A smart safety cane for human fall detection," *Int. J. Ad Hoc Ubiquitous Comput.*, vol. 20, no. 1, pp. 49–65, 2015.
[106] "iStand Smartcane," 2018. [Online]. Available: https://istandtoday.com/. [Accessed: 01-Nov-2018].
[107] "Dring Smartcane," 2018. [Online]. Available: https://dring.io/11-canne-connectee-fayet. [Accessed: 01-Nov-2018].
[108] H. Ping, "Anti-falling walking stick for old person," 2015. [Online]. Available: https://worldwide.espacenet.com/publicationDetails/biblio?II=2&ND=3&adjacent=true&locale=en_EP&FT=D&date=20150114&CC=CN&NR=104273812A&KC=A. [Accessed: 12-Nov-2018].
[109] Y. Ota, S. Sano, M. Ryumae, and K. Sato, "Robotic cane devices," 2010. [Online]. Available: https://worldwide.espacenet.com/publicationDetails/biblio?II=0&ND=3&adjacent=true&locale=en_EP&FT=D&date=20130214&CC=US&NR=2013041507A1&KC=A1. [Accessed: 12-Nov-2018].
[110] "WALKING SUPPORT DEVICE AND FALL PREVENTION METHOD USING THE SAME," 2015. [Online]. Available: https://worldwide.espacenet.com/publicationDetails/biblio?II=0&ND=3&adjacent=true&locale=en_EP&FT=D&date=20151207&CC=JP&NR=2015217155A&KC=A. [Accessed: 12-Nov-2018].
[111] M. Ashfak Habib, M. S. Mohktar, S. Bahyah Kamaruzzaman, K. Seang Lim, T. Maw Pin, and F. Ibrahim, "Smartphone-based solutions for fall detection and prevention: Challenges and open issues," *Sensors (Switzerland)*, vol. 14, no. 4, pp. 7181–7208, 2014.
[112] STMicroeletronics, "NUCLEO-F303K8." [Online]. Available: https://www.st.com/en/evaluation-tools/nucleo-f303k8.html/. [Accessed: 22-Aug-2019].
[113] MBed, "NUCLEO-F303K8." [Online]. Available: https://os.mbed.com/platforms/ST-Nucleo-F303K8/. [Accessed: 22-Aug-2019].
[114] STMicroeletronics, "STM32CubeMX." [Online]. Available: https://www.st.com/en/development-tools/stm32cubemx.html. [Accessed: 22-Aug-2019].
[115] Adafruit Industries, "Micro SD Card Breakout Board Tutorial." [Online]. Available: https://learn.adafruit.com/adafruit-micro-sd-breakout-board-card-tutorial?view=all. [Accessed: 22-Aug-2019].
[116] R. Mustafaoğlu, B. Unver, and V. Karatosun, "Evaluation of stair climbing in elderly people," *J. Back Musculoskelet. Rehabil.*, vol. 28, no. 3, pp. 509–516, Jun. 2015.

[117] H. J. Lee and L. S. Chou, “Balance control during stair negotiation in older adults,” *J. Biomech.*, vol. 40, no. 11, pp. 2530–2536, 2007.
[118] R. Boonsinsukh, L. Panichareon, V. Saengsirisuwan, and P. Phansuwan-Pujito, “Clinical Identification for the Use of Light Touch Cues with a Cane in Gait Rehabilitation Poststroke,” *Top. Stroke Rehabil.*, vol. 18, no. sup1, pp. 633–642, Oct. 2011.
[119] M. R. Afzal, I. Hussain, Y. Jan, and J. Yoon, “Design of a haptic cane for walking stability and rehabilitation,” *Int. Conf. Control. Autom. Syst.*, no. Iccas, pp. 1450–1454, 2013.
[120] M. Studio, “ALBERT.” [Online]. Available: https://www.miio-studio.com/albert. [Accessed: 23-Aug-2019].
[121] R. Velik, “Effect of On-Demand Cueing on Freezing of Gait in Parkinson’ s Patients,” *Int. J. Medical, Pharm. Sci. Eng.*, vol. 6, no. 6, pp. 10–15, 2012.
[122] M. Caroline, E. Bruno, A. Samuel, S. Horacio, and H. M. Abiel, “Fisiología de la vibración,” *Rev Mex Neuroci*, vol. 15, no. 15, pp. 163–170, 2014.
[123] K. Myles and M. Binseel, “The Tactile Modality: A Review of Tactile Sensitivity and Human Tactile Interfaces,” *Army Res. Lab.*, pp. 1–27, Jan. 2007.
[124] T. L. White, *Suitable Body Locations and Vibrotactile Cueing Types for Dismounted Soldiers*, no. May. 2010.
[125] MaxBotix, “LV-MaxSonar-EZ.” [Online]. Available: https://www.maxbotix.com/documents/LV-MaxSonar-EZ_Datasheet.pdf. [Accessed: 25-Aug-2019].
[126] P. Microdrives, “Model No. 310-103.005 10mm Vibration Motor.” [Online]. Available: https://www.precisionmicrodrives.com/product/310-103-005-10mm-vibration-motor-3mm-type. [Accessed: 24-Aug-2019].
[127] T. Instruments, “DRV2605.” [Online]. Available: http://www.ti.com/lit/ds/symlink/drv2605.pdf. [Accessed: 27-Aug-2019].
[128] InvenSense, “MPU-9250.” [Online]. Available: http://www.invensense.com/wp-content/uploads/2015/02/PS-MPU-9250A-01-v1.1.pdf. [Accessed: 29-Aug-2019].
[129] C. V Bouten, K. T. Koekkoek, M. Verduin, R. Kodde, and J. D. Janssen, “A triaxial accelerometer and portable data processing unit for the assessment of daily physical activity.,” *IEEE Trans. Biomed. Eng.*, vol. 44, no. 3, pp. 136–47, Mar. 1997.
[130] A. T. Özdemir, “An Analysis on Sensor Locations of the Human Body for Wearable Fall Detection Devices: Principles and Practice.,” *Sensors (Basel).*, vol. 16, no. 8, p. 1161, Jul. 2016.
[131] D. Rodríguez-Martín, C. Pérez-López, A. Samà, J. Cabestany, and A. Català, “A Wearable Inertial Measurement Unit for Long-Term Monitoring in the Dependency Care Area,” *Sensors*, vol. 13, no. 10, pp. 14079–14104, Oct. 2013.
[132] I. Eletronics, “FSR 402 Data Sheet.” [Online]. Available: http://www.trossenrobotics.com/productdocs/2010-10-26-DataSheet-FSR402-Layout2.pdf. [Accessed: 29-Aug-2019].
[133] D. Razum, G. Seketa, J. Vugrin, and I. Lackovic, “Optimal threshold selection for threshold-based fall detection algorithms with multiple features,” in *2018 41st International Convention on Information and Communication Technology, Electronics and Microelectronics (MIPRO)*, 2018, pp. 1513–1516.
[134] A. K. Bourke, J. V. O’Brien, and G. M. Lyons, “Evaluation of a threshold-based tri-axial accelerometer fall detection algorithm,” *Gait Posture*, vol. 26, no. 2, pp. 194–199, 2007.
[135] N. Otanasap, “Pre-impact fall detection based on wearable device using dynamic threshold model,” *Parallel Distrib. Comput. Appl. Technol. PDCAT Proc.*, pp. 362–365, 2017.
[136] M. N. Nyan, F. E. H. Tay, A. W. Y. Tan, and K. H. W. Seah, “Distinguishing fall activities from normal activities by angular rate characteristics and high-speed camera characterization,” *Med. Eng. Phys.*, vol. 28, no. 8, pp. 842–849, 2006.

[137] A. Ligeza, *Artificial Intelligence: A Modern Approach*, vol. 9, no. 2. 1995.
[138] A. Nath, S. Agarwal, and A. Ghosh, "Classification of Machine Learning Algorithms," *Int. J. Innov. Res. Adv. Eng.*, vol. 3, no. March, pp. 6–11, 2016.
[139] S. Wang, J. Tang, and H. Liu, "Feature Selection," *Encyclopedia of Machine Learning and Data Mining*. 2016.
[140] Y. Choi, A. S. Ralhan, and S. Ko, "A study on machine learning algorithms for fall detection and movement classification," *2011 Int. Conf. Inf. Sci. Appl. ICISA 2011*, 2011.
[141] M. Daoudi, *Data Mining*, vol. 11, no. 3. Elsevier, 2017.
[142] N. Shibuya *et al.*, "A real-time fall detection system using a wearable gait analysis sensor and a Support Vector Machine (SVM) classifier," *2015 8th Int. Conf. Mob. Comput. Ubiquitous Networking, ICMU 2015*, pp. 66–67, 2015.
[143] H. (Howe) Liu, J. Eaves, W. Wang, J. Womack, and P. Bullock, "Assessment of canes used by older adults in senior living communities," *Arch. Gerontol. Geriatr.*, vol. 52, no. 3, pp. 299–303, May 2011.
[144] T. Roman de Mettelinge and D. Cambier, "Understanding the Relationship Between Walking Aids and Falls in Older Adults," *J. Geriatr. Phys. Ther.*, vol. 38, no. 3, pp. 127–132, 2015.
[145] J. Taborri, E. Palermo, S. Rossi, and P. Cappa, "Gait partitioning methods: A systematic review," *Sensors (Switzerland)*, vol. 16, no. 1, pp. 40–42, 2016.
[146] N. Abaid, P. Cappa, E. Palermo, M. Petrarca, and M. Porfiri, "Gait Detection in Children with and without Hemiplegia Using Single-Axis Wearable Gyroscopes," *PLoS One*, vol. 8, no. 9, pp. 1–8, 2013.
[147] P. Catalfamo, S. Ghoussayni, and D. Ewins, "Gait event detection on level ground and incline walking using a rate gyroscope," *Sensors*, vol. 10, no. 6, pp. 5683–5702, 2010.
[148] "Proper Ambulation with a Cane." [Online]. Available: https://www.physio-pedia.com/Proper_Ambulation_with_a_Cane. [Accessed: 12-Nov-2019].
[149] K. Aminian, B. Najafi, C. Büla, P. F. Leyvraz, and P. Robert, "Spatio-temporal parameters of gait measured by an ambulatory system using miniature gyroscopes," *J. Biomech.*, vol. 35, no. 5, pp. 689–699, 2002.
[150] A. T. M. Willemsen, J. A. van Alsté, and H. B. K. Boom, "Real-time gait assessment utilizing a new way of accelerometry," *J. Biomech.*, vol. 23, no. 8, pp. 859–863, 1990.
[151] R. Williamson and B. J. Andrews, "Gait event detection for FES using accelerometers and supervised machine learning," *IEEE Trans. Rehabil. Eng.*, vol. 8, no. 3, pp. 312–319, 2000.
[152] J. Figueiredo, P. Felix, L. Costa, J. C. Moreno, and C. P. Santos, "Gait Event Detection in Controlled and Real-Life Situations: Repeated Measures From Healthy Subjects," *IEEE Trans. Neural Syst. Rehabil. Eng.*, vol. 26, no. 10, pp. 1945–1956, Oct. 2018.
[153] H. B. Moss, D. S. Leslie, and P. Rayson, "Using J-K fold Cross Validation to Reduce Variance When Tuning NLP Models," pp. 2978–2989, 2018.
[154] H. C. van Houwelingen and W. Sauerbrei, "Cross-Validation, Shrinkage and Variable Selection in Linear Regression Revisited," *Open J. Stat.*, vol. 03, no. 02, pp. 79–102, 2013.
[155] J. Huang, P. Di, K. Wakita, T. Fukuda, and K. Sekiyama, "Study of Fall Detection Using Intelligent Cane Based on Sensor Fusion Force Sencr rage ptb a pln," pp. 495–500, 2008.
[156] P. Di, J. Huang, S. Nakagawa, K. Sekiyama, and T. Fukuda, "Fall detection for elderly by using an intelligent cane robot based on center of pressure (COP) stability theory," *2014 Int. Symp. Micro-NanoMechatronics Hum. Sci. MHS 2014*, pp. 3–6, 2015.
[157] N. F. Ribeiro, J. André, L. Costa, and C. P. Santos, "Development of a Strategy to Predict and Detect Falls Using Wearable Sensors," *J. Med. Syst.*, vol. 43, no. 5, 2019.

APPENDICES

Appendix 1

In this appendix it is represented the complete results regarding chapter 6.

Table I: Algorithm performance in controlled situations with ground truth the manual segmentation

Gait Event	ACC	Delay		Advance		ND within range	ND by Cane
		%	ms	%	ms		
FGC	83.92	14.37	19.25±10.61	69.36	45.34±25.31	14.92	1.16
FBC	46.34	43.25	55.32±27.90	8.47	43.92±30.44	52.49	1.16
MSM	0.74	28.57	35.00±0.00	71.43	58.00±30.33	98.09	1.16
PCO	0.96	11.11	90.00±0.00	77.78	78.57±21.74	97.87	1.17
FCO	22.60	34.91	51.42±16.85	57.08	53.06±28.32	76.33	1.01
CMSW	98.51	0.95	6.67±4.08	0.76	19.29±29.50	0.42	1.01

Table II: Algorithm performance in Real-Life situations (Level-ground Surfaces) with ground the manual segmentation

Gait Event	ACC	Delay		Advance		ND within range	ND by Cane
		%	ms	%	ms		
FGC	72.38	0.76	15.00±0.00	96.94	54.13±23.87	22.65	4.97
FBC	49.45	29.61	35.19±23.31	30.17	44.07±26.74	45.58	4.97
MSM	8.84	15.63	43.00±16.81	68.75	62.27±28.52	86.19	4.97
PCO	12.98	8.51	38.75±31.98	85.10	67.50±24.62	82.59	4.41
FCO	46.54	2.38	10.00±4.08	74.40	42.60±23.98	49.58	3.88
CMSW	93.54	0.60	5.00±0.00	1.50	7.60±4.2.52	2.52	3.93

Table III: Algorithm performance in Real-Life situations (Inclined Surfaces) with ground the manual segmentation

Gait Event	ACC	Delay		Advance		ND within range	ND by Cane
		%	ms	%	ms		
FGC	72.19	1.83	12.50±3.54	95.41	51.68±24.98	19.21	8.61
FBC	56.95	18.60	47.50±28.87	29.07	53.00±28.46	34.44	8.61
MSM	7.28	0	0.00±0.00	81.81	77.22±19.22	84.11	8.61
PCO	10.60	18.75	13.33±10.41	75.00	77.92±20.05	78.80	10.60

Gait Event	ACC	Delay		Advance		ND within range	ND by Cane
		%	ms	%	ms		
FCO	38.93	5.17	16.67±10.41	77.59	42.89±25.79	52.35	8.72
CMSW	87.42	0	0.00±0.00	0.76	5.00±0.00	3.97	8.61

Table IV: Algorithm performance in Real-Life situations (Stairs) with ground the manual segmentation

Gait Event	ACC	Delay		Advance		ND within range	ND by Cane
		%	ms	%	ms		
FGC	52.78	17.54	18.50±11.07	75.43	54.30±22.00	17.59	29.63
FBC	34.26	32.43	34.17±21.30	29.73	30.00±22.36	36.11	29.63
MSM	11.11	16.67	80.00±21.21	41.67	52.00±38.01	59.26	29.63
PCO	17.59	26.32	30.00±27.16	68.42	78.46±23.66	52.77	29.63
FCO	34.26	24.32	69.44±36.70	45.95	46.76±26.34	42.59	23.15
CMSW	77.36	0	0.00±0.00	0	0.00±0.00	0	22.65

Table V: Comparison of the best classification results (ACC, SENS, SPEC, PREC, F1S, MCC), selected by the highest ACC, for the different machine learning classifiers trained with the features ranked by the CFS feature selection method (fist stage)

Classifiers	Overall Performance						Number of Features
	ACC	SENS	SPEC	PREC	F1S	MCC	
KNN Squared Inverse	77.67	77.90	95.50	77.93	77.87	73.41	120
KNN Equal	77.67	77.90	95.50	77.93	77.87	73.41	120
KNN Inverse	77.67	77.90	95.50	77.93	77.87	73.41	120
DA Linear	77.07	76.42	95.39	78.83	76.77	72.79	75
DA Quadratic	70.13	68.71	93.99	71.20	68.23	63.54	75
Ensemble Learning	94.35	94.29	98.86	94.38	94.32	93.13	113
Decision Tree	90.04	90.00	98.00	89.96	89.90	87.97	117
Regression Model - Linear	46.88	46.48	89.24	54.09	45.67	38.21	120
Regression Model – Pure Quadratic	58.17	57.38	91.54	64.07	57.03	51.24	120

Table VI: Comparison of the best classification results (ACC, SENS, SPEC, PREC, F1S, MCC), selected by the highest ACC, for the different machine learning classifiers trained with the features ranked by the Laplacian Score feature selection method (fist stage)

Classifiers	Overall Performance						Number of Features
	ACC	SENS	SPEC	PREC	F1S	MCC	
KNN Squared Inverse	86.27	86.61	97.23	86.45	86.45	83.74	60
KNN Equal	86.27	86.61	97.23	86.45	86.45	83.74	60
KNN Inverse	86.27	86.61	97.23	86.45	86.45	83.74	60
DA Linear	69.40	69.18	93.90	70.58	68.71	63.44	102
DA Quadratic	65.32	64.03	93.09	66.60	63.82	58.01	95
Ensemble Learning	95.72	95.63	99.14	95.70	95.65	94.80	111
Decision Tree	90.95	90.79	98.18	90.80	90.79	88.97	110
Regression Model - Linear	57.49	56.23	91.41	62.80	55.36	49.75	120
Regression Model – Pure Quadratic	61.78	60.80	92.28	66.14	60.61	54.98	120

Table VII: Comparison of the best classification results ((ACC, SENS, SPEC, PREC, F1S, MCC), selected by the highest ACC, for the different machine learning classifiers trained with the features ranked by the LASSO feature selection method (fist stage)

Classifiers	Overall Performance						Number of Features
	ACC	SENS	SPEC	PREC	F1S	MCC	
KNN Squared Inverse	90.86	90.85	98.16	90.72	90.75	88.94	34
KNN Equal	90.86	90.85	98.16	90.72	90.75	88.94	34
KNN Inverse	90.86	90.85	98.16	90.72	90.75	88.94	34
DA Linear	69.41	69.14	93.88	71.61	69.20	63.95	117
DA Quadratic	64.20	61.69	92.80	64.39	60.88	55.33	118
Ensemble Learning	93.17	92.86	98.62	93.26	93.03	91.68	119
Decision Tree	86.89	86.54	97.37	86.50	86.52	83.89	117
Regression Model - Linear	43.37	43.83	88.61	47.40	40.54	32.30	119
Regression Model – Pure Quadratic	50.76	50.15	90.10	53.96	48.71	41.16	120

Table VIII: Comparison of the best classification results (ACC, SENS, SPEC, PREC, F1S, MCC), selected by the highest ACC, for the different machine learning classifiers trained with the features ranked by the LLCFS feature selection method (fist stage)

Classifiers	Overall Performance						Number of Features
	ACC	SENS	SPEC	PREC	F1S	MCC	
KNN Squared Inverse	84.39	84.59	96.86	84.49	84.43	81.37	120
KNN Equal	84.39	84.59	96.86	84.49	84.43	81.37	120
KNN Inverse	84.39	84.59	96.86	84.49	84.43	81.37	120
DA Linear	75.91	75.68	95.20	76.42	75.46	71.05	116
DA Quadratic	72.87	72.25	94.57	73.85	72.10	67.39	31
Ensemble Learning	96.10	96.03	99.22	96..06	96.02	95.26	118
Decision Tree	91.83	91.73	98.36	91.74	91.73	90.09	120
Regression Model - Linear	60.51	59.36	92.02	65.22	59.32	53.50	120
Regression Model – Pure Quadratic	63.96	62.93	92.72	67.83	63.03	57.48	120

Table IX: Comparison of the best classification results (ACC, SENS, SPEC, PREC, F1S, MCC), selected by the highest ACC, for the different machine learning classifiers trained with the features ranked by the PCA feature selection method (fist stage)

Classifiers	Overall Performance						Number of Features
	ACC	SENS	SPEC	PREC	F1S	MCC	
KNN Squared Inverse	92.38	92.51	98.47	92.36	92.40	90.89	62
KNN Equal	92.38	92.51	98.47	92.36	92.40	90.89	62
KNN Inverse	92.38	92.51	98.47	92.36	92.40	90.89	62
DA Linear	68.12	67.66	93.63	69.72	67.24	61.94	120
DA Quadratic	62.86	61.16	92.61	64.35	60.72	54.81	106
Ensemble Learning	95.08	94.95	99.01	95.06	94.98	94.01	103
Decision Tree	91.11	90.95	98.21	90.95	90.95	89.17	104
Regression Model - Linear	58.17	57.20	91.54	63.78	57.05	51.04	120
Regression Model – Pure Quadratic	61.62	60.70	62.24	63.31	60.69	54.97	119

Table X: Comparison of the best classification results (ACC, SENS, SPEC, PREC, F1S, MCC), selected by the highest ACC, for the different machine learning classifiers trained with the features ranked by the Relieff feature selection method (fist stage)

Classifiers	Overall Performance						Number of Features
	ACC	SENS	SPEC	PREC	F1S	MCC	
KNN Squared Inverse	86.44	86.63	97.27	86.45	86.49	83.80	119
KNN Equal	86.44	86.63	97.27	86.45	86.49	83.80	119
KNN Inverse	86.44	86.63	97.27	86.45	86.49	83.80	119
DA Linear	77.99	77.14	95.57	73.93	77.35	73.80	37
DA Quadratic	77.18	76.70	95.43	78.31	76.62	72.72	31
Ensemble Learning	94.26	94.09	98.84	94.27	94.17	93.02	120
Decision Tree	90.76	90.61	98.14	90.62	90.62	88.76	119
Regression Model - Linear	56.43	55.54	91.19	62.61	55.40	49.21	110
Regression Model – Pure Quadratic	60.63	59.68	92.03	65.84	59.83	53.99	120

Table XI: Comparison of the best classification results ((ACC, SENS, SPEC, PREC, F1S, MCC), selected by the highest ACC, for the different machine learning classifiers trained with the features ranked by the UDFS feature selection method (fist stage)

Classifiers	Overall Performance						Number of Features
	ACC	SENS	SPEC	PREC	F1S	MCC	
KNN Squared Inverse	94.49	94.51	98.90	94.24	94.36	93.26	20
KNN Equal	94.49	94.51	98.90	94.24	94.36	93.26	20
KNN Inverse	94.49	94.51	98.90	94.24	94.36	93.26	20
DA Linear	76.04	75.77	95.22	76.67	75.62	71.26	70
DA Quadratic	71.11	70.25	94.24	71.74	70.12	65.01	108
Ensemble Learning	94.71	94.65	98.93	94.75	94.68	93.63	118
Decision Tree	89.86	89.84	97.96	89.79	89.81	87.78	118
Regression Model - Linear	52.88	52.05	90.46	58.45	51.74	44.72	120
Regression Model – Pure Quadratic	59.59	58.66	91.83	64.45	58.66	52.60	119

Table XII: Comparison of the best classification results (ACC, SENS, SPEC, PREC, F1S, MCC), selected by the highest ACC, for the different machine learning classifiers trained with the features ranked by the UFSOL feature selection method (fist stage)

Classifiers	Overall Performance						Number of Features
	ACC	SENS	SPEC	PREC	F1S	MCC	
KNN Squared Inverse	92.08	92.12	98.41	92.01	92.04	90.47	30
KNN Equal	92.08	92.12	98.41	92.01	92.04	90.47	30
KNN Inverse	92.08	92.12	98.41	92.01	92.04	90.47	30
DA Linear	67.11	66.82	93.39	70.96	67.10	67.85	82
DA Quadratic	53.89	52.10	90.70	55.58	49.24	43.40	84
Ensemble Learning	93.88	93.66	98.77	93.91	93.77	92.55	88
Decision Tree	88.49	88.25	97.69	88.24	88.24	85.93	93
Regression Model - Linear	40.60	40.02	88.09	44.28	37.06	28.69	120
Regression Model – Pure Quadratic	45.22	44.56	89.00	48.02	41.98	33.97	119

Table XIII: Comparison of the classification results (ACC, SENS, SPEC, PREC, F1S, MCC),), of the machine learning models, KNN and Ensemble Leaning, trained with the features ranked by the UDFS and LLCFS method, respectively and validated with a 10-5-Fold CV (second stage)

Feature Selection Melhod	Classifiers	Overall Performance						Number of Features
		ACC	SENS	SPEC	PREC	F1S	MCC	
UDFS	KNN SquaredInverse	98.22	97.34	99.63	97.33	97.33	96.97	20
		97.27	96.01	99.42	96.21	96.11	95.54	10
		97.75	96.72	99.53	96.78	96.74	96.28	15
LLCFS	Emsemble Learning	98.46	97.63	99.68	97.87	97.75	97.43	118
		92.71	89.50	98.36	92.56	90.91	89.45	20
		95.38	93.30	98.97	95.11	94.16	93.21	30
		97.86	96.69	99.54	97.13	96.91	96.47	35
		98.18	97.17	99.62	97.46	97.31	96.94	40

Table XIV: Performance Metrics for each gait event (ACC, SENS, SPEC, PREC, F1S, MCC) with the combination of the 20 most significant features through the UDFS feature selection method with the KNN algorithm as classifier (second stage)

Gait Event	ACC	SENS	SPEC	PREC	F1S	MCC
FGC	93.59	93.59	99.50	96.51	95.02	94.33
FBC	98.88	98.87	99.13	98.59	98.73	97.96
MSM	96.34	96.33	99.56	96.34	96.34	95.90
PCO	92.87	92.86	99.66	91.90	92.38	92.07
FCO	98.39	98.39	99.74	98.68	98.52	98.25
CMS	98.40	98.40	99.29	96.90	97.64	97.11

Appendix 2

In this appendix it is represented the complete results regarding Chapter 7.

Table XV: Comparison of the best classification results (ACC, SENS, SPEC, PREC, F1S and MCC), selected by the highest ACC, for the different machine learning classifiers trained with the features ranked by the Relief feature selection method for PFS detection (first stage)

Classifiers	ACC	SENS	SPEC	PREC	F1S	MCC	Number of Features
Support Vector Machines - Linear	95.84	97.80	87.74	97.04	97.42	86.62	53
Support Vector Machines - Polynomial	99.89	99.92	99.74	99.94	99.93	99.65	60
Support Vector Machines - Gaussian	99.02	99.43	99.34	99.35	99.39	96.89	58
KNN Squared Inverse	99.95	99.96	99.96	99.98	99.97	99.84	106
KNN Equal	99.95	99.96	99.96	99.98	99.97	99.84	106
KNN Inverse	99.95	99.96	99.96	99.98	99.97	99.84	106
DA Linear	92.22	94.29	83.30	96.05	95.16	75.39	5
DA Quadratic	92.14	95.31	78.50	95.02	95.17	74.18	5
Ensemble Learning	99.93	99.96	99.84	99.96	99.96	99.78	30
Decision Tree	99.78	99.87	99.39	99.86	99.87	99.28	34
Regression Model - Linear	95.07	98.21	81.49	95.82	97.00	83.35	118
Regression Model – Pure Quadratic	95.40	98.23	83.22	96.19	97.20	84.55	119

Table XVI: Comparison of the best classification results (ACC, SENS, SPEC, PREC, F1S and MCC), selected by the highest ACC, for the different machine learning classifiers trained with the features ranked by the Laplacian Score for PFS detection (first stage)

Classifiers	ACC	SENS	SPEC	PREC	F1S	MCC	Number of Features
Support Vector Machines - Linear	96.24	97.94	89.26	97.40	97.67	87.96	55
Support Vector Machines - Polynomial	99.89	99.92	99.78	99.95	99.93	99.67	51
Support Vector Machines - Gaussian	99.35	99.52	98.63	99.67	99.59	97.93	60
KNN Squared Inverse	98.85	99.29	96.97	99.30	99.29	96.25	12
KNN Equal	98.85	99.29	96.97	99.30	99.29	96.25	12
KNN Inverse	98.85	99.29	96.97	99.30	99.29	96.25	12
DA Linear	80.97	91.92	81.16	95.46	93.66	69.15	8
DA Quadratic	90.17	92.30	80.97	95.43	93.84	67.74	11
Ensemble Learning	99.94	99.94	99.90	99.98	99.96	99.79	67
Decision Tree	99.71	99.82	99.25	99.83	99.82	99.06	118
Regression Model - Linear	95.19	98.21	82.17	95.96	97.09	83.81	119
Regression Model – Pure Quadratic	95.66	98.32	84.22	96.41	97.35	85.46	118

Table XVII: Comparison of the best classification results (ACC, SENS, SPEC, PREC, F1S and MCC), selected by the highest ACC, for the different machine learning classifiers trained with the features ranked by the UDFS for PFS detection (first stage)

Classifiers	ACC	SENS	SPEC	PREC	F1S	MCC	Number of Features
Support Vector Machines - Linear	80.47	99.91	0.51	80.51	89.17	3.93	41
Support Vector Machines - Polynomial	80.45	100	0.01	80.45	89.16	0.91	1
Support Vector Machines - Gaussian	82.02	99.92	4.61	81.91	90.02	19.07	60
KNN Squared Inverse	95.92	97.74	88.06	97.24	97.49	86.55	120
KNN Equal	95.92	97.74	88.06	97.24	97.49	86.55	120
KNN Inverse	95.92	97.74	88.06	97.24	97.49	86.55	120
DA Linear	81.17	100	0.06	81.17	89.61	2.28	4
DA Quadratic	81.16	100	0.00	81.16	89.60	NaN	1
Ensemble Learning	94.73	99.98	72.10	93.92	96.85	82.23	120
Decision Tree	90.57	94.31	74.48	94.09	94.02	69.05	120
Regression Model - linear	82.80	99.51	10.66	82.78	90.38	25.98	116
Regression Model - pure quadratic	83.39	99.06	15.81	83.53	90.64	30.66	119

Table XVIII: Comparison of the best classification results (ACC, SENS, SPEC, PREC, F1S and MCC), selected by the highest ACC, for the different machine learning classifiers trained with the features ranked by the LLC feature selection method for PFS detection (first stage)

Classifier	ACC	SENS	SPEC	PREC	F1S	MCC	Number of Features
Support Vector Machines - Linear	95.75	97.84	88.64	97.24	97.36	86.44	55
Support Vector Machines - Polynomial	99.26	99.51	98.21	99.56	99.54	97.64	58
Support Vector Machines - Gaussian	97.89	99.11	92.87	98.28	98.69	93.21	59
KNN Squared Inverse	97.82	98.83	93.46	98.49	98.66	92.82	120
KNN Equal	97.82	98.83	93.46	98.49	98.66	92.82	120
KNN Inverse	97.82	98.83	93.46	98.49	98.66	92.82	120
DA Linear	91.38	93.53	82.10	95.75	94.62	72.97	14
DA Quadratic	90.78	93.57	78.79	95.00	94.28	70.65	17
Ensemble Learning	99.94	99.95	99.89	99.97	99.96	99.80	84
Decision Tree	99.72	99.83	99.25	99.83	99.83	99.08	78
Regression Model - linear	95.20	98.27	81.82	95.91	97.08	83.79	116
Regression Model – Pure Quadratic	95.69	98.33	84.33	96.43	97.37	85.57	117

Table XIX: Comparison of the best classification results (ACC, SENS, SPEC, PREC, F1S and MCC), selected by the highest ACC, for the different machine learning classifiers trained with the features ranked by the CFS for PFS detection (first stage)

Classifier	ACC	SENS	SPEC	PREC	F1S	MCC	Number of Features
Support Vector Machines - Linear	85.12	98.07	31.83	85.54	91.38	44.29	55
Support Vector Machines - Polynomial	96.09	97.95	88.41	97.20	97.58	87.43	58
Support Vector Machines - Gaussian	90.67	97.81	61.31	91.23	94.40	68.07	60
KNN Squared Inverse	95.09	97.43	85.01	96.55	96.99	83.71	120
KNN Equal	95.09	97.43	85.01	96.55	96.99	83.71	120
KNN Inverse	95.09	97.43	85.01	96.55	96.99	83.71	120
DA Linear	87.41	88.77	81.58	95.40	91.97	63.97	101
DA Quadratic	81.16	100	0.00	81.16	89.60	NaN	1
Ensemble Learning	99.92	99.95	99.8	99.95	99.95	99.73	85
Decision Tree	99.66	99.8	99.06	99.78	99.79	98.89	96
Regression Model - Linear	94.86	97.84	81.99	95.91	96.87	82.72	118
Regression Model - pure quadratic	95.26	97.88	83.96	96.34	97.10	84.15	113

Table XX: Comparison of the best classification results (ACC, SENS, SPEC, PREC, F1S and MCC), selected by the highest ACC, for the different machine learning classifiers trained with the features ranked by the UFSOL feature selection method for PFS detection (first stage)

Classifier	ACC	SENS	SPEC	PREC	F1S	MCC	Number of Features
Support Vector Machines - Linear	81.23	99.88	0.87	81.28	89.63	5.83	15
Support Vector Machines - Polynomial	81.20	99.92	0.58	81.24	89.62	4.65	2
Support Vector Machines - Gaussian	84.63	99.69	22.72	84.14	91.26	42.01	59
KNN Squared Inverse	99.14	99.56	97.34	99.38	99.47	97.18	118
KNN Equal	99.14	99.56	97.34	99.38	99.47	97.18	118
KNN Inverse	99.14	99.56	97.34	99.38	99.47	97.18	118
DA Linear	80.80	98.88	2.91	81.44	89.32	5.86	1
DA Quadratic	79.23	96.44	5.1	81.41	88.29	3.13	1
Ensemble Learning	99.36	99.89	97.05	99.32	99.61	97.89	114
Decision Tree	99.35	99.64	98.11	99.56	99.60	97.87	118
Regression Model - Linear	86.52	97.92	37.42	87.09	92.18	48.92	120
Regression Model – Pure Quadratic	89.99	98.96	51.02	89.77	94.14	63.86	120

Table XXI: Comparison of the best classification results (ACC, SENS, SPEC, PREC, F1S and MCC), selected by the highest ACC, for the different machine learning classifiers trained with the features ranked by the Lasso feature selection method for PFS detection (first stage)

Classifier	ACC	SENS	SPEC	PREC	F1S	MCC	Number of Features
Support Vector Machines - Linear	90.71	98.09	58.93	91.14	94.49	67.07	46
Support Vector Machines - Polynomial	98.12	98.63	95.92	99.05	98.84	93.89	53
Support Vector Machines - Gaussian	94.92	99.27	76.19	94.73	96.94	82.75	51
KNN Squared Inverse	99.58	99.77	98.76	99.71	99.74	98.61	51
KNN Equal	99.58	99.77	98.76	99.71	99.74	98.61	51
KNN Inverse	99.58	99.77	98.76	99.71	99.74	98.61	51
DA Linear	82.28	93.81	32.60	85.71	89.58	32.79	39
DA Quadratic	81.11	93.26	28.75	84.94	88.91	27.64	20
Ensemble Learning	99.91	99.95	99.77	99.95	99.95	99.72	50
Decision Tree	99.68	99.81	99.12	99.79	99.80	98.96	50
Regression Model - linear	92.42	98.48	66.20	92.65	95.48	73.54	119
Regression Model – Pure Quadratic	94.76	98.33	79.32	95.36	96.82	82.21	120

Table XXII: Comparison of the classification results (ACC, SENS, SPEC, Precision, F1S and MCC), of the machine learning models, KNN and Support Vector Machines, trained with the features ranked by the Laplacian Score and validated with a 10-5-Fold CV (second stage)

Feature Selection Method	Classifier	ACC	SENS	SPEC	PREC	F1S	MCC	Number of Features
Laplacian	Support Vector Machines - Polynomial	60.78	58.33	71.32	89.76	70.71	23.22	10
		53.42	53.41	64.74	86.81	66.11	17.23	12
		59.99	59.08	63.89	87.58	70.56	18.05	20
		97.11	97.88	93.81	98.55	98.22	90.68	30
		99.09	98.92	98.63	99.91	99.92	99.58	51
	KNN Squared Inverse	98.84	99.24	97.12	99.33	99.28	96.21	10
		99.08	99.39	97.72	99.47	99.43	97.00	12
		98.22	98.98	94.97	98.83	98.90	94.18	20

Table XXIII: Comparison the post-processing filter results (ACC, SENS, SPEC, Precision, F1S and MCC) with different windows size and sample number with the non-use of the filter (third stage)

With/Without Filter	Window Size	Number of Samples	ACC	SENS	SPEC	PREC	F1S	MCC
Without	NA		98.15	98.11	100.	100	99.04	73.15
With	20	20	99.76	99.93	92.29	99.82	99.88	94.51
	39	39	99.65	100	84.44	99.64	99.82	91.73
	100	33	99.45	99.73	86.92	99.70	99.71	87.27

Appendix 3

In this appendix it is represented the complete list of features computed for chapter 6 and 7.

Table XXIV:Complete list of features used both in Chapter 6 and 7 with feature label, its description and the corresponding reference.

Feature Number	Feature Label	Feature Description	Reference
1	Raw - Acc X	Raw acceleration (X axis)	[82]
2	Raw - Acc Y	Raw acceleration (Y axis)	[82]
3	Raw - Acc Z	Raw acceleration (Z axis)	[82]
4	Raw - Gyr X	Raw angular velocity (X axis)	NA
5	Raw - Gyr Y	Raw angular velocity (Y axis)	NA
6	Raw - Gyr Z	Raw angular velocity (Z axis)	NA
7	BP Filter - Acc X	Band-pass filtered acceleration (X axis)	NA
8	BP Filter - Acc Y	Band-pass filtered acceleration (Y axis)	NA
9	BP Filter - Acc Z	Band-pass filtered acceleration (Z axis)	NA
10	BP Filter - Gyr X	Band-pass filtered angular velocity (X axis)	NA
11	BP Filter - Gyr Y	Band-pass filtered angular velocity (Y axis)	NA
12	BP Filter - Gyr Z	Band-pass filtered angular velocity (Z axis)	NA
13	HP Filter - Acc X	High-pass filtered acceleration (X axis)	NA
14	HP Filter - Acc Y	High-pass filtered acceleration (Y axis)	NA
15	HP Filter - Acc Z	High-pass filtered acceleration (Z axis)	NA
16	HP Filter - Gyr X	High-pass filtered angular velocity (X axis)	NA
17	HP Filter - Gyr Y	High-pass filtered angular velocity (Y axis)	NA
18	HP Filter - Gyr Z	High-pass filtered angular velocity (Z axis)	NA
19	SVM Acc High Pass	SVM of High-pass filtered acceleration	[58]
20	SVM Acc Band Pass	SVM of Band-pass filtered acceleration	[58]
21	SVM Acc RAW	SVM of Raw acceleration	[58]
22	SVM Gyr High Pass	SVM of High-pass filtered Angular Velocity	[19]
23	SVM Gyr Band Pass	SVM of Band-pass filtered Angular Velocity	[19]
24	SVM Gyr RAW	SVM of Raw Angular Velocity	[19]
25	CHA	Cumulative Horizontal Acceleration	[81]
26	Velocity X	Velocity (X axis)	[81]
27	Velocity Y	Velocity (Y axis)	[81]
28	Velocity Z	Velocity (Z axis)	[81]
29	Displacement X	Displacement (X Axis)	[81]
30	Displacement Y	Displacement (Y Axis)	[81]
31	Displacement Z	Displacement (Z Axis)	[81]
32	CHD	Cumulative Horizontal Displacement	[81]
33	Cumulative horizontal SL - X	Sway Length of Cumulative Horizontal acceleration (X axis)	[81]
34	Cumulative horizontal SL - Y	Sway Length of Cumulative Horizontal acceleration (Y axis)	[81]
35	Cumulative horizontal SL - Z	Sway Length of Cumulative Horizontal acceleration (Z axis)	[81]
36	Mean sway velocity - X	Mean sway velocity (X Axis)	[81]

Feature Number	Feature Label	Feature Description	Reference
37	Mean sway velocity - Y	Mean sway velocity (Y Axis)	[81]
38	Mean sway velocity - Z	Mean sway velocity (Z Axis)	[81]
39	Displacement range - X	Displacement range (X axis)	[81]
40	Displacement range - Y	Displacement range (Y axis)	[81]
41	Displacement range - Z	Displacement range (Z axis)	[81]
42	Skewness - Acc X	Skewness of acceleration (X axis)	[67]
43	Skewness - Acc Y	Skewness of acceleration (Y axis)	[67]
44	Skewness - Acc Z	Skewness of acceleration (Z axis)	[67]
45	Skewness SVM - Acc BP	Skewness of band-pass filtered SVM acceleration	[67]
46	Skewness - Gyr X	Skewness of angular velocity (X axis)	[67]
47	Skewness - Gyr Y	Skewness of angular velocity (Y axis)	[67]
48	Skewness - Gyr Z	Skewness of angular velocity (Z axis)	[67]
49	Skewness SVM -Gyr BP	Skewness of band-pass filtered SVM angular velocity	[67]
50	Kurtosis - Acc X	Kurtosis of acceleration (X axis)	[67]
51	Kurtosis - Acc Y	Kurtosis of acceleration (Y axis)	[67]
52	Kurtosis - Acc Z	Kurtosis of acceleration (Z axis)	[67]
53	Kurtosis SVM - Acc BP	Kurtosis of band-pass filtered SVM acceleration	[67]
54	Kurtosis - Gyr X	Kurtosis of angular velocity (X axis)	[67]
55	Kurtosis - Gyr Y	Kurtosis of angular velocity (Y axis)	[67]
56	Kurtosis - Gyr Z	Kurtosis of angular velocity (Z axis)	[67]
57	Kurtosis SVM - Gyr BP	Kurtosis of band-pass filtered SVM angular velocity	[67]
58	Kurtosis - Acc X SMF	Kurtosis of smooth-median filter acceleration (X axis)	[67]
59	Kurtosis - Acc Y SMF	Kurtosis of smooth-median filter acceleration (Y axis)	[67]
60	Kurtosis - Acc Z SMF	Kurtosis of smooth-median filter acceleration (Z axis)	[67]
61	Kurtosis SVM - Acc BP SMF	Kurtosis of SVM acceleration band-pass and smooth-median filtered	[67]
62	Kurtosis - Gyr X SMF	Kurtosis of smooth-median filter angular velocity (X axis)	[67]
63	Kurtosis - Gyr Y SMF	Kurtosis of smooth-median filter angular velocity (Y axis)	[67]
64	Kurtosis - Gyr Z SMF	Kurtosis of smooth-median filter angular velocity (Z axis)	[67]
65	Kurtosis SVM - Gyr BP SMF	Kurtosis of SVM Angular Velocity band-pass and smooth-median filtered	[67]
66	Min - Acc X	Minimum Acceleration (X axis)	[65]
67	Min - Acc Y	Minimum Acceleration (Y axis)	[65]
68	Min - Acc Z	Minimum Acceleration (Z axis)	[65]
69	Min - Gyr X	Minimum Angular Velocity (X axis)	[65]
70	Min - Gyr Y	Minimum Angular Velocity (Y axis)	[65]
71	Min - Gyr Z	Minimum Angular Velocity (Z axis)	[65]
72	Min SVM - Acc	Minimum SVM of Acceleration	[65]
73	Min SVM - Gyr	Minimum SVM of Angular Velocity	[65]
74	Max - Acc X	Maximum Acceleration (X axis)	[65]
75	Max - Acc Y	Maximum Acceleration (Y axis)	[65]
76	Max - Acc Z	Maximum Acceleration (Z axis)	[65]
77	Max - Gyr X	Maximum Angular Velocity (X axis)	[65]
78	Max - Gyr Y	Maximum Angular Velocity (Y axis)	[65]

Feature Number	Feature Label	Feature Description	Reference
79	Max - Gyr Z	Maximum Angular Velocity (Z axis)	[65]
80	Max SVM - Acc	Maximum SVM of Acceleration	[65]
81	Max SVM - Gyr	Maximum SVM of Angular Velocity	[65]
82	Mean - Acc X	Mean Acceleration (X axis)	[67]
83	Mean - Acc Y	Mean Acceleration (Y axis)	[67]
84	Mean - Acc Z	Mean Acceleration (Z axis)	[67]
85	Mean - Gyr X	Mean Angular Velocity (X axis)	[67]
86	Mean - Gyr Y	Mean Angular Velocity (Y axis)	[67]
87	Mean - Gyr Z	Mean Angular Velocity (Z axis)	[67]
88	Mean SVM - Acc	Mean SVM of Acceleration	[67]
89	Mean SVM - Gyr	Mean SVM of Angular Velocity	[67]
90	Variance - Acc X	Variance of Acceleration (X axis)	[67]
91	Variance - Acc Y	Variance of Acceleration (Y axis)	[67]
92	Variance - Acc Z	Variance of Acceleration (Z axis)	[67]
93	Variance - Gyr X	Variance of Angular Velocity (X axis)	[67]
94	Variance - Gyr Y	Variance of Angular Velocity (Y axis)	[67]
95	Variance - Gyr Z	Variance of Angular Velocity (Z axis)	[67]
96	Variance - SVM Acc	Variance of SVM of Acceleration	[67]
97	Variance - SVM Gyr	Variance of SVM of Angular Velocity	[67]
98	Std - Acc X	Standard Deviation of Acceleration (X Axis)	NA
99	Std - Acc Y	Standard Deviation of Acceleration (Y Axis)	NA
100	Std - Acc Z	Standard Deviation of Acceleration (Z Axis)	NA
101	Std - Gyr X	Standard Deviation of Angular Velocity (X Axis)	NA
102	Std - Gyr Y	Standard Deviation of Angular Velocity (Y Axis)	NA
103	Std - Gyr Z	Standard Deviation of Angular Velocity (Z Axis)	NA
104	Std SVM - Acc	Standard Deviation of Acceleration SVM	NA
105	Std SVM - Gyr	Standard Deviation of Angular Velocity SVM	NA
106	Min SVM - Acc LP	Minimum of SVM Acceleration Low-Pass Filtered	NA
107	Max SVM - Acc LP	Maximum of SVM Acceleration Low-Pass Filtered	NA
108	Mean SVM - Acc LP	Mean of SVM Acceleration Low-Pass Filtered	NA
109	Var SVM - Acc LP	Variance of SVM Acceleration Low-Pass Filtered	NA
110	Std SVM - Acc LP	Standard Deviation of SVM Acceleration Low-Pass Filtered	NA
111	Min SVM - Gyr LP	Minimum of SVM Angular Velocity Low-Pass Filtered	NA
112	Max SVM - Gyr LP	Maximum of SVM Angular Velocity Low-Pass Filtered	NA
113	Mean SVM - Gyr LP	Mean of SVM Angular Velocity Low-Pass Filtered	NA
114	Var SVM - Gyr LP	Variance of SVM Angular Velocity Low-Pass Filtered	NA
115	Std SVM - Gyr LP	Standard Deviation of SVM Angular Velocity Low-Pass Filtered	NA
116	Correlation - Acc X - Y	Correlation Between Accelerantion X and Y axis	[84]
117	Correlation - Acc X - Z	Correlation Between Accelerantion X and Z axis	[84]
118	Correlation - Acc Y - Z	Correlation Between Accelerantion Y and Z axis	[84]
119	Correlation - Gyr X - Y	Correlation Between Angular Velocity X and Y axis	[84]
120	Correlation - Gyr X - Z	Correlation Between Angular Velocity X and Z axis	[84]

Feature Number	Feature Label	Feature Description	Reference
121	Correlation - Gyr Y - Z	Correlation Between Angular Velocity Y and Z axis	[84]
122	Energy Acc X	Acceleration Energy (X axis)	[83]
123	Energy Acc Y	Acceleration Energy (Y axis)	[83]
124	Energy Acc Z	Acceleration Energy (Z axis)	[83]
125	Total Energy - Acc SVM BP	Total Energy of Band-Pass Filtered SVM acceleration	[83]
126	Dynamic Sum Vector	Dynamic Sum Vector	[58]
127	Z2	Vertical Acceleration	[58]
128	Total angular change	Total angular change	[19]
129	Resultant angular acceleration	Resultant angular acceleration	[19]
130	% of window where the LP Acc SVM is < 0.9	Percentage of Low-Pass Filtered Acceleration SVM lower than 0.9	[84]
131	ASMA	Activity Signal Magnitude Area	[60]
132	SMA	Signal Magnitude Are	[61]
133	PP Values - Acc X	Peak-to-peak values of Acceleration (X axis)	[87]
134	PP Values - Acc Y	Peak-to-peak values of Acceleration (Y axis)	[87]
135	PP Values - Acc Z	Peak-to-peak values of Acceleration (Z axis)	[87]
136	PP Values - Gyr X	Peak-to-peak values of Angular Velocity (X axis)	[87]
137	PP Values - Gyr Y	Peak-to-peak values of Angular Velocity (Y axis)	[87]
138	PP Values - Gyr Z	Peak-to-peak values of Angular Velocity (Z axis)	[87]
139	PP Values - SVM Acc BP	Peak-to-peak Values of Band-Pass filtered Acceleration SVM	[87]
140	PP Values - SVM Gyr BP	Peak-to-peak Values of Band-Pass filtered Angular Velocity SVM	[87]
141	RMS -Acc X	Root Mean Square of Acceleration (X axis)	[87]
142	RMS - Acc Y	Root Mean Square of Acceleration (Y axis)	[87]
143	RMS - Acc Z	Root Mean Square of Acceleration (Z axis)	[87]
144	RMS - Gyr X	Root Mean Square of Angular Velocity (X axis)	[87]
145	RMS - Gyr Y	Root Mean Square of Angular Velocity (Y axis)	[87]
146	RMS - Gyr Z	Root Mean Square of Angular Velocity (Z axis)	[87]
147	RMS - SVM Acc	Root Mean Square of Acceleration SVM	[87]
148	RMS - SVM Gyr	Root Mean Square of Angular Velocity SVM	[87]
149	RI - Acc X	Ration Index of Acceleration (X axis)	[87]
150	RI - Acc Y	Ration Index of Acceleration (Y axis)	[87]
151	RI - Acc Z	Ration Index of Acceleration (Z axis)	[87]
152	RI - SVM Acc	Ratio Index of Acceleration SVM	[87]
153	RI - Gyr X	Ration Index of Angular Velocity (X axis)	[87]
154	RI - Gyr Y	Ration Index of Angular Velocity (Y axis)	[87]
155	RI - Gyr Z	Ration Index of Angular Velocity (Z axis)	[87]
156	RI - SVM Gyr	Ratio Index of Angular Velocity SVM	[87]
157	RI - Acc X PP	Ration Index of Peak-to-peak of Acceleration (X axis)	[87]
158	RI - Acc Y PP	Ration Index of Peak-to-peak of Acceleration (Y axis)	[87]
159	RI - Acc Z PP	Ration Index of Peak-to-peak of Acceleration (Z axis)	[87]
160	RI - Gyr X PP	Ration Index of Peak-to-peak of Angular Velocity (X axis)	[87]
161	RI - Gyr Y PP	Ration Index of Peak-to-peak of Angular Velocity (Y axis)	[87]
162	RI - Gyr Z PP	Ration Index of Peak-to-peak of Angular Velocity (Z axis)	[87]

Feature Number	Feature Label	Feature Description	Reference
163	GC - Acc X	Gravity component of Acceleration (X Axis)	NA
164	GC - Acc Y	Gravity component of Acceleration (Y Axis)	NA
165	GC- Acc Z	Gravity component of Acceleration (Z Axis)	NA
166	Quaternion	First element of quaternion vector	[57]
167	Quaternion	Second element of quaternion vector	[57]
168	Quaternion	Third element of quaternion vector	[57]
169	Quaternion	Fourth element of quaternion vector	[57]
170	Roll	Roll (Madgwick Sensor-Fusion Algorithm)	[57]
171	Pitch	Pitch (Madgwick Sensor-Fusion Algorithm)	[57]
172	Yaw	Yaw (Madgwick Sensor-Fusion Algorithm)	[57]
173	Acc of absolute vertical direction	Absolute vertical acceleration	[11]
174	RAC SVM	SVM of Resultant angle change	[70]
175	RAC - X	Resultant angle change (X axis)	[70]
176	RAC - Y	Resultant angle change (Y axis)	[70]
177	RAC - Y	Resultant angle change (Z axis)	[70]
178	MRAA	Maximum resultant angular acceleration	[70]
179	FF	Sum of Fluctuation Frequency of all axis	[70]
180	FF DX	Fluctuation Frequency (X axis)	[70]
181	FF DY	Fluctuation Frequency (Y axis)	[70]
182	FF DZ	Fluctuation Frequency (Z axis)	[70]
183	Transf - X	Trapz of the Fast Fourier Transform of Acceleration (X axis)	[86]
184	Transf - Y	Trapz of the Fast Fourier Transform of Acceleration (Y axis)	[86]
185	Transf - Z	Trapz of the Fast Fourier Transform of Acceleration (Z axis)	[86]
186	HR X	Harmonic Ratio (X axis)	[87]
187	HR Y	Harmonic Ratio (Y axis)	[87]
188	HR Z	Harmonic Ratio (Z axis)	[87]
189	HR - SVM	SVM of Harmonic Ratio	[87]
190	Wavelet_STD 2 - Gyr X	Standard deviations of the angular velocity (X axis) at level 2	[86]
191	Wavelet_STD 3 - Gyr X	Standard deviations of the angular velocity (X axis) at level 3	[86]
192	Wavelet_STD 4 - Gyr X	Standard deviations of the angular velocity (X axis) at level 4	[86]
193	Wavelet_STD 5 - Gyr X	Standard deviations of the angular velocity (X axis) at level 5	[86]
194	Wavelet_RMS 2 - Gyr X	Root Mean Square of the angular velocity (X axis) at level 2	[86]
195	Wavelet_RMS 3 - Gyr X	Root Mean Square of the angular velocity (X axis) at level 3	[86]
196	Wavelet_RMS 4 - Gyr X	Root Mean Square of the angular velocity (X axis) at level 4	[86]
197	Wavelet_RMS 5 - Gyr X	Root Mean Square of the angular velocity (X axis) at level 5	[86]
198	SumSquaredWavelet - Gyr X	Sum of squared wavelet coefficients from level 2 to 6 from the Angular velocity (X axis)	[86]
199	Wavelet_STD 2 - Gyr Y	Standard deviations of the angular velocity (Y axis) at level 2	[86]
200	Wavelet_STD 3 - Gyr Y	Standard deviations of the angular velocity (Y axis) at level 3	[86]
201	Wavelet_STD 4 - Gyr Y	Standard deviations of the angular velocity (Y axis) at level 4	[86]
202	Wavelet_STD 5 - Gyr Y	Standard deviations of the angular velocity (Y axis) at level 5	[86]
203	Wavelet_RMS 2 - Gyr Y	Root Mean Square of the angular velocity (Y axis) at level 2	[86]
204	Wavelet_RMS 3 - Gyr Y	Root Mean Square of the angular velocity (Y axis) at level 3	[86]

Feature Number	Feature Label	Feature Description	Reference
205	Wavelet_RMS 4 - Gyr Y	Root Mean Square of the angular velocity (Y axis) at level 4	[86]
206	Wavelet_RMS 5 - Gyr Y	Root Mean Square of the angular velocity (Y axis) at level 5	[86]
207	SumSquaredWavelet - Gyr Y	Sum of squared wavelet coefficients from level 2 to 6 from the Angular velocity (Y axis)	[86]
208	Wavelet_STD 2 - Gyr Z	Standard deviations of the angular velocity (Z axis) at level 2	[86]
209	Wavelet_STD 3 - Gyr Z	Standard deviations of the angular velocity (Z axis) at level 3	[86]
210	Wavelet_STD 4 - Gyr Z	Standard deviations of the angular velocity (Z axis) at level 4	[86]
211	Wavelet_STD 5 - Gyr Z	Standard deviations of the angular velocity (Z axis) at level 5	[86]
212	Wavelet_RMS 2 - Gyr Z	Root Mean Square of the angular velocity (Z axis) at level 2	[86]
213	Wavelet_RMS 3 - Gyr Z	Root Mean Square of the angular velocity (Z axis) at level 3	[86]
214	Wavelet_RMS 4 - Gyr Z	Root Mean Square of the angular velocity (Z axis) at level 4	[86]
215	Wavelet_RMS 5 - Gyr Z	Root Mean Square of the angular velocity (Z axis) at level 5	[86]
216	SumSquaredWavelet - Gyr Z	Sum of squared wavelet coefficients from level 2 to 6 from the Angular velocity (Z axis)	[86]
217	Wavelet_STD 2 - Gyr SVM	SVM of the Standard deviations of the angular velocity at level 2	[86]
218	Wavelet_STD 3 - Gyr SVM	SVM of the Standard deviations of the angular velocity at level 3	[86]
219	Wavelet_STD 4 - Gyr SVM	SVM of the Standard deviations of the angular velocity at level 4	[86]
220	Wavelet_STD 5 - Gyr SVM	SVM of the Standard deviations of the angular velocity at level 5	[86]
221	Wavelet_RMS 2 - Gyr SVM	SVM of the Root Mean Square of the angular velocity at level 2	[86]
222	Wavelet_RMS 3 - Gyr SVM	SVM of the Root Mean Square of the angular velocity at level 3	[86]
223	Wavelet_RMS 4 - Gyr SVM	SVM of the Root Mean Square of the angular velocity at level 4	[86]
224	Wavelet_RMS 5 - Gyr SVM	SVM of the Root Mean Square of the angular velocity at level 5	[86]
225	SumSquaredWavelet - Gyr SVM	SVM of the Sum of squared wavelet coefficients from level 2 to 6 from the Angular velocity	[86]
226	Wavelet_STD 2 - Acc X	Standard deviations of the Acceleration (X axis) at level 2	[86]
227	Wavelet_STD 3 - Acc X	Standard deviations of the Acceleration (X axis) at level 3	[86]
228	Wavelet_STD 4 - Acc X	Standard deviations of the Acceleration (X axis) at level 4	[86]
229	Wavelet_STD 5 - Acc X	Standard deviations of the Acceleration (X axis) at level 5	[86]
230	Wavelet_RMS 2 - Acc X	Root Mean Square of the Acceleration (X axis) at level 2	[86]
231	Wavelet_RMS 3 - Acc X	Root Mean Square of the Acceleration (X axis) at level 3	[86]
232	Wavelet_RMS 4 - Acc X	Root Mean Square of the Acceleration (X axis) at level 4	[86]
233	Wavelet_RMS 5 - Acc X	Root Mean Square of the Acceleration (X axis) at level 5	[86]
234	SumSquaredWavelet - Acc X	Sum of squared wavelet coefficients from level 2 to 6 from the Acceleration (X axis)	[86]
235	Wavelet_STD 2 - Acc Y	Standard deviations of the Acceleration (Y axis) at level 2	[86]
236	Wavelet_STD 3 - Acc Y	Standard deviations of the Acceleration (Y axis) at level 3	[86]
237	Wavelet_STD 4 - Acc Y	Standard deviations of the Acceleration (Y axis) at level 4	[86]
238	Wavelet_STD 5 - Acc Y	Standard deviations of the Acceleration (Y axis) at level 5	[86]
239	Wavelet_RMS 2 - Acc Y	Root Mean Square of the Acceleration (Y axis) at level 2	[86]
240	Wavelet_RMS 3 - Acc Y	Root Mean Square of the Acceleration (Y axis) at level 3	[86]
241	Wavelet_RMS 4 - Acc Y	Root Mean Square of the Acceleration (Y axis) at level 4	[86]

Feature Number	Feature Label	Feature Description	Reference
242	Wavelet_RMS 5 - Acc Y	Root Mean Square of the Acceleration (Y axis) at level 5	[86]
243	SumSquaredWavelet - Acc Y	Sum of squared wavelet coefficients from level 2 to 6 from the Acceleration (Y axis)	[86]
244	Wavelet_STD 2 - Acc Z	Standard deviations of the Acceleration (Z axis) at level 2	[86]
245	Wavelet_STD 3 - Acc Z	Standard deviations of the Acceleration (Z axis) at level 3	[86]
246	Wavelet_STD 4 - Acc Z	Standard deviations of the Acceleration (Z axis) at level 4	[86]
247	Wavelet_STD 5 - Acc Z	Standard deviations of the Acceleration (Z axis) at level 5	[86]
248	Wavelet_RMS 2 - Acc Z	Root Mean Square of the Acceleration (Z axis) at level 2	[86]
249	Wavelet_RMS 3 - Acc Z	Root Mean Square of the Acceleration (Z axis) at level 3	[86]
250	Wavelet_RMS 4 - Acc Z	Root Mean Square of the Acceleration (Z axis) at level 4	[86]
251	Wavelet_RMS 5 - Acc Z	Root Mean Square of the Acceleration (Z axis) at level 5	[86]
252	SumSquaredWavelet - Acc Z	Sum of squared wavelet coefficients from level 2 to 6 from the Acceleration (Z axis)	[86]
253	Wavelet_STD 2 - Acc SVM	SVM of the Standard deviations of the Acceleration at level 2	[86]
254	Wavelet_STD 3 - Acc SVM	SVM of the Standard deviations of the Acceleration at level 3	[86]
255	Wavelet_STD 4 - Acc SVM	SVM of the Standard deviations of the Acceleration at level 4	[86]
256	Wavelet_STD 5 - Acc SVM	SVM of the Standard deviations of the Acceleration at level 5	[86]
257	Wavelet_RMS 2 - Acc SVM	SVM of the Root Mean Square of the Acceleration at level 2	[86]
258	Wavelet_RMS 3 - Acc SVM	SVM of the Root Mean Square of the Acceleration at level 3	[86]
259	Wavelet_RMS 4 - Acc SVM	SVM of the Root Mean Square of the Acceleration at level 4	[86]
260	Wavelet_RMS 5 - Acc SVM	SVM of the Root Mean Square of the Acceleration at level 5	[86]
261	Sum Squared Wavelet - Acc SVM	SVM of the Sum of squared wavelet coefficients from level 2 to 6 from the Acceleration	[86]
262	RAC - SVM	SVM of Resultant of Average Acceleration (X axis)	[62]
263	RAC - X	Resultant of Average Acceleration (X axis)	[62]
264	RAC - Y	Resultant of Average Acceleration (Y axis)	[62]
265	RAC - Z	Resultant of Average Acceleration (Z axis)	[62]
266	RSD - SVM	SVM of Resultant of Standard Deviation	[62]
267	RSD - X	Resultant of Standard Deviation (X axis)	[62]
268	RSD - Y	Resultant of Standard Deviation (Y axis)	[62]
269	RSD - Z	Resultant of Standard Deviation (Z axis)	[62]
270	Slope	Slope	[64]
271	Fast Change Vector	Fast Change Vector	[66]
272	Acceleration in the horizontal Plane	SVM of Acceleration in the horizontal Plane	[64]
273	EMA	Acceleration exponential moving average	[65]
274	Rotational Angle - SVM Acc	Rotational Angle of Acceleration SVM	[64]
275	Z-score	Z-Score	[62]
276	entropy - Acc X	Acceleration Entropy (X axis)	[85]
277	entropy - Acc Y	Acceleration Entropy (Y axis)	[85]
278	entropy - Acc Z	Acceleration Entropy (Z axis)	[85]
279	entropy - Gyr X	Angular Velocity Entropy (X axis)	[85]
280	entropy - Gyr Y	Angular Velocity Entropy (Y axis)	[85]
281	entropy - Gyr Z	Angular Velocity Entropy (Z axis)	[85]
282	entropy - SVM Acc	Acceleration SVM Entropy	[85]

Feature Number	Feature Label	Feature Description	Reference
283	entropy - SVM Gyr	Angular Velocity SVM Entropy	[85]
284	MAD	Magnitude of Angular Displacement	[57]
285	Rotational Angle - SVM LP Acc	Rotational Angle of Low-Pass filtered Acceleration SVM	[64]
286	Resultant of Delta Changes - Acc	Acceleration Resultant of Delta Changes	[62]
287	Resultant of Delta Changes - Gyr	Angular Velocity Resultant of Delta Changes	[62]
288	FSR	ASCane FSR	NA